Principles of local computation in the entorhinal cortex

DISSERTATION

zur Erlangung des akademischen Grades
Doctor rerum naturalium
(Dr.rer.nat.)
eingereicht an der
Lebenswissenschaftlichen Fakultät
der Humboldt-Universität zu Berlin
von

MSc Neurosciences
Eric Torsten Reifenstein

Präsident der Humboldt-Universität zu Berlin
Prof. Dr. Jan-Hendrik Olbertz

Dekan der Lebenswissenschaftlichen Fakultät
Prof. Dr. Richard Lucius

Gutachter/innen:

1. Prof. Dr. Susanne Schreiber
2. Prof. Dr. Sen Cheng
3. Prof. Dr. Christian Leibold

Tag der mündlichen Prüfung: 21.07.2016

Abstract

Every day, animals are exposed to sequences of events that are worth recalling. It is a common problem, however, that the time scale of behavior and the time scale for the induction of neuronal learning differ by multiple orders of magnitude. One possible solution could be a phenomenon called "phase precession" – the gradual shift of spike phases with respect to the theta oscillation in the local field potential. Phase precession allows for the temporal compression of behavioral sequences of events to the time scale of synaptic plasticity. In this thesis, I investigate the phase-precession phenomenon in the medial entorhinal cortex of the rat. I find that entorhinal grid cells show phase precession at the behaviorally relevant single-trial level and that phase precession is stronger in single trials than in pooled-trial data. Single-trial analysis further revealed that phase precession (i) exists in cells across all layers of medial entorhinal cortex and (ii) is altered by the complex movement patterns of rats in two-dimensional environments. Finally, I show that phase precession is cell-type specific: stellate cells in layer II of the medial entorhinal cortex exhibit clear phase precession whereas pyramidal cells in the same layer do not. These results have broad implications for pinpointing the origin and possible mechanisms of phase precession.

Zusammenfassung

Lebewesen sind jeden Tag Sequenzen von Ereignissen ausgesetzt, die sie sich merken wollen. Es ist jedoch ein allgemeines Problem, dass sich die Zeitskalen des Verhaltens und der Induzierung von neuronalem Lernen um mehrere Größenordnungen unterscheiden. Eine mögliche Lösung könnte "Phasenpräzession" sein – das graduelle Verschieben von Aktionspotential-Phasen relativ zur Theta-Oszillation im lokalen Feldpotential. Phasenpräzession ermöglicht es, Verhaltens-Sequenzen zeitlich zu komprimieren, herunter bis auf die Zeitskala von synaptischer Plastizität. In dieser Arbeit untersuche ich das Phasenpräzessions-Phänomen im medialen entorhinalen Kortex der Ratte. Ich entdecke, dass entorhinale Gitterzellen auf der für das Verhalten relevanten Einzellaufebene Phasenpräzession zeigen und dass die Phasenpräzession in Einzelläufen stärker ist als in zusammengefassten Daten vieler Läufe. Die Analyse von Einzelläufen zeigt zudem, dass Phasenpräzession (i) in Zellen aus allen Schichten des entorhinalen Kortex existiert und (ii) von den komplexen Bewegungsmustern der Ratten in zweidimensionalen Umgebungen abhängt. Zum Abschluss zeige ich, dass Phasenpräzession zelltyp-spezifisch ist: Sternzellen in Schicht II des medialen entorhinalen Kortex weisen klare Phasenpräzession auf, wohingegen Pyramidenzellen in der selben Schicht dies nicht tun. Diese Ergebnisse haben weitreichende Implikationen sowohl für das Lokalisieren des Ursprungs als auch für die möglichen Mechanismen von Phasenpräzession.

Contents

List of Figures

1 Introduction

In Sir Arthur Conan Doyle's "The Adventure of the Engineer's Thumb" the hydraulic engineer Victor Hatherlay reports the incidents of an adventurous night to Sherlock Holmes:

> He dashed her to one side, and, rushing to the window, cut at me with his heavy weapon. I had let myself go, and was hanging by the hands to the sill, when his blow fell. I was conscious of a dull pain, my grip loosened, and I fell into the garden below. I was shaken but not hurt by the fall; so I picked myself up and rushed off among the bushes as hard as I could run, for I understood that I was far from being out of danger yet. Suddenly, however, as I ran, a deadly dizziness and sickness came over me. I glanced down at my hand, which was throbbing painfully, and then, for the first time, saw that my thumb had been cut off and that the blood was pouring from my wound. I endeavoured to tie my handkerchief round it, but there came a sudden buzzing in my ears, and next moment I fell in a dead faint among the rose-bushes.

While Hatherlay recollects the events of that night, many questions arise: Who is the assassin? Who is the woman he dashed aside? How does a hydraulic engineer end up losing his thumb? All of these questions are valid – and Sherlock Holmes proceeds to tackle them. However, I believe the most pressing question is: How does the engineer manage to recall the correct order of events? Or to be more specific: what are the neuronal mechanisms for remembering the correct sequence of the events?

To put this scenario more generally, let us consider a sequence of behavioral events which occur over the course of a few seconds (e.g. getting your thumb cut off, falling from a window, and running through the garden). In contrast to that, neurons in the nervous system usually act on much shorter time scales. It is a big challenge for the nervous system to bridge the gap between those time scales.

Let us consider a small number of neurons that each represent a single event of the behavioral sequence. Each of those neurons is assumed to elicit a burst of action potentials (or "spikes") in response to the event that it represents. If the nervous system aims to learn the sequence of events, the spikes of cells representing successive events are required to be close in time to allow for the modification of synaptic weights, so called "spike-time dependent plasticity" (Levy and Steward, 1983, Gerstner et al., 1996, Markram et al., 1997, Kempter et al., 1997, Bi and Poo, 1998). This implies that the events should have some temporal overlap or if they do not – like in our example – then at least the corresponding activity of the different neurons should overlap. Additionally, the order of the sequence should be preserved in the firing of the neurons.

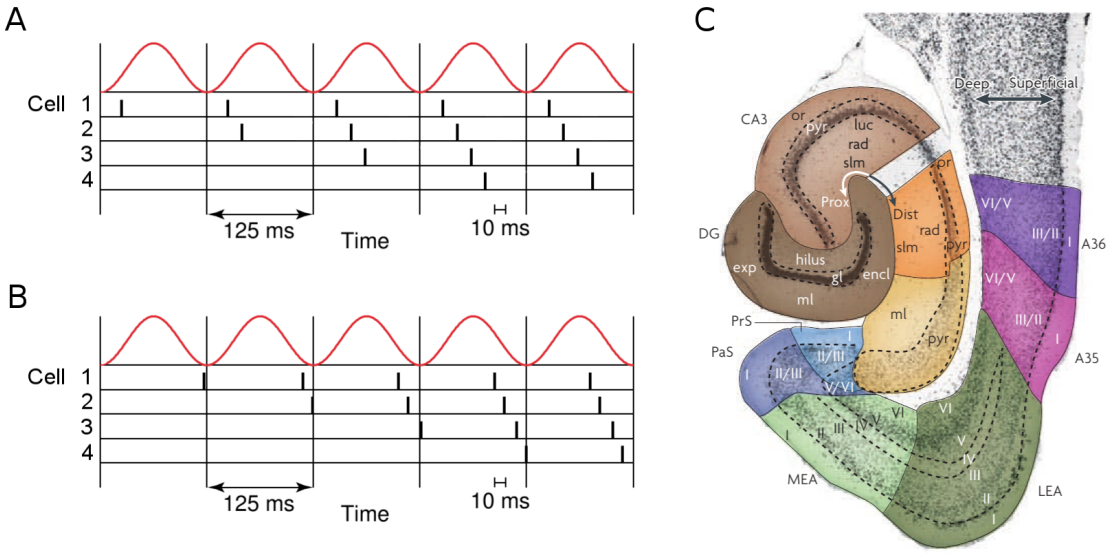

Figure 1.1: (A) Using phase-locked cells for the temporal compression of a sequence. Each cell corresponds to one phase of firing. The individual firing phases are organized such that the sequence of cells (from cell 1 to 4) is compressed to the time scale of a single cycle of the background oscillation. The background oscillation is shown in red. Black ticks mark the spikes of the cells. (B) Using phase-shifting cells for the temporal compression of a sequence. Each cell shifts its firing phases from late to early in the cycle, starting at the same initial phase for all cells. If the amount of phase shift per cycle is approximately the same for all cells, the sequence of cells is temporally compressed to a single cycle of the background oscillation. Adapted with permission from Melamed et al. (2004). (C) A Nissl-stained horizontal cross section in which the cortical layers are marked. The Roman numerals indicate cortical layers. A35 and A36, Brodmann areas 35 and 36; CA, cornu ammonis; dist, distal; encl, enclosed blade of the DG; exp, exposed blade of the DG; gl, granule cell layer; LEA, lateral entorhinal area; luc, stratum lucidum; MEA, medial entorhinal area; ml, molecular layer; or, stratum oriens; PaS; parasubiculum; prox, proximal; PrS, presubiculum; pyr, pyramidal cell layer; rad, stratum radiatum; slm, stratum lacunosum-moleculare. The CA1 is shown in orange. The subiculum is shown in yellow. The other subregions are explicitly marked. Adapted with permission from van Strien et al. (2000).

For the sake of the argument, let us assume an ongoing background oscillation at the intra-burst frequency of the cells, so we are able to assign phases to the cells' spikes. How can the spiking activity be organized such that the spikes of cells representing successive events are close in time? In one scenario, we can imagine different cells to be phase-locked to different phases of the oscillation, according to a cell's position in the behavioral sequence (Fig. 1.1A). Neighboring positions would thus be encoded by neighboring phases. Unfortunately, the order of events might change for a different sequence, e.g. first running through the garden, then getting your thumb cut off. Therefore, the firing phase of a cell would have to be dynamically tuned to fit its position in the sequence, which can be very demanding if a cell participates in multiple sequences. Alternatively, each cell could start firing at the same phase, but fire at a slightly higher frequency compared to the background oscillation (Skaggs et al., 1996; Fig. 1.1B). Consequently, a cell would elicit its first spike at the initial phase, but then, the longer it stays active, the earlier the following spikes in next cycles would occur. At the single cell level, the representation of sequences would hence be manifested as a progressive shift of the phases of spikes with respect to the background oscillation. This phenomenon has indeed been observed in a brain region called the "hippocampal formation".[1]

1.1 Hippocampal formation and phase precession

The hippocampal formation is an evolutionarily very old brain structure belonging to the limbic system. It consists of the hippocampus and adjacent cortical areas (Fig. 1.1C). The hippocampus contains multiple subregions: Cornu Ammonis 1 (CA1), Cornu Ammonis 2 (CA2), Cornu Ammonis 3 (CA3), and Dentate Gyrus (DG). These subregions are distinguished on the basis of different indicators such as cell morphology, connectivity and gene expression (Ramón y Cajal, 1893, Lorente de Nó, 1934, Amaral and Lavenex, 2007, Cembrowski et al., 2016). The hippocampus can be found in all mammalian species but also birds (Colombo and Broadbent, 2000, Shettleworth, 2003) and fish (Rodríguez et al., 2002, Broglio et al., 2005) have brain structures that are considered homologous to it. The mammalian

[1] There are alternative ideas to bridge the gap between the time scales of (slow) behavioral events and (fast) neuronal learning. These include "skipping neurons" in synfire chains (Abeles, 1991, Gerstner et al., 1993, Aviel et al., 2002), slow transitions between different neuronal populations that each represent the memory of a different event (Abbott and Blum, 1996, Markram et al., 1998, van Vreeswijk and Hansel, 2001) and slowing down the neuronal time scale by large loops spanning multiple brain regions (Kistler et al., 2000). In this thesis, I will focus on phase precession as a candidate mechanisms for temporal compression.

hippocampus plays a major role in the formation and consolidation of memories, as found by a plethora of lesion studies (Scoville and Milner, 1957, Rosenbaum et al., 2004, Savage et al., 2004, Lavenex et al., 2006).

Throughout the hippocampal formation, the previously hypothesized background oscillation (p.3) can indeed be found. The so-called theta rhythm oscillates at about 8 Hz and is observed in both, the extracellular field potential (Arnolds et al., 1980, Bland, 1986, Buzsáki, 2002) and the subthreshold potentials of individual neurons (Alonso and Klink, 1993, Kamondi et al., 1998, Schreiber et al., 2004, Domnisoru et al., 2013). Interestingly, many neurons oscillate slightly faster than the extracellular field potential, leading to the phenomenon of phase precession.

The term "phase precession" refers to the fact that the theta phases (i.e. the spike phases with respect to the theta oscillation) of a neuron's action potentials successively change from late to early in the theta cycle over the course of a few theta periods. As mentioned before, this consistent shift of spike phase might be used to compress behavioral sequences of events to the time scale of synaptic plasticity.

But what are the events that are represented by the cells? The answer to this question is not entirely clear. Potential candidates might be spatially tuned cells in the hippocampus and its surrounding regions. So-called place cells are active when the animal visits a certain location of the environment (the 'place field') and inactive when the animal moves to other locations (Fig. 1.2A, O'Keefe and Dostrovsky, 1971, O'Keefe, 1976, Wilson and McNaughton, 1993). Place cells can be found in all subregions of the hippocampus proper (CA1: O'Keefe and Dostrovsky, 1971; CA2: Mankin et al., 2015; CA3: Leutgeb and Leutgeb, 2007; DG: Jung and McNaughton, 1993) and have been shown to exhibit phase precession (O'Keefe and Recce, 1993). For hippocampal place cells, it thus seems clear that the events are defined as visits of the place field. However, the events need not be linked to space at all. Anything that correlates to the firing of a neuron could potentially be such an event of a sequence. Another example from the hippocampus are the so-called "time cells", which are active at a certain point in time during the waiting period in a delayed choice experiment (MacDonald et al., 2011, Kraus et al., 2013). In human hippocampus and entorhinal cortex, some cells respond to complex visual stimuli like faces, houses, and animals (Kreiman et al., 2000). In regions beyond the hippocampus, many more examples can be found besides visual objects (Gross et al., 1972, Logothetis and Sheinberg, 1996). Cells can represent things like complex

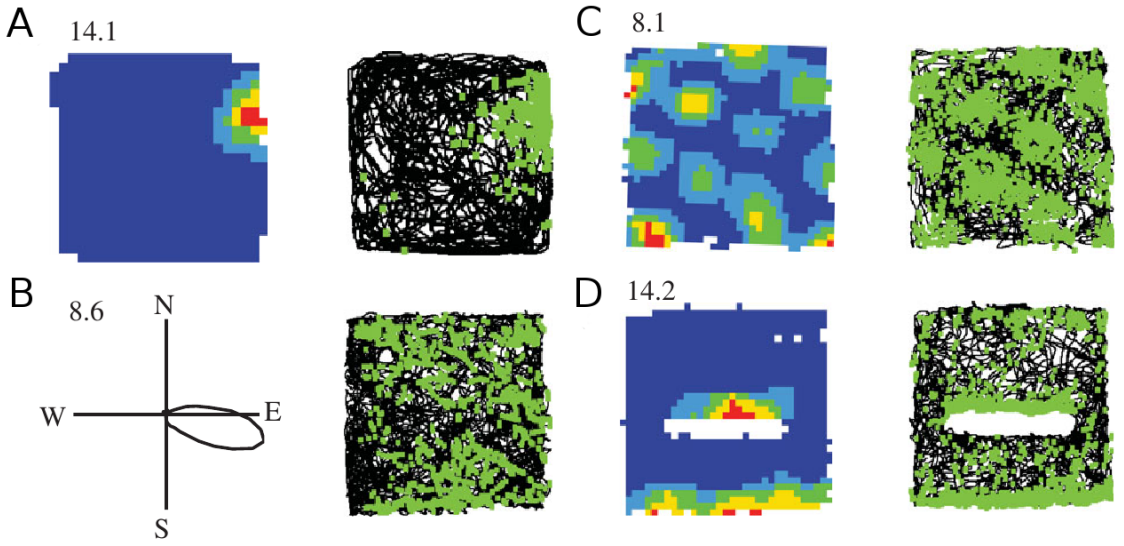

Figure 1.2: Different types of cells showing movement-related activity in the hippocampal formation. For each example cell (except for B), the firing-rate map (left) and the animal's trajectory in black with superimposed spikes in green (right) are shown. Numbers above the firing-rate maps are the peak firing rates (in spikes/s). The environment was a 1 m^2 box for all the experiments. (A) Place cell: the cell is active in one particular location of the box. (B) Head-direction cell: the cell is active when the animal moves in a certain direction, as demonstrated by the polar plot of the firing rate. This head-direction cell does not show clear spatial tuning, which can be seen by the scatter of spikes in space. (C) Grid cell: this type of cell has multiple firing fields which are arranged in a hexagonal grid. (D) Border cell: the cell is active at one (or more) of the borders of the box. To illustrate this property, an additional border was introduced to the environment. Modified from Hartley et al. (2013).

sensory input (e.g. certain odors (Schoenbaum and Eichenbaum, 1995)), higher cognitive qualities (like attention (Lynch et al., 1977) or planning (Goldman-Rakic, 1987)), or even represent sequences of events (Allen et al., 2016). For any of these cells to participate in a sequence that is imprinted in the synaptic weights, it would be hypothesized that they showed phase precession. So far, this has not been investigated.

More generally, the behavioral correlate of phase-precessing cells is mostly unclear. Phase precession has been observed in a number of brain regions apart from the hippocampus (Hafting et al., 2008, van der Meer and Redish, 2011, Malhotra et al., 2012). The most famous example is the medial entorhinal cortex, a region of associational cortex adjacent to the hippocampus. It harbors different types of spatially tuned cells: grid cells show multiple firing fields that are arranged in a hexagonal grid (Fig. 1.2C, Hafting et al.,2005), border cells are active when the animal moves along a certain boundary of the environment (Fig. 1.2D, Solstad et al., 2008), head-direction cells are tuned to direction (Fig. 1.2B, Sargolini et al.,

2006, Giocomo et al., 2014), speed cells fire according to the animal's speed (Kropff et al., 2015), and cue cells signal the proximity of visual cues in an environement (Kinkhabwala et al., 2015). It is currently not clear which of them show phase precession. I will try to shed some light on this question later in this thesis.

1.2 Connectivity in the hippocampal formation

The different subregions of hippocampus and the different layers of medial entorhinal cortex are highly interconnected (Fig. 1.3, see Moser et al., 2014 for a review). More specifically, layer II of the medial entorhinal cortex sends output via the "perforant path" to the hippocampal subregion DG, which projects to CA3 via the so called "mossy fibers". A number of fibers originate from layer II and project directly to CA3 and CA2. Those connections are often considered part of the perforant path. From CA3, signals are sent to CA1 – these connections are called "Schaffer collaterals" – and then on to the deep layers (V and VI) of the medial entorhinal cortex. This entire series of connections is often referred to as the "hippocampal loop". Additionally, cells in layers III, V and VI of the medial entorhinal cortex directly project to CA1 ("temporoammonic pathway", also considered part of the perforant path). Many further connections complicate the picture. As an example, CA2 is interconnected with CA3, receives input from DG and projects to CA1 as well as back to layer II of the medial entorhinal cortex. Within the medial entorhinal cortex, all cortical layers seem to be reciprocally interconnected (Moser et al., 2014).

Considering all these connections raises the question whether phase precession is created in one subregion and passed on to others (Jaramillo et al., 2014), or whether there are independent phase-precession generating mechanisms in different subregions. To work our way towards an answer to this question, we need to know whether phase precession exists in the different subregions of the hippocampal formation.

The phase-precession phenomenon was first described for cells in CA1 (O'Keefe and Recce, 1993). Later, Skaggs et al. (1996) reported phase precession also in CA3 and DG. Finally, Mankin et al. (2015) completed the picture for the hippocampus by demonstrating phase precession in CA2. Regarding medial entorhinal cortex, Hafting et al. (2008) pioneered phase-precession investigations. They showed the phenomenon in layers II, V and VI.

All the hitherto mentioned phase-precession studies analyzed the phenomenon in pooled

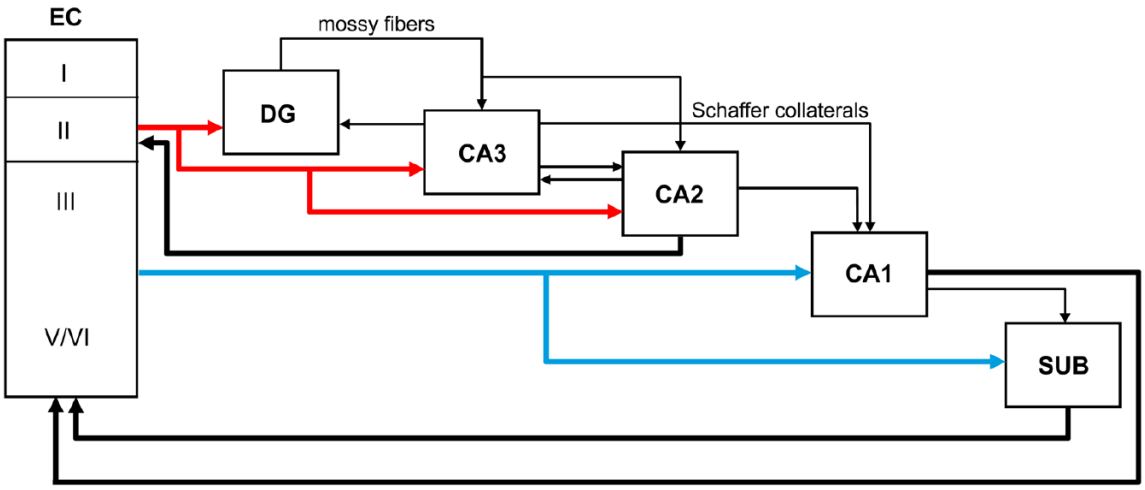

Figure 1.3: Schematic diagram showing the main excitatory connections between DG, the CA fields, the subicular complex (SUB), and entorhinal cortex (EC). Adapted from Llorens-Martín et al. (2014).

data: spikes from one cell were collected over many repetitions of the event, i.e. repeated traversals of a cell's firing field. Phase precession was then quantified by measuring the slope and the correlation between the theta phase and the position or time of all the pooled spikes. This procedure comes with the disadvantage that the estimated parameters of phase precession might be blurred by pooling over many runs.

1.3 Single-run analysis of entorhinal phase precession

It seems likely that the behaving animal needs to make use of phase information within individual runs – it usually does not have the opportunity to pool over multiple runs. Furthermore, according to the sequence-learning hypothesis (Skaggs et al., 1996, Tsodyks et al., 1996) and also other functional hypotheses like temporal coding (Harris et al., 2002, Mehta et al., 2002, Huxter et al., 2003, Leibold et al., 2008, Thurley et al., 2008), recall of sequences (Hasselmo and Eichenbaum, 2005, Lisman et al., 2005) and spatial navigation (Burgess et al., 1994, Koene et al., 2003, Lengyel et al., 2005), phase precession is expected to occur during individual events, i.e. in individual field traversals. Until recently, only one study performed such a single-run analysis: Schmidt et al. (2009) demonstrated phase precession in individual field traversals in CA1 place cells. Such an analysis had not been performed in the entorhinal cortex.

Using extracellularly recorded spikes recorded from grid cells in layer II of the medial

entorhinal cortex (Hafting et al., 2008), I analyzed phase precession in a single-run fashion (Reifenstein et al., 2012). I found that layer II grid cells phase precess in single runs. In those individual field traversals, the theta phase and the position of the rat on a linear track are even tighter correlated and slopes are steeper than expected from pooled data. Furthermore, I showed that phase precession is independent in successively visited grid fields of the same cell, indicating that different grid fields of the same cell could independently contribute to sequence learning.

As mentioned above, I explored entorhinal phase precession for rats running on linear tracks (Reifenstein et al., 2012). At that time, due to the correlation between theta phase and space, it seemed plausible to assume that theta phase could be used to estimate the position of the animal. I showed that this estimation could pinpoint the position with an accuracy of a few centimeters. Furthermore, I found that the theta phase contained more spatial information than the firing rate for a given firing field. These findings link space and phase for movements of the animal in one-dimensional environments. But how do the findings generalize to two-dimensional environments?

I tackled this question in Reifenstein et al. (2014). Apart from the issue of the rat's environment, my previous analysis (Reifenstein et al., 2012) had been restricted to cells recorded in layer II of the medial entorhinal cortex. In Reifenstein et al. (2014), I extended the analysis to grid cells from all entorhinal layers and performed a single-run analysis to investigate how differently shaped trajectories through the two-dimensional firing fields affect phase precession.

It is known that layer II of the medial entorhinal cortex does not consist of only one population of principal cells. Instead, two populations of excitatory cells, namely "stellate cells" and "pyramidal cells" can be distinguished. These two populations differ in their morphology (Fig. 1.4, Alonso and Klink, 1993, Tang et al., 2014) and show different projection patterns. Stellate cells project to the DG, whereas pyramidal cells send output to CA1 (Varga et al., 2010, Kitamura et al., 2014, Ray et al., 2014). Furthermore, stellate cells and pyramidal cells differ in their electrophysiological properties, such as subthreshold resonance, firing-rate adaptation and sag potentials (Alonso and Klink, 1993, Engel et al., 2008).

As mentioned before, it has been known that layer II cells show phase precession. But does phase coding differ between stellate cells and pyramidal cells? Due to methodological limitations, it is not simple to address this question. Juxtacellular recordings provide

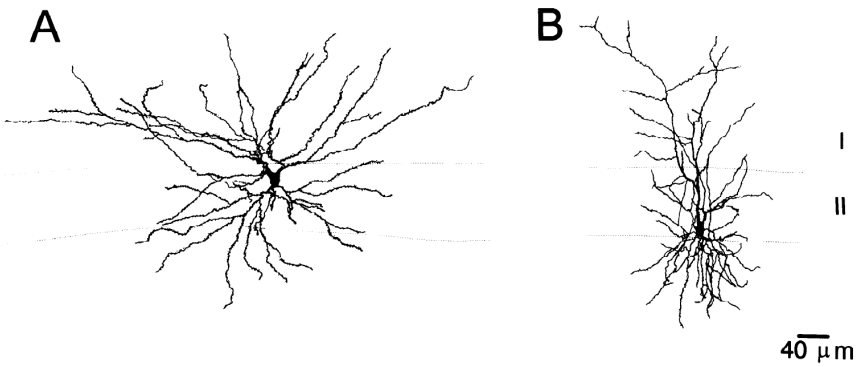

Figure 1.4: Morphology of (A) a stellate cell and (B) a pyramidal cell in layer II of the medial entorhinal cortex layer. Adapted from Alonso and Klink (1993).

unequivocal information about cell identity, but are exceedingly difficult and yield short recording durations. Calcium imaging in optogenetically identified cells allows the experimentator to monitor multiple cells at once, but the temporal resolution is too low to resolve the timing of individual spikes. In Reifenstein et al. (2016), I circumvented these problems by employing a computational classification procedure proposed by Tang et al. (2014), which allowed me to separate stellate cells from pyramidal cells in data from extracellular recordings.

The following three sections consist of the studies Reifenstein et al. (2012), Reifenstein et al. (2014) and Reifenstein et al. (2016). In these chapters, all results and related discussions are presented. The thesis will conclude with a general discussion that aims to put the findings in a broader picture. Please note that parts of Reifenstein et al. (2012) were already part of my Master's thesis.

2 Grid cells in rat entorhinal cortex encode physical space with independent firing fields and phase precession at the single-trial level

Published in the *Proceedings of the National Academy of Sciences* on April, 14 2012.

I wish to point out that the information-theoretical section and parts of the single-trial analysis of this study were already part of my Master's thesis. Therefore, this study is *not* part of the formal requirement for two first-author publications. Nevertheless, I believe that the findings of this study greatly add to the general picture, so I would like to include the study as a chapter of this thesis.

Grid cells in rat entorhinal cortex encode physical space with independent firing fields and phase precession at the single-trial level

Eric T. Reifenstein[a,b], Richard Kempter[b], Susanne Schreiber[b], Martin B. Stemmler[a], and Andreas V. M. Herz[a,1]

[a]Department of Biology II, Ludwig-Maximilians-Universität München, and Bernstein Center for Computational Neuroscience Munich, 82152 Planegg-Martinsried, Germany; and [b]Institute for Theoretical Biology, Humboldt-Universität zu Berlin, and Bernstein Center for Computational Neuroscience Berlin, 10115 Berlin, Germany

Edited* by John J. Hopfield, Princeton University, Princeton, NJ, and approved March 08, 2012 (received for review June 14, 2011)

When a rat moves, grid cells in its entorhinal cortex become active in multiple regions of the external world that form a hexagonal lattice. As the animal traverses one such "firing field," spikes tend to occur at successively earlier theta phases of the local field potential. This phenomenon is called phase precession. Here, we show that spike phases provide 80% more spatial information than spike counts and that they improve position estimates from single neurons down to a few centimeters. To understand what limits the resolution and how variable spike phases are across different field traversals, we analyze spike trains run by run. We find that the multiple firing fields of a grid cell operate as independent elements for encoding physical space. In addition, phase precession is significantly stronger than the pooled-run data suggest. Despite the inherent stochasticity of grid-cell firing, phase precession is therefore a robust phenomenon at the single-trial level, making a theta-phase code for spatial navigation feasible.

neural coding | spatial representation | spike-timing code | oscillator-interference model

Finding and remembering paths to follow through an environment relies on specialized neural circuits in which subgroups of neurons encode different spatial locations. A spatial region that causes a cell to fire spikes defines a "firing field"; for instance, place cells in CA1 of hippocampus often have a single firing field, whereas grid cells in the medial entorhinal cortex (mEC) have multiple, regularly spaced firing fields that are arranged in hexagonal grids (1–5).

Spatial location is represented not only in the firing rates of such cells (Fig. 1*A*), but also in the timing of spikes relative to global rhythms in the network (Fig. 1*B*). A prominent 6- to 11-Hz network oscillation—the "theta rhythm"—modulates the firing patterns of nerve cells throughout the entire entorhinal–hippocampal formation during exploratory behavior and accompanies the spatial periodicity of rodent grid cells (6, 7). By adding up the spikes recorded on many runs of the rodent through the same firing field, Hafting et al. (8) observed a pattern of progressively earlier phases relative to the theta rhythm for the spikes of layer II mEC grid cells. This phenomenon is termed phase precession and was first described in place cells from the hippocampus (9–12).

The observation that spatial position correlates negatively with the average phase of spikes does not answer the question of whether the animal can use this phenomenon for estimating its location at the single-run level. In fact, not only could the average, pooled behavior mask the variability of phase precession in single runs, but even more drastically, single-run phase precession could be unrelated to pooled phase precession. For instance, single runs could exhibit no or only little phase precession, whereas pooled runs would exhibit phase precession (Fig. 1*C*). The spikes on single runs could even recess in phase, yet still lead to phase precession in the pooled data. Single-run phase precession could also be stronger than the pooled runs suggest (Fig. 1*D*). Moreover, runs with strong phase precession could be interspersed with runs in which the spikes lock to a particular theta phase of the local field potential (LFP). There is also another aspect of grid-cell activity that needs to be taken into account: From one firing field to the next one visited, the discharge of a single grid cell may or may not be correlated. Hence it is an open question whether the nervous system can actually make use of phase coding in mEC, notwithstanding the trends seen in pooled data or at the single-run level in hippocampal place cells (13).

Results

Extracellularly isolated cells from layer II medial entorhinal cortex and the LFP were recorded by Hafting et al. (8) from rats running along a linear track, and made available by E. I. Moser (Norwegian University of Science and Technology, Trondheim, Norway). Many cells had multiple firing fields, corresponding to different locations at which the cell spiked (Fig. 1*A*). To analyze the relationship between the timing of spikes and the background theta rhythm in the LFP, we computed an instantaneous theta phase of the LFP by taking the Hilbert transform of the LFP signal, band-passed between 6 and 11 Hz. During the traversal of a single grid field, the firing rate first rises and then falls (Fig. 1*A*). At the same time, the average spike phase relative to the ongoing theta rhythm decreases (Fig. 1*B*). Hence, both the phase and the number of spikes within a theta cycle are a function of the rat's position within the firing field.

To quantify phase precession, regression analyses were performed. Because phase is a circular variable, traditional linear correlation analysis, as in Hafting et al. (8), may yield slope and correlation estimates that do not reflect the true structure in the data (Fig. S1). Therefore, we turned to circular–linear methods (14, 15). Indeed, the median linear correlation for a set of 291 grid fields from 67 cells, pooled across runs for each field, is found to be -0.28 ± 0.02, whereas the median circular–linear correlation coefficient is only -0.05 ± 0.04.

Such weak correlations could imply that the theta phase of spikes in single entorhinal grid cells is not a reliable indicator of spatial location, so we asked how well the phase of spikes relative to the theta LFP predicts the rat's position compared with the spike count. For any single run through a given location, the number and phase of a grid cell's spikes varies. By pooling over different runs through a grid field, we map the joint probability distribution of the rat's position and either the spike count or the spike phase (Fig. 2 *A* and *B*). Kernel density methods yield smoothed estimates for these distributions (*Materials and Methods*). In the example of Fig. 2*A*,

Author contributions: E.T.R., R.K., S.S., M.B.S., and A.V.M.H. designed research; E.T.R. performed research; E.T.R., M.B.S., and A.V.M.H. analyzed data; and E.T.R., R.K., S.S., M.B.S., and A.V.M.H. wrote the paper.

The authors declare no conflict of interest.

*This Direct Submission article had a prearranged editor.

Freely available online through the PNAS open access option.

[1]To whom correspondence should be addressed. E-mail: herz@bio.lmu.de.

This article contains supporting information online at www.pnas.org/lookup/suppl/doi:10.1073/pnas.1109599109/-/DCSupplemental.

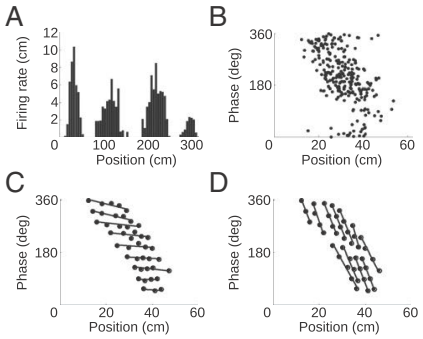

Fig. 1. The animal's position within the firing field modulates both the firing rate and theta phase. (*A*) Average firing rate of a grid cell for a rat running 42 times from left to right along a linear track. (*B*) The phase relative to the ongoing theta rhythm of all spikes from the leftmost grid field in *A*. Each dot depicts a single spike. (*C* and *D*) Hypothetical cases for which the relationship between the spike phase and the animal's position differs radically between single runs and pooled-run data. (*C*) Example in which spikes tend to be phase locked to the LFP oscillation, so that all subsequent spikes in later theta cycles follow at about the same phase as the initial spike. If the phase of the initial spike depends on the spatial coordinate, then the pooled-run data can mimic phase precession. (*D*) Phase precession in single runs can also be stronger than suggested by pooled data. Pooled phase precession in *C* and *D* is identical and could thus belie the phase–position relationship in single runs.

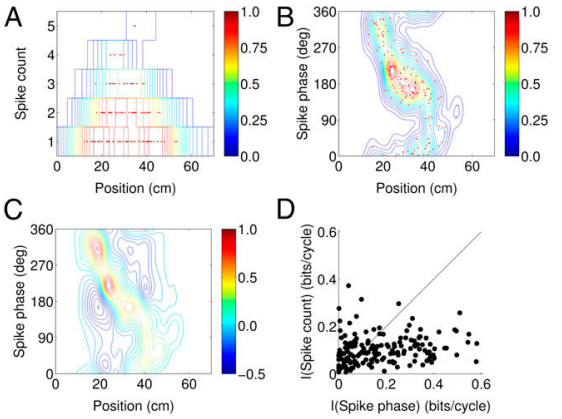

Fig. 2. The phase of spikes relative to the theta rhythm and the spike count per theta period convey spatial information. (*A*) Smoothed probability density of the position and the spike count in a theta cycle, $p_{X,N}(x,n)$, obtained by kernel density estimation (*Materials and Methods*) for the grid field depicted in Fig. 1*B*. The probability density (color bar) is normalized relative to the maximum value. Observed counts are indicated by red dots. (*B*) Normalized joint probability density of the position and phase of spikes relative to its theta cycle, $p_{X,\Theta}(x,\theta)$, for the same grid field. Red dots depict the phase of the first spike in each theta cycle, measured across different theta cycles and different runs. The average phase decreases as a function of position, whereas the spike count's relationship to position is inherently ambiguous: for instance, the average spike count at $x \approx 20$ cm$(\bar{n} \approx 1.75)$ is nearly the same as that at $x \approx 40$ cm$(\bar{n} \approx 1.65)$, whereas the (circular) average phases are 285° and 104°, respectively. (*C*) The difference $p_{X,\Theta}(x,\theta) - p_X(x)p_\Theta(\theta)$ reflects the strong correlation between phase and position induced by precession. (*D*) Theta phase conveys more information about position than does spike count ($p < 0.001$), as demonstrated by compound data from all grid fields (n = 166).

the most likely number of spikes within a theta cycle, given that the grid cell spiked at all, was always one, regardless of the rat's position within the grid field. Higher numbers of spikes only occurred toward the center of the grid field. Likewise, any particular location on the linear track leads to a specific range of possible phases for the first spikes within a theta cycle (Fig. 2*B*).

To quantify the effect of these uncertainties, we estimated the information the two different spike measures convey about the position. If position and phase were statistically independent, for instance, their joint probability $p_{X,\Theta}(x,\theta)$ would be equal to the product of the marginal probability distributions, $p_X(x)p_\Theta(\theta)$; Fig. 2*C* shows that this is not the case. Here, the joint probability clearly exceeds the product of the marginals along a negatively slanted diagonal throughout the grid field.

Different positions within a grid field map onto different expected spike phases; however, firing rates rise toward the center and then fall again, so that generally two positions are associated with the same average spike count. This ambiguity implies additional uncertainty, reducing the information available in the spike count to about half of that contained in the spike phase (0.102 ± 0.005 vs. 0.18 ± 0.01 bits/cycle). On a grid field-by-grid field basis, too, phase conveys more information about position than spike count ($P < 0.001$; Fig. 2*D*).

How precisely can one estimate the rat's position from the theta phase or spike count? A lower bound on the accuracy can be given by estimating the Fisher information (see Materials and Methods) using the kernel density estimates of the probability distributions. On average, the spike count allows one to discriminate nearby positions down to 9.3 ± 0.6 cm, whereas the theta phase differentiates positions to an accuracy of 5.8 ± 0.6 cm, i.e., about 1/10th of the grid field's size (56.0 ± 1.2 cm).

Information measures based on pooled data, however, reveal nothing about spatial encoding in single runs. For instance, the phase precession shown schematically in Fig. 1 *C* and *D* would yield the same average information between position and phase. A run-by-run analysis is warranted.

Just how few spikes participate in phase precession can be appreciated by a closer examination of single runs. In over half the runs, fewer than five spikes were elicited. Often, spikes on a single run reflect a nearly linear progression of phase with position (Fig. 3*A*); in some cases, connecting the spikes by lines in the phase vs. position diagram reveals a zigzag pattern in which one or more spikes follow the leading spike in a given theta cycle (Fig. 3*B*). Such "follower" spikes within the same theta cycle amount to about one-half of all spikes and occur with highly variable phase delays that can be >90°. After removing these unreliable spikes and considering only the leading spikes, a clearer signature of phase precession emerges (Fig. 3 *C* and *D*), even though the median number of spikes drops from five to three (Fig. 3*E*).

The median correlation in single runs is −0.33 ± 0.03 for leading spikes, compared with −0.24 ± 0.02 for all spikes (Fig. 3*F*, n = 5,948 runs with more than two leading spikes), although the distribution of correlation values is extremely broad; in fact, all possible correlation values from −1 to +1 are observed (Fig. 3*G*). The average slope, which measures the theta phase shift per distance traveled, changes from a mean value of −9.6 ± 0.1 degrees (deg)/cm for all spikes to −11.1 ± 0.1 deg/cm for the leading spikes (Fig. 3*H*; n = 5,948). The SD of either underlying distribution is large: 11.7 deg/cm for all spikes and 9.3 deg/cm for the leading spikes (Fig. 3*I*). Nonetheless, the difference in the mean slope of 1.5 deg/cm is highly significant ($P < 10^{-5}$).

Pooling can conceal the properties of phase precession during single runs. Comparing the pooled leading spikes to the leading spikes on single runs, the median correlation coefficient in many grid fields is more negative on single runs (Fig. 4*A*; $P < 0.001$). Apart from the inherent variability manifest in Fig. 3, the schematic of Fig. 1*D*, therefore, resembles phase precession on single runs: the average phase slope is about 30% more negative and significantly less variable than the pooled slope (Fig. 4*B*; paired t test: $P < 0.001$).

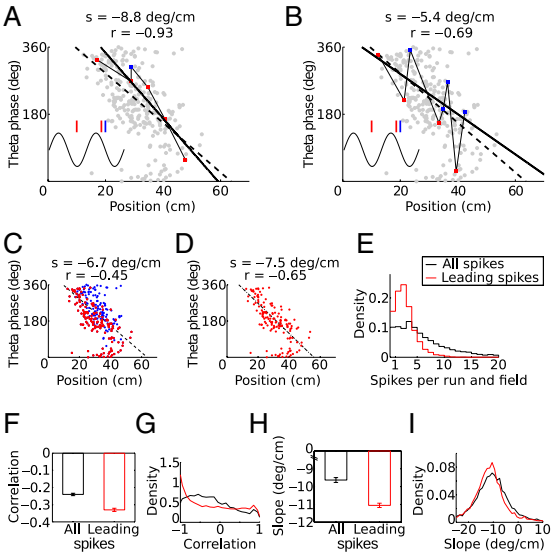

Fig. 3. Phase precession in single runs through grid fields. In each run, multiple theta cycles occur within a grid field. (*A* and *B*) Two typical single runs (red and blue squares connected by thin solid line; red squares, leading spikes; blue squares, later spikes within the same theta cycle, as sketched in the *Insets*) through the grid field shown in Figs. 1 and 2. Solid lines depict the circular fit to the single runs; dashed lines depict circular fit to all runs. Spikes from other runs through the grid field are shown in light gray. The slope *s* and the correlation coefficient *r* are given above the graphs. (*C*) Regression fit to all spikes across all runs through the grid field. (*D*) Regression fit to all of the leading spikes within each theta cycle of this grid field, after discarding any later spikes within the same cycle. (*E*) Histograms of spike counts per single run and grid field for all firing fields and grid cells (black line, median: 5) and for only the leading spikes (red line, median: 3). (*F*) Median circular correlation coefficient of all spikes and of leading spikes on single runs (-0.24 ± 0.02 vs. -0.33 ± 0.03). (*G*) Histograms of single-run correlation coefficients for all spikes (black line) and for leading spikes (red line). The two distributions are significantly different (Kolmogorov–Smirnov test: $P < 0.001$). (*H*) Slopes of circular fits for all spikes in a single run and for leading spikes (-9.6 ± 0.1 vs. -11.1 ± 0.1 deg/cm). (*I*) Histogram of the slopes fitted to all spikes and to only leading spikes. Some 9.7% of the slopes fall outside of the range shown. The two distributions differ significantly from one another (Kolmogorov–Smirnov test: $P < 0.001$).

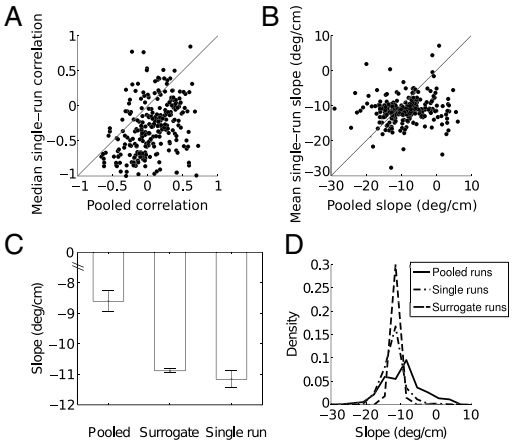

Fig. 4. Pooling spikes across runs distorts salient features of phase precession. Shown are results for the leading spikes in each theta cycle; averaged data from a single grid field are denoted by a dot. (*A*) The median single-run phase–position correlation is more negative than the pooled-data correlation (Wilcoxon rank-sum test: $p < 10^{-5}$, $n = 291$). (*B*) The mean single-run slope is less variable than the pooled slope (paired *t* test: $p < 10^{-5}$). (*C*) The phase changes ~30% more rapidly with position in single runs than predicted by the pooled runs, yielding a steeper slope (-11.2 ± 0.3 vs. -8.6 ± 0.3 deg/cm, averaged per grid field, not per run). The slopes of artificial, surrogate single runs (-10.9 ± 0.1 deg/cm) and actual runs are not significantly different. Surrogate single runs for a grid field were created by drawing leading spikes from the pooled data of that field, and the number of spikes in surrogate runs matched the number of spikes in the actual runs. (*D*) Circular regression of phase vs. position is more variable across grid fields if multiple runs are pooled first. The SD in the slope of pooled phase precession is 6.0 deg/cm, compared with 4.7 deg/cm in the mean slope of single runs.

To test whether the changes in the correlation coefficients and slopes of phase precession could be explained by the low number of leading spikes in single runs, we drew surrogate runs at random from the pooled data of leading spikes, using the same spike-count distribution as in the actual single runs. For each grid field ($n = 291$), we computed the median circular phase–position correlation in surrogate and actual single runs, as before. The median of the median correlations in surrogate and actual single runs was $r = -0.29 \pm 0.02$ and $r = -0.34 \pm 0.05$, respectively. Per grid field, the phase precessed at -10.9 ± 0.1 deg/cm in surrogate single runs, and at -11.2 ± 0.3 deg/cm in the actual single runs (Fig. 4*C*); though the mean values were not significantly different, the underlying distributions for the slopes differed between surrogate and actual runs (Fig. 4*D*).

Remarkably, the mean single-run slopes are less variable across grid fields than the pooled-data slopes across grid fields (Fig. 4*D*): 4.7 deg/cm (SD) for single runs vs. 6.0 deg/cm. In particular, the pooled data for some grid fields show no phase precession or even phase recession (zero or positive slope in the phase vs. position diagram). However, with the exception of four grid fields, the majority of single runs always precessed (Fig. 4*B*).

Unlike the firing fields of place cells, grid fields regularly repeat. If phase precession codes the animal's position, instead of being just a side effect of the theta rhythm, we need to investigate whether neural activity in one field depends on activity in the field visited previously (Fig. 5). Across runs, we compared the phase of the first spike in the present field with the phase of specific spikes in the prior field: the first spike (Fig. 5*B*), the last leading spike (Fig. 5*C*), or the last spike (Fig. 5*D*). For all three combinations, the joint probabilities were indistinguishable from the product of the respective marginal distributions, as shown by a generalized Kolmogorov–Smirnov test ($P = 0.83$, $P = 0.74$, $P = 0.74$, respectively; *Materials and Methods*). Similarly, neither the number of spikes ($P = 0.81$), nor the leading spike count ($P = 0.99$), nor the phase-precession slopes (all spikes: $P = 0.94$, leading spikes: $P = 0.94$) exhibited any significant field-to-field dependencies on single runs. We also asked whether phase precession in the next field is simply an extension of the precession in the previous field, as forecast by elementary oscillator-interference models for the generation of grid fields (16). Extrapolating the regression line fitted to one field failed to predict the phase of the first spike in the next field, however (Fig. 5 *E* and *F*; circular correlation $r = 0.01$, $P = 0.64$). The same was true when we also took the number of elapsed theta cycles into account (circular correlation $r = -0.01$, $P = 0.64$). To reveal subtle effects that might not have been captured by the above analyses, we finally tested whether single-run deviations from the mean response in each field (measured as the phase of the first spike, phase-precession slope, spike count, leading spike count, or leading spike slope) were correlated along the rat's track, but did not find any significant trends (circular correlation $r = 0.015$, $P =$

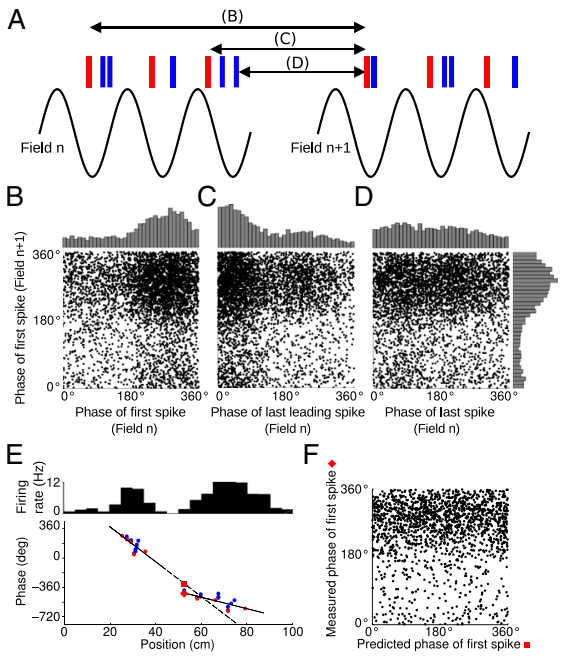

Fig. 5. Relation between successive firing fields of a grid cell. (*A*) The first-spike phase in field *n* + 1 (*Right*) could depend on various parameters of the cell's activity in field *n* (*Left*), such as the phase of the first spike, phase of the last leading spike, or phase of the last spike. As in Fig. 3, leading spikes are drawn in red, followers in blue. (*B–D*) The corresponding joint-probability distributions together with the respective marginal probabilities. The product structure of the joint-probability distributions indicates that the individual firing fields of one grid cell operate as independent encoders of physical space. In line with this observation, phase precession in one field does not predict the phase of the first spike in the next field, as illustrated in *E* and evidenced by population data (*F*).

0.31; Pearson's $r = 0.01$, $P = 0.53$; Pearson's $r = -0.02$, $P = 0.09$; Pearson's $r = 0.002$, $P = 0.89$; Pearson's $r = -0.002$, $P = 0.99$; respectively). Together, these findings indicate that the different firing fields of a grid cell provide independent information to downstream processing stages in the hippocampus.

Discussion

The negative correlation between a rat's location and the theta phase of grid-cell spikes (8, 17) invites the conjecture that the animal's brain works with these phases to navigate through the environment. This conjecture is at the core of various computational models (10, 16, 18) but had not been tested on experimental data. In the present analysis, we used the spike trains from single entorhinal grid cells recorded by Hafting et al. (8) to estimate the spatial information conveyed by theta phase and spike count, and studied the differences between single runs and pooled runs through grid fields as well as relations between individual grid fields.

Given the trial-to-trial variability of the theta phase of spikes throughout the entorhinal–hippocampal complex, one needs to prove that the phase contains useful information about the animal's position. This task is not always trivial: for an ensemble of simultaneously recorded, phase-precessing neurons in hippocampal CA1, Jensen and Lisman (19) used a Bayesian reconstruction algorithm to show that adding phase information improves the spatial resolution more than simply using the firing rate, narrowing the uncertainty from 4 cm to 3 cm under ideal conditions. However, an earlier study found that including the phases in the reconstruction algorithm led to no improvement (20).

For grid cells, firing fields repeat in a regular pattern. The spike phase of a single cell yields an instantaneous position estimate that is local and unique up to the intrinsic length scale of the grid. The coherence of the ongoing theta rhythm and cell-intrinsic mechanisms might induce dependencies between the discharge patterns evoked in different grid fields of the same cell. Our analysis shows that this is not the case (Fig. 5), and that each firing field of a grid cell can be regarded as an independent encoder of physical space. Because the animals were moving rapidly, passing through successive grid fields within as few as 10 theta cycles, this is a surprising result. Our finding suggests that the neural noise level is small enough to enable single-run phase-precession patterns within a grid field, yet large enough to decorrelate the activity from field to field. This interpretation is in accordance with in-vitro data (21) that show that EC stellate cells generate stochastic sub-threshold membrane potential oscillations whose low coherence may be responsible for the fast decorrelations observed in vivo.

As grid fields independently encode position in the phase, each one can be considered in isolation, so that we can estimate probability distributions for position and phase from pooling multiple runs through individual grid fields. Here, we found that the spike count within a theta cycle resolved the rat's position within a grid field to an average accuracy of 9.3 cm, whereas the spike phases improves that value to 5.8 cm, only little more than 1/10th of the mean grid-field size of 56 cm.

Phase precession on single grid-field traversals differed qualitatively from the average phase precession obtained by pooling many runs. In single runs, the change in phase with distance traveled was more pronounced, and the measured correlation between position and phase was more negative. Using surrogate data to take sample-size effects into account revealed that both observations are compatible with the reduced number of spikes in single runs. We conclude that phase precession is clearly present in the behaviorally relevant situation and that traditional pooling underestimates its strength by ∼30%.

In the hippocampal CA1 region, the correlations between phase and position also tend to be more negative on single runs (13). A cardinal difference between entorhinal grid cells and hippocampal place cells exists, however: inside a CA1 cell's place field, bursts frequently occur within theta cycles; a grid cell, in contrast, fires comparatively few bursts. The median number of spikes elicited during the traversal of a place field is ten (13), much higher than the five spikes in a grid field. Nonetheless, the leading spike in each theta cycle yielded a clear signature of phase precession in mEC. These leading spikes might be effective triggers of spiking activity in other areas—a much longer time delay (median: 92 ms) precedes them, compared with the delay that precedes follower spikes (median: 12 ms), so that the effect of leading spikes will be less prone to synaptic depression and adaptation downstream. Phase precession in place cells could thus be inherited from the phase precession of the leading spikes in mEC. Assuming that precisely timed activity of multiple grid cells is required to fire a single place cell, one might expect a reduction of the single-run phase range from EC to hippocampus. Indeed, the median single-run phase precession in entorhinal grid cells is 250°, whereas Schmidt et al. (13) observe that phase precession in CA1 during single runs typically extends over 180°, or half the full range of phases from 0° to 360° encompassed by pooled-run data.

Phase-precession measures in mEC grid cells were highly variable across single runs (Fig. 3 *F–I*), and the same phenomenon is observed in CA1 place cells. Information quantifies the uncertainty induced by variability, without pinpointing the source of uncertainty. Intrinsic noise, spike time jitter, and the LFP itself all contribute.

Population rhythms sculpt the timing of spikes (22–24), yet the LFP's theta phase is not synchronized to the location of the rat: at the moment when the rat enters a grid field, the theta phase is different on every run. In contrast, the oscillation phase in visual and auditory cortex is consistent in response to repeated

presentations of the same stimulus (25, 26). Cells throughout the mEC show a preference for spiking at particular phases of the theta and gamma rhythm in the LFP (17, 27); precession implies that the preferred phase shifts as the rat traverses the cell's firing field. The difference between the initial phase upon grid field entry and the preferred phase for spiking will affect when, and hence where, a grid cell will spike first. As a consequence, the pooled portrait of phase precession can be interpreted as the sum of the steeper phase precession sequences on individual runs; on each run, the line of phase precession is subject to a variable lateral shift along the position axis. Four factors, however, complicate this simple picture. First, single-run phase precession is not only steeper, on average, but also highly variable. Second, many entorhinal grid cells skip different theta cycles on different runs (27, 28). Third, the theta band LFP itself is noisy and not perfectly coherent in time. Fourth, any coupling to the gamma-band LFP will also shift the timing of grid cell spikes and thereby perturb the map between theta phase and the rat's position.

As the wide-range synchrony in the theta LFP organizes the spiking across different neurons (28), the single-run characteristics of phase precession, including the field-to-field independence, become decisive, and not the averaged precession properties derived from pooling over multiple runs. Indeed, firing sequences in simultaneously recorded place cells in CA1 have been shown to be more highly structured than predicted from the pooled, average phase–position relationship (29); the same may hold true for simultaneously recorded grid cells in mEC, but this remains to be seen.

Materials and Methods

Both published and previously unpublished data recorded by Hafting et al. (8) were reanalyzed (http://www.ntnu.no/cbm/moser/gridcell). In these experiments, grid cells were recorded extracellularly from layer II in the mEC of eight rats that ran on a linear track (length: 320 cm). Data include single-unit activity, the LFP sampled at a frequency of 250 Hz, and the position of the rat, as tracked by a diode fixed to the animal's head (8).

For our analysis, the spikes on each run were partitioned into firing fields, using the same criteria as Hafting et al. (8). Grid fields on runs from left to right were not generally the same as grid fields on runs in the reverse direction, and so were treated separately. Runs from right to left were mirrored for the data analysis, so that fields are always entered from the left and exited on the right. A total of 291 grid fields from 67 units were analyzed. Unlike Hafting et al. (8), we did not exclude fields with low spatial coherence between neighboring bins. In total, there were 9,561 single runs. The number of single runs per grid field ranged from 6 to 97. The raw LFP signal was filtered in the theta range (6–11 Hz). Using the Hilbert transform of the filtered signal, every spike was assigned an instantaneous theta phase. Two sets of spikes were considered: (*i*) the set of all spikes in a grid field and (*ii*) only the first spikes in each theta cycle (these spikes were termed leading spikes). In these two sets, there were 66,365 and 31,734 spikes, respectively. The phase precession properties associated with the leading spikes also held for other methods of choosing a single spike within a theta cycle (e.g., the average or the last spike in each theta cycle).

Phase precession was quantified by two measures (13–15): the slope s from circular–linear regression, which results from fitting the model $\theta = s \cdot (x - x_0)$ to the data by maximizing

$$R = \sqrt{\left(\frac{1}{n}\sum_{i=1}^{n}\cos(\theta_i - sx_i)\right)^2 + \left(\frac{1}{n}\sum_{i=1}^{n}\sin(\theta_i - sx_i)\right)^2},$$

and the circular–linear correlation coefficient

$$r = \frac{\sum_i \sin(\theta_i - \bar{\theta})\sin(\varphi_i - \bar{\varphi})}{\sqrt{\sum_i \sin^2(\theta_i - \bar{\theta})\sum_j \sin^2(\varphi_j - \bar{\varphi})}},$$

where θ_i denotes the theta phase of the i-th spike, $\varphi_i = s \cdot x_i \bmod 2\pi$ is a circular variable that is derived from the animal's position x_i, and $\bar{\varphi} = \arg\left(\frac{1}{n}\sum_{j=1}^{n}\exp(i\varphi_j)\right)$ and $\bar{\theta} = \arg\left(\frac{1}{n}\sum_{j=1}^{n}\exp(i\theta_j)\right)$ are the circular sample mean values (14).

Linear–linear correlation (30) is inherently ambiguous, because phase is a circular variable. Typically, one adds a phase offset to all spike phases in a given grid field and searches for the offset that leads to the largest (absolute) correlation. As a consequence of the optimization step, the estimated linear–linear correlation coefficient is nonzero, even if phase and position are completely uncorrelated (14, 15). When sample sizes are small, this effect is exacerbated. In contrast, the median circular–linear correlation coefficient is independent of any phase offset and is much more conservative, yielding lower values for the correlation coefficients, as also observed by Huxter et al. (31) in CA1. Fig. S1 compares the values of the linear–linear and circular–linear fits across all grid fields in the data set. The circular–linear slopes provided a better visual match to the data and were much steeper, on average, than the original mean value of -2.77 ± 0.31 deg/cm (8), which was derived by averaging across linear regressions.

The statistical likelihood of observing specific properties of phase precession in single runs was estimated by drawing surrogate runs from the pooled data. Each spike is associated with a position and a phase, so that the set of all (position, phase) pairs from actual runs is $\{(x_i, \theta_i)\}$. For each true run, a surrogate run with the same number of spikes was created, drawing the position and phase for each spike randomly from $\{(x_i, \theta_i)\}$ without replacement.

Mutual information is used to estimate how well the rat's position is encoded in the theta phase of action potentials or in the spike count within individual theta cycles. For two random variables, X and Φ, the mutual information is defined as

$$I(\Phi, X) = \int_{\Phi,X}\int p_{\Phi,X}(\varphi, x)\log\left(\frac{p_{\Phi,X}(\varphi, x)}{p_{\Phi}(\varphi)p_X(x)}\right)d\varphi dx,$$

where $p_{\Phi,X}(\varphi, x)$ denotes the joint probability density of the two random variables, and $p_{\Phi}(\varphi)$ and $p_x(x)$ are the marginal probability densities.

Whereas the mutual information reflects the global uncertainty about one random variable, given the other random variable, the Fisher information, defined as

$$I_F(x) = \int_{\Phi} p_{\Phi|X}(\varphi|x)\left(\frac{\partial}{\partial x}\log p_{\Phi|X}(\varphi|x)\right)^2 d\varphi,$$

measures the local uncertainty. Here, $p_{\Phi|X}(\varphi|x)$ is the conditional probability of observing a theta-based variable φ given a position x. It can be shown that the variance of any unbiased estimator is bounded from below by the Cramér–Rao inequality

$$\sigma_x^2 \geq \frac{1}{I_F(x)}.$$

Though an ideal observer can, in many instances, construct an estimator that reaches the lower bound, it should be stressed that not all estimators are ideal (20), and that we measure the theoretical resolution limit. Both information measures require knowledge of the underlying probability distributions. Because the data are finitely sampled, the distributions can only be approximated. For this purpose, we use the kernel density estimation method described by Botev et al. (32). The number of measured spikes was sufficient to estimate the probability density in 166 grid fields.

Unless stated otherwise, the SEM is used as the measure of uncertainty. To test for significance, we generally used two-sample two-tailed t tests, testing for equal means of the two data samples. Because correlation coefficients turned out to stem from strongly skewed distributions, median values are given together with their 95% confidence intervals. The Wilcoxon rank-sum test was used to test whether the medians of two sets of sampled correlation data were the same. To test whether two data samples stem from the same underlying distribution, the Kolmogorov–Smirnov test was applied. Its 2D extension due to Fasano and Franceschini (33) tested for potential field-to-field dependencies by comparing the measured joint probability distribution with the product distribution obtained from the respective marginals. Here, mean P values were obtained from 100 data shuffles. In general, the P value indicates the likelihood of observing a result that is as least as extreme as the one that was actually observed, assuming that the null hypothesis (equal means, equal medians, or same distribution, respectively) is true. $P < 0.05$ was considered significant.

ACKNOWLEDGMENTS. We thank E. I. Moser and coworkers for their hospitality to E.T.R, and for making data recorded by T. Hafting and coworkers publicly available; science benefits greatly when such altruistic data-sharing occurs. We also thank C. Kluger, A. Mathis, R. Schmidt, and K. Thurley for stimulating discussions. This work was supported by Deutsche Forschungsgemeinschaft Grants SFB 618 and GRK 1123, and German Federal Ministry for Education and Research Grants 01GQ0440, 01GQ0901, 01GQ0972, and 01GQ1001A.

1. Fyhn M, Molden S, Witter MP, Moser EI, Moser MB (2004) Spatial representation in the entorhinal cortex. *Science* 305:1258–1264.
2. Hafting T, Fyhn M, Molden S, Moser MB, Moser EI (2005) Microstructure of a spatial map in the entorhinal cortex. *Nature* 436:801–806.
3. Barry C, Hayman R, Burgess N, Jeffery KJ (2007) Experience-dependent rescaling of entorhinal grids. *Nat Neurosci* 10:682–684.
4. Moser EI, Kropff E, Moser MB (2008) Place cells, grid cells, and the brain's spatial representation system. *Annu Rev Neurosci* 31:69–89.
5. Boccara CN, et al. (2010) Grid cells in pre- and parasubiculum. *Nat Neurosci* 13: 987–994.
6. Brandon MP, et al. (2011) Reduction of theta rhythm dissociates grid cell spatial periodicity from directional tuning. *Science* 332:595–599.
7. Koenig J, Linder AN, Leutgeb JK, Leutgeb S (2011) The spatial periodicity of grid cells is not sustained during reduced theta oscillations. *Science* 332:592–595.
8. Hafting T, Fyhn M, Bonnevie T, Moser MB, Moser EI (2008) Hippocampus-independent phase precession in entorhinal grid cells. *Nature* 453:1248–1252.
9. O'Keefe J, Recce ML (1993) Phase relationship between hippocampal place units and the EEG theta rhythm. *Hippocampus* 3:317–330.
10. Skaggs WE, McNaughton BL, Wilson MA, Barnes CA (1996) Theta phase precession in hippocampal neuronal populations and the compression of temporal sequences. *Hippocampus* 6:149–172.
11. Harris KD, et al. (2002) Spike train dynamics predicts theta-related phase precession in hippocampal pyramidal cells. *Nature* 417:738–741.
12. Huxter J, Burgess N, O'Keefe J (2003) Independent rate and temporal coding in hippocampal pyramidal cells. *Nature* 425:828–832.
13. Schmidt R, et al. (2009) Single-trial phase precession in the hippocampus. *J Neurosci* 29:13232–13241.
14. Jammalamadaka SR, SenGupta A (2001) *Topics in Circular Statistics* (World Scientific, Singapore).
15. Kempter R, Leibold C, Buzsáki G, Diba, K, Schmidt R (2012) Quantifying circular-linear associations: Hippocampal phase precession. *J Neurosci Meth*, in press.
16. Burgess N, Barry C, O'Keefe J (2007) An oscillatory interference model of grid cell firing. *Hippocampus* 17:801–812.
17. Mizuseki K, Sirota A, Pastalkova E, Buzsáki G (2009) Theta oscillations provide temporal windows for local circuit computation in the entorhinal-hippocampal loop. *Neuron* 64:267–280.
18. Kamondi A, Acsády L, Wang XJ, Buzsáki G (1998) Theta oscillations in somata and dendrites of hippocampal pyramidal cells in vivo: Activity-dependent phase-precession of action potentials. *Hippocampus* 8:244–261.
19. Jensen O, Lisman JE (2000) Position reconstruction from an ensemble of hippocampal place cells: Contribution of theta phase coding. *J Neurophysiol* 83:2602–2609.
20. Zhang K, Ginzburg I, McNaughton BL, Sejnowski TJ (1998) Interpreting neuronal population activity by reconstruction: Unified framework with application to hippocampal place cells. *J Neurophysiol* 79:1017–1044.
21. Erchova I, Kreck G, Heinemann U, Herz AVM (2004) Dynamics of rat entorhinal cortex layer II and III cells: characteristics of membrane potential resonance at rest predict oscillation properties near threshold. *J Physiol* 560:89–110.
22. Chrobak JJ, Buzsáki G (1998) Gamma oscillations in the entorhinal cortex of the freely behaving rat. *J Neurosci* 18:388–398.
23. Lisman J (2005) The theta/gamma discrete phase code occurring during the hippocampal phase precession may be a more general brain coding scheme. *Hippocampus* 15:913–922.
24. Whittingstall K, Logothetis NK (2009) Frequency-band coupling in surface EEG reflects spiking activity in monkey visual cortex. *Neuron* 64:281–289.
25. Montemurro MA, Rasch MJ, Murayama Y, Logothetis NK, Panzeri S (2008) Phase-of-firing coding of natural visual stimuli in primary visual cortex. *Curr Biol* 18:375–380.
26. Kayser C, Montemurro MA, Logothetis NK, Panzeri S (2009) Spike-phase coding boosts and stabilizes information carried by spatial and temporal spike patterns. *Neuron* 61:597–608.
27. Deshmukh SS, Yoganarasimha D, Voicu H, Knierim JJ (2010) Theta modulation in the medial and the lateral entorhinal cortices. *J Neurophysiol* 104:994–1006.
28. Quilichini P, Sirota A, Buzsáki G (2010) Intrinsic circuit organization and theta-gamma oscillation dynamics in the entorhinal cortex of the rat. *J Neurosci* 30:11128–11142.
29. Foster DJ, Wilson MA (2007) Hippocampal theta sequences. *Hippocampus* 17: 1093–1099.
30. Mehta MR, Lee AK, Wilson MA (2002) Role of experience and oscillations in transforming a rate code into a temporal code. *Nature* 417:741–746.
31. Huxter JR, Senior TJ, Allen K, Csicsvari J (2008) Theta phase-specific codes for two-dimensional position, trajectory and heading in the hippocampus. *Nat Neurosci* 11: 587–594.
32. Botev ZI, Grotowski JF, Kroese DP (2010) Kernel density estimation via diffusion. *Ann Stat* 38:2916–2957.
33. Fasano G, Franceschini A (1987) A multidimensional version of the Kolmogorov–Smirnov test. *Mon Not R Astron Soc* 225:155–170.

Supporting Information

Reifenstein et al. 10.1073/pnas.1109599109

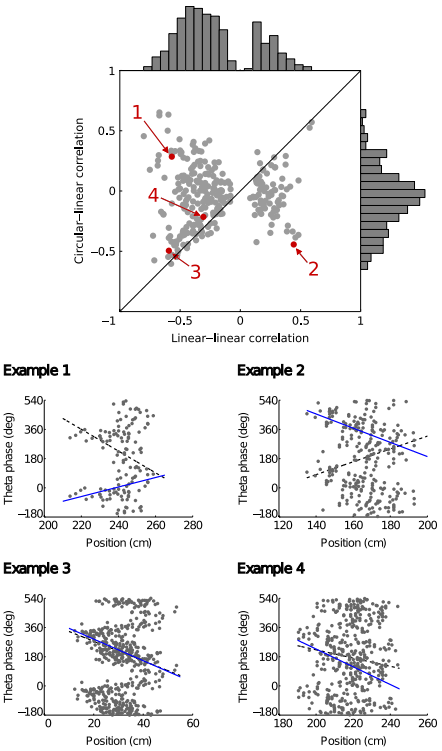

Fig. S1. Comparison of phase–position correlation measures for pooled runs from 67 units with a total of 291 grid fields (1). (*Upper*) The linear–linear correlation yields a bimodal distribution, whereas the circular–linear correlation (*Materials and Methods*) results in a unimodal distribution. Note that the linear–linear correlation is never zero. Selected examples are highlighted in red and numbered—the phase–position diagrams for these cases are displayed below (*Lower*). Clusters of phases can bias both the circular–linear and the linear–linear fit, so that the estimated slope in the phase–position diagram becomes positive (examples 1 and 2). However, even when both fits yield a negative correlation (in the absence of bimodality), the linear–linear fit typically underestimates the slope of phase precession (examples 3 and 4). Aberrant linear–linear correlation fits were also noted by Hafting et al. (in supplementary figure 10*A* of ref. 1).

1. Hafting T, Fyhn M, Bonnevie T, Moser MB, Moser EI (2008) Hippocampus-independent phase precession in entorhinal grid cells. *Nature* 453:1248–1252.

3 Movement-dependence and Layer Specificity of Entorhinal Phase Precession in Two-Dimensional Environments

Published in *PLoS One* on June, 24 2014.

OPEN ACCESS Freely available online

PLOS ONE

Movement Dependence and Layer Specificity of Entorhinal Phase Precession in Two-Dimensional Environments

Eric Reifenstein[1]*, Martin Stemmler[2], Andreas V. M. Herz[2], Richard Kempter[1], Susanne Schreiber[1]

1 Institute for Theoretical Biology, Department of Biology, Humboldt-Universität zu Berlin, Berlin, Germany and Bernstein Center for Computational Neuroscience Berlin, Berlin, Germany, **2** Department Biology II, Ludwig-Maximilians-Universität München, Planegg-Martinsried, Germany; and Bernstein Center for Computational Neuroscience Munich, Munich, Germany

Abstract

As a rat moves, grid cells in its entorhinal cortex (EC) discharge at multiple locations of the external world, and the firing fields of each grid cell span a hexagonal lattice. For movements on linear tracks, spikes tend to occur at successively earlier phases of the theta-band filtered local field potential during the traversal of a firing field – a phenomenon termed phase precession. The complex movement patterns observed in two-dimensional (2D) open-field environments may fundamentally alter phase precession. To study this question at the behaviorally relevant single-run level, we analyzed EC spike patterns as a function of the distance traveled by the rat along each trajectory. This analysis revealed that cells across all EC layers fire spikes that phase-precess; indeed, the rate and extent of phase precession were the same, only the correlation between spike phase and path length was weaker in EC layer III. Both slope and correlation of phase precession were surprisingly similar on linear tracks and in 2D open-field environments despite strong differences in the movement statistics, including running speed. While the phase-precession slope did not correlate with the average running speed, it did depend on specific properties of the animal's path. The longer a curving path through a grid-field in a 2D environment, the shallower was the rate of phase precession, while runs that grazed a grid field tangentially led to a steeper phase-precession slope than runs through the field center. Oscillatory interference models for grid cells do not reproduce the observed phenomena.

Citation: Reifenstein E, Stemmler M, Herz AVM, Kempter R, Schreiber S (2014) Movement Dependence and Layer Specificity of Entorhinal Phase Precession in Two-Dimensional Environments. PLoS ONE 9(6): e100638. doi:10.1371/journal.pone.0100638

Editor: Maurice J. Chacron, McGill University, Canada

Received February 6, 2014; **Accepted** May 29, 2014; **Published** June 24, 2014

Funding: This work was supported by the Deutsche Forschungsgemeinschaft Grants SFB 618 TP B3 and GRK 1123, and the German Federal Ministry for Education and Research Grants 01GQ0440, 01GQ0901, 01GQ0972, and 01GQ1001A. The funders had no role in study design, data collection and analysis, decision to publish, or preparation of the manuscript.

Competing Interests: The authors have declared that no competing interests exist.

* Email: eric.reifenstein@bccn-berlin.de

Introduction

Large-scale oscillations can organize the spikes of individual neurons [1]. In some cases, neural discharges are precisely orchestrated such that spike phases relative to an ongoing oscillation of the local field potential (LFP) convey information about a visual scene, the identity of a memory item, or the location of an animal [2–4]. The entorhinal-hippocampal complex in rodents, for instance, exhibits prominent LFP oscillations in the theta band (6–11 Hz) when the animal explores its environment. For certain neurons within this complex, the theta-band spike phase decreases with distance traveled through the neuron's firing field, a phenomenon known as phase precession [5].

Many neurons in the entorhinal-hippocampal complex are spatially tuned. Grid cells in the medial entorhinal cortex (mEC) form some of the most elaborate spatial firing rate maps known – multiple receptive fields arranged in a hexagonal grid [6]. Hippocampal place cells, in contrast, often have only a single firing field in a given environment, although firing fields do repeat under certain conditions [7–10].

On linear tracks, grid cells show phase precession [11], just as place cells do. In two-dimensional environments, the spikes of place cells as well as grid cells precess in pooled-run data [12–14], but it is unknown whether the same is true for individual field traversals. Single-run phase precession has been shown for linear-track data from hippocampal place cells [15]. For entorhinal grid cells, the spacing and size of firing fields differs between one- and two-dimensional environments [11,16]. Moreover, a rat's behavior changes within these two environments: on a linear track, the animal runs in a stereotyped, goal-directed manner, while foraging in a two-dimensional environment, the animal's trajectories and its running speed are highly variable. Paths can curve, go through the center of the grid field, or swerve and miss it completely; the time spent in the grid field varies as the rat slows down or speeds up.

These factors might severely change or even obscure the signatures of grid-cell phase precession. Therefore, we examined phase-precession on a run-by-run basis in two-dimensional environments – a strategy previously applied to linear-track data [15,17,18]. We first evaluated phase-precession properties in dependence upon the properties of the two-dimensional path. Because cells in different mEC layers differ in their preferred spike phases [17], we also investigated the layer specificity of phase precession at the single-run level.

The results of our data analysis provide additional constraints for computational models. One class of model relies on a baseline theta oscillation and additional oscillators whose frequencies increase linearly with speed along certain preferred directions [19,20]. As the carrier frequency of the resulting beat pattern is higher than the baseline frequency, spikes will precess relative to this baseline. Other models explain grid fields through attractor dynamics [21–23]. Yet attractor networks do not intrinsically explain phase precession, but require additional mechanisms, such as after-spike dynamics [24] or oscillatory interference [22]. An intracellular ramp depolarization poses another common explanation for phase precession [25]. However, it does not explain phase precession at the edges of a firing field. Therefore, we focus on different versions of the oscillatory interference model and ask whether they can reproduce single-run phase precession as in the experimental data.

Materials and Methods

We reanalyzed – both published and previously unpublished – data that were recorded by Hafting et al. [11] and Sargolini et al. [26]. In these experiments, extracellular recordings were performed in the medial entorhinal cortex (mEC) of 7 rats that explored a 1 m^2 square box [26] or ran on a linear track [11]. Data include sorted single-unit activity, the local field potential (LFP) sampled at 250 Hz and recorded from the same electrode as the spiking activity (low-pass filtered at 500 Hz, single pole), and the position of the rat, which was tracked by a diode fixed to the animal's head. The data recorded by Hafting et al. [11] and Sargolini et al. [26] are available at http://www.ntnu.no/cbm/moser/gridcell.

For our analysis, spikes were partitioned into firing fields, and each spike was assigned spatial coordinates, convolving these coordinates with a Gaussian kernel of width 5 cm and dividing by the time spent at each location resulted in a firing-rate map. The borders of a candidate firing field were obtained by initially thresholding the firing-rate map at 20% of the overall peak rate (bin size: 1 cm×1 cm). Those borders were then further extended to 20% of the individual firing field's peak rate. Fields with an area of less than 200 cm^2 or a circumference of more than 160 cm were excluded from the analysis (74 out of 388); the remaining grid fields were almost circular. We also tested different values for the initial firing-rate threshold (see Fig. S1 in File S1), which led to either smaller fields (threshold of 25%) or even merged fields (low threshold values like 5% or 10%). We were able to replicate all of our findings for a threshold value of 15%.

For each cell the gridness score [27] was calculated. Cells with a gridness score of less than 0 were excluded from the analysis. Eighty-seven units with a total of 314 grid fields were analyzed. As the borders of the environment limit an animal's movements, we separately analyzed the dependence of phase precession on the properties of the rat's path by considering the 115 grid fields that had no overlap with the boundaries of the box; we confirmed that the results presented for all 314 grid fields were not affected by the overlap of fields with the boundaries. The average area of the 115 central fields was 509 cm^2, corresponding to an average field diameter of 24.9 cm if one assumes a circular field shape.

All told, there were 7139 single-firing-field crossings, or "runs"; on 4396 of these, the cell fired spikes. For each run, four properties were assessed: (1) path length, measured along the animal's trajectory from entry to exit of the firing field; (2) path tortuosity, the ratio of the actual path length to the length of the straight line connecting entry to exit; (3) path eccentricity, measured as the shortest distance between the path and the location of the maximum firing rate within the field (the "firing-field peak"), and (4) average speed within the firing field. The statistics of these run properties are shown in Figure 1. Note that many runs were short, straight, and tangential. These runs usually showed only little spiking activity. Runs with a tortuosity of <1.4 were considered "straight runs". We also checked that our main results still hold if only runs were taken that lasted at least 3 theta cycles and on which the rat did not move slower than 1 cm/s at any time during field traversal (see Figures S3, S4 and S5 in File S1).

The LFP signal was band-pass filtered in the theta frequency range (6–11 Hz). Every spike was assigned an instantaneous theta phase, using the Hilbert transform of the filtered signal. This procedure sets phase 0° to the ascending slope of the oscillation; the peak hence is associated with a phase of 90°. In contrast, Hafting et al. [11] defined the peak of the oscillation as phase 0°. Phase precession was quantified by two measures [15,18,28]: first, the slope m from circular-linear regression, which results from fitting the model $\theta = m(x-x_0)$ to the data (where θ is the phase, x is the spatial variable and x_0 the spatial offset) by maximizing

$$R=\sqrt{\left(\frac{1}{n}\sum_{k=1}^{n} cos(\theta_k - m\,x_k)\right)^2+\left(\frac{1}{n}\sum_{k=1}^{n} sin(\theta_k - m\,x_k)\right)^2}$$

and, second, the circular-linear correlation coefficient

$$r=\frac{\sum_{k=1}^{n} sin(\theta_k-\overline{\theta})sin\left(\phi_k-\overline{\phi}\right)}{\sqrt{\sum_{k=1}^{n} sin^2(\theta_k-\overline{\theta})\ \sum_{h=1}^{n} sin^2\left(\phi_h-\overline{\phi}\right)}}$$

where θ_k denotes the theta phase of the k-th spike (n spikes in total), and $\phi_k = m{\cdot}x_k \mod 2\pi$ is a circular variable that is derived from the animal's position x_k. The phases $\overline{\phi}=arg\left(\frac{1}{n}\sum_{k=1}^{n} exp(i\phi_k)\right)$ and $\overline{\theta}=arg\left(\frac{1}{n}\sum_{k=1}^{n} exp(i\theta_k)\right)$ are the circular sample mean values. The significance value p (null hypothesis: $r=0$) can be calculated as $p=1-\mathrm{erf}(|z|/\sqrt{2})$, where $\mathrm{erf}(\cdot)$ depicts the error function and $z=r\sqrt{n\ \lambda_{20}\ \lambda_{02}/\lambda_{22}}$ with $\lambda_{ij}=n^{-1}\ \sum_{k=1}^{n} sin^i(\theta_k-\overline{\theta})sin^j\left(\phi_k-\overline{\phi}\right)$ [28,29].

Due to the circular nature of the phase variable, fitting the phase-precession slope m is often ambiguous for low spike numbers. The analysis was therefore performed on runs with more than four spikes (n = 2466). Results were similar if this criterion was changed to require more than 3, 5 or 6 spikes per run (Fig. S6 in File S1). To avoid overfitting the data by a helix that spirals around the phase-position cylinder many times, we restricted slopes to [−60,60] deg/cm. Restrictions to [−50,50] and [−80,80] deg/cm gave similar results (Fig. S7 in File S1).

To assess directional influences on phase precession, we measured the linear-circular correlation [30,31] between entry direction to the firing field and phase-precession slope on a field-by-field basis. Note that this measure is different from the circular-linear correlation used throughout the manuscript: for the analysis shown in Fig. 2D, the angular variable is the independent variable, whereas in the remaining manuscript the angular variable is the dependent variable. The linear-circular correlation takes values between 0 and 1 and allows for the calculation of a p-value. P-values below 0.05 were used to indicate a statistically significant correlation. To reliably measure the correlation and p-value, only

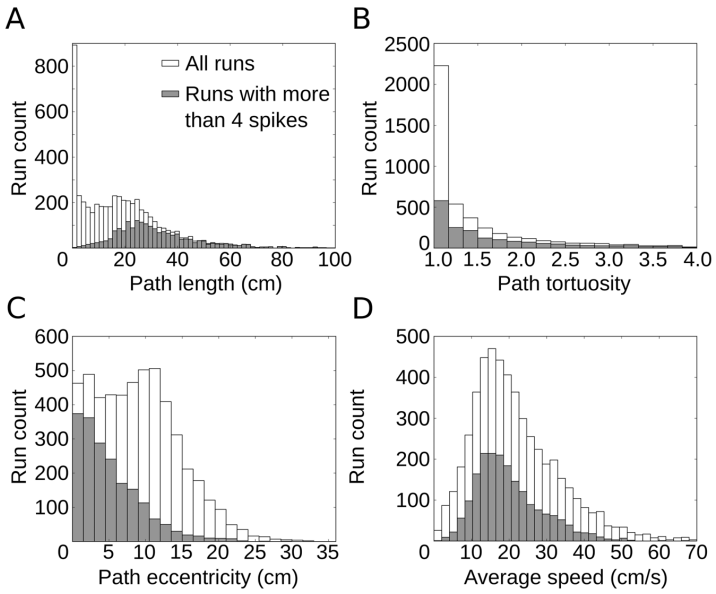

Figure 1. Statistical properties of runs through single grid fields. (A) Distribution of path length within grid fields for all runs and for all runs with more than four spikes. In many runs, the animal's paths graze the field. Most of these very short runs show only little spiking activity. (B) Distribution of path tortuosity, as measured by the ratio of the actual path length to the length of the straight line connecting field entry to field exit. Short runs from (A) are usually straight. (C) Distribution of path eccentricity, the shortest distance between the path and the location of the maximum firing rate within the field (the "firing-field peak"). Note that many runs with large eccentricities have only few spikes. (D) Distribution of average speed in single runs. The constraint on spiking activity only mildly affects this distribution.
doi:10.1371/journal.pone.0100638.g001

fields that contributed more than four runs were included in this analysis.

To test for significance of a difference between mean values of two data samples, we generally used two-sample two-tailed t-tests. As correlation coefficients turned out to stem from strongly skewed distributions, the Wilcoxon rank-sum test – assessing whether the medians of two sets of sampled data are the same – was used to analyze correlations. To compare the means of multiple groups, we used one-way ANOVA. Moreover, to disentangle the influences of path length, tortuosity, eccentricity, and speed on the phase-precession slope, a 4-way ANOVA without interaction terms was used. P-values were obtained by comparing the full model to a reduced model without the factor in question; e.g. for path length, the full model (4 parameters) was compared to a model that contained only tortuosity, eccentricity, and speed.

We used the Rayleigh test to test for circular uniformity. Additionally, we used the vector strength to quantify theta phase preference. The p-value indicates the likelihood of observing a result that is as least as extreme as the one that was actually observed, assuming that the null hypothesis ("equal means", "equal medians" or "data is uniform", respectively) is true. The null hypothesis was rejected when $p<0.05$.

Three variants of the oscillatory interference model were implemented [19,32]. In the first two models, a voltage-like variable $v=\Pi_{i=1}^{3}[cos(\theta_i)+cos(\omega_s t)]$ results from the threefold superposition of cosines, with $\frac{d\theta_i}{dt}=\omega_s+\beta\cdot s\cdot cos(\phi-\phi_i)$, where $\beta=2\pi\cdot 0.022\mathrm{cm}^{-1}$ and $\omega_s=2\pi\cdot f_s$ with $f_s=10\ Hz$. The parameters s andϕ are the speed and direction of the animal's movement. The preferred directions ϕ_i of the three oscillators were chosen to be 60° apart for the first version and 120° apart for the second version of the model.

In the third model of oscillatory interference, three pairs of oscillators were used, for a total of six. By imposing half-wave rectification, the frequency of each oscillator never falls below the theta frequency $\omega_s=2\pi\cdot f_s$ with $f_s=10\ Hz$. The equation for the voltage-like variable reads $v=\Pi_{i=1}^{3}[cos(\theta_{i,1})+cos(\theta_{i,2})]$ with $\frac{d\theta_{i,1}}{dt}=\omega_s+\Theta(\beta\cdot s\cdot cos(\phi-\phi_i))$ and $\frac{d\theta_{i,2}}{dt}=\omega_s+\Theta(\beta\cdot s\cdot cos(\phi-(\phi_i+\pi)))$. Here, $\Theta(x)=x \mathrm{if} x>0$, but is zero otherwise. The three preferred directions were 0°, 60°, and 120°.

In all versions of the model, spikes were produced by applying a threshold to the voltage variable. Spikes phases were assigned with respect to the baseline oscillation at an angular frequency ω_s. Thresholds were chosen to approximate grid-field sizes in the experimental data. In the first two models $v_{\mathrm{thresh}}=1.2$, while the third model had $v_{\mathrm{thresh}}=3.5$.

Results

To answer key open questions about phase precession in rat entorhinal cortex, we analyzed in-vivo data recorded in freely moving animals in 1D and 2D environments on the basis of individual runs. In contrast to estimates that consider data pooled across multiple runs or firing fields [5,11–14,17,33], the single-run approach enabled us to directly relate phase precession to the properties of the animal's paths through a cell's spatial firing field. Moreover, we addressed how phase precession depends on the anatomical layer of the spiking cell for pooled and single-run estimates of phase precession. Complementing this approach, we

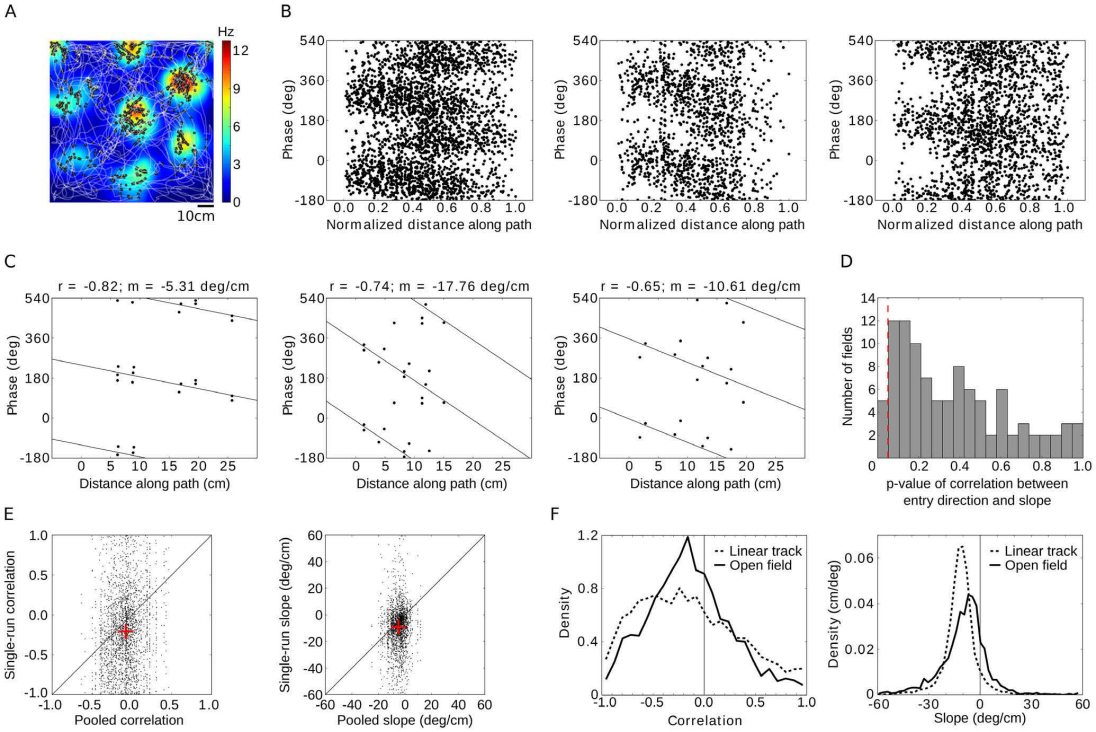

Figure 2. Grid cells exhibit phase precession in two-dimensional environments. (A) Trajectory (white line) of a rat over 10 minutes in a 1 m^2 square enclosure together with the firing pattern (black dots) and color-coded firing-rate map of a single grid cell. Data from Sargolini et al. [26]. Note that many different paths traverse each grid field. (B) Spike phase relative to the local field potential for all passages through three example grid fields. Runs with varying directions and originating from various points in the two-dimensional environment are pooled. The position along each path within the firing field is normalized by the path's total length. (C) Three examples of single runs with different phase-precession slopes *m* and circular-linear correlation values *r*. Circular-linear regression lines are indicated. (D) Running direction has no consistent influence on the phase-precession slope. Histogram of p-values of the correlation between entry direction of the animal into a firing field and single-run phase-precession slope. The analysis is restricted to straight runs. Red dashed line indicates significance level $p = 0.05$. (E) Comparison of single-run phase precession and phase precession assessed by pooling all runs through a particular grid field. Each dot represents a single run; the left panel shows the place-phase correlation, the right panel depicts the slope of phase versus location. A negative slope implies phase precession; note the large variability across different runs. Red crosses denote the average correlation and the average slope. The diagonal line marks the identity. (F) Single-run phase precession in one and two-dimensional environments. (*left*) Distribution of circular-linear correlation values for runs on a linear track (dashed lines) and in the square arena (full lines). (*right*) Distribution of phase-precession slopes for the same two conditions. Despite the large speed and movement differences between the linear track and the open field, the phase-precession statistics are similar.
doi:10.1371/journal.pone.0100638.g002

used the single-run analysis to test whether the observed features of phase precession were reproduced by models that explain both the formation of the spatial firing-rate map for grid cells and their phase precession as the result of multiple oscillations at different frequencies.

Phase precession prevails in single runs through 2D environments

Extracellularly isolated cells in the medial entorhinal cortex (mEC) and the corresponding local field potential (LFP) were recorded by Sargolini et al. [26] in rats that explored a square arena (1 m^2) while searching for food; the data were made available by E.I. Moser (Norwegian University of Science and Technology, Trondheim, Norway). Eighty-seven recorded cells showed spatial firing maps with hexagonal grid structure, resulting in a total of 314 clearly discernible firing fields (see also Materials and Methods). The paths taken through these grid fields varied widely (Fig. 2A). We tested how the phase of grid-cell firing changes along a rat's path within a firing field, as measured by the distance traveled. We found that grid cells fired at earlier phases as the animal moved along its path. Three typical examples of such phase-precession patterns, pooled over all traversals (or "runs") through a given firing field, are shown in Fig. 2B. For visualization of the pooled data, the traveled distance was normalized by the total path length in each run. Throughout the manuscript, all analyses were performed using the absolute traveled distance along the path (in cm). Phase precession also occurred at the level of single runs, as demonstrated by three sample runs from different cells and animals with clearly negative phase-precession slopes (Fig. 2C).

The running direction at field entry spanned 360°. Yet, running direction had no consistent influence on the phase-precession slope (Fig. 2D). We measured the linear-circular correlation coefficient between the running direction at field entry and the slope on a

field-by-field basis (see also Materials and Methods). The resulting distribution of p-values of the linear-circular correlation is shown for straight runs (tortuosity <1.4). Only 5 out of 100 fields showed a significant correlation between entry direction and slope, as expected by the statistical significance criterion of 5%. Similarly, when all runs (straight and curved) were included in the analysis, entry direction and slope were significantly correlated in only 4 out 190 fields (about 2%). For those analyses, fields were required to have more than 4 runs – straight runs or all runs, respectively.

Despite the propensity of grid-cell spikes to precess on single runs, the properties of phase precession varied greatly from run to run. The resulting correlation coefficients between phase and distance traveled along the path (Fig. 2E, left panel) and phase-precession slopes (Fig. 2E, right panel) were broadly distributed. Nevertheless, single-run phase precession turned out to be more tightly correlated and steeper than pooled phase precession (Fig. 2E, Wilcoxon rank-sum test $p<10^{-8}$ for the correlation, t-test $p<10^{-8}$ for the slope). At the single-run level, the median circular-linear correlation was $r=-0.17$ (95% confidence interval $[-0.19, -0.15]$) and the phase precessed by -8.4 ± 0.3 deg/cm on average. Figure 2F compares the phase precession in 1D and in 2D environments, again at the single-run level [11,18]. The correlations on the linear track were stronger, $r=-0.20$ (95% confidence interval $[-0.22, -0.19]$), and the slope of the relation between phase and position (-10.2 ± 0.1 deg/cm) was about 20% steeper than in the square enclosure. We also found that the firing rate influences the phase-precession correlation, but has no effect on the slope (see Fig. S8 in File S1 for details).

Dependence of phase precession on specific path features

Rather different paths can be taken through a grid field – long or short, curved or straight, fast or slow (see also Fig. 1). Therefore, we investigated whether phase precession depended on the properties of the path taken. We found that the longer the path, the shallower the slope of phase precession became (Fig. 3A, Pearson correlation $r=0.17$, $p<10^{-12}$; see also Fig. 3H). Fields with smaller diameters were generally associated with steeper phase-precession slopes (Pearson correlation $r=0.35$, $p<10^{-8}$), but even within a single field of fixed size, longer paths were associated with shallower slopes of phase precession. Overall, the majority of firing fields (across all cells) showed a positive correlation between phase-precession slope and path length (Fig. 3B), in agreement with Fig. 3A. Measuring the phase-precession slopes during the first and second half of long runs (>60 cm) revealed that the slope during the second half was significantly shallower than during the first half (Fig. 3C, $p<10^{-5}$, t-test). The total phase shift during phase precession, measured as precession slope times run distance, was substantial even for short runs with relatively few spikes ($\sim150^\circ$). For longer paths, the phase range first increased and then approached a value of about 210° (Fig. 3D; average range for runs longer than 50 cm: $211^\circ\pm9^\circ$). Thus phase precession started off more steeply and flattened out later in a run through a grid field.

The rat's path in a 2D environment need not be straight. In general, long runs resulted from winding trajectories through a firing field. To quantify the influence of curving paths on phase precession, we defined the tortuosity of a path as the distance along that path divided by the length of the straight line between field entry and exit of the path in question. We found that phase precession became shallower as a function of the path's tortuosity (Fig. 3E, $r=0.13$, $p<10^{-7}$), as it did for longer paths (Fig. 3A). Moreover, rats ran more slowly on meandering paths ($r=-0.39$, $p<10^{-10}$), so that slower speeds tended to result in slower rates of phase precession (Fig. 3F, $r=-0.10$, $p=10^{-5}$). When we restricted the analysis to straight runs (Materials and Methods), however, we found no significant correlation between speed and slope (Fig. 3F, $r=-0.05$, $p=0.14$).

In contrast to data from 1D environments, paths in 2D allowed us to directly address the question whether phase precession differs between runs that pass through the center of a field and those that only skirt the grid field tangentially. We defined the eccentricity of a path as the shortest Euclidean distance between the path and the center of the firing field. Slope and eccentricity correlated negatively for all runs (Fig. 3G, $r=-0.09$, $p<0.04$): the more a run "grazed" the firing field, the steeper the phase precession slope. The distance between field entry and exit was shorter on tangential runs (correlation between path length and eccentricity $r=-0.31$, $p<10^{-10}$), consistent with the analysis of pooled runs by Jeewajee et al. [13] and Climer et al. [14], and shorter runs generally showed a steeper slope of phase precession (Fig. 3A). Restricting the analysis to straight runs weakened the correlation between slope and eccentricity, path length, and speed (Fig. 3H).

Based on the correlation and p-values, path length and tortuosity seemed to be the most important factors. To investigate this question more closely, we performed an analysis of variance on the effect of path length, tortuosity, eccentricity, and speed on the slope, quantifying how much each of these four components contributes to explaining the slope value (see Methods). We found that path length ($p<10^{-5}$) and tortuosity ($p=0.02$) significantly improved the model's performance, whereas eccentricity ($p=0.05$) and speed ($p=0.31$) did not. In summary, phase precession depended on the properties of a path through the firing field, and path length and path tortuosity were the most important factors.

In hippocampal place cells recorded in rats running on a linear track, the correlation of spike phase with spatial location on a run-by-run basis is as strong as the correlation with time [15]. Whether the same is true for grid cells in 2D environments is not obvious, as time and Euclidean distance traveled do not correlate nearly as strongly when the rat has more freedom to move. Hence we next measured the correlation and slope of the spike phases with respect to time elapsed since field entry. We found the median correlation and the mean slope to be clearly negative (median time-phase correlation: -0.17, mean time-phase slope: -86.9 deg/s, see Fig. 4A, B). Interestingly, the median of time-phase correlations was statistically indistinguishable from the median of position-phase correlations in single runs (Fig. 4C, Wilcoxon rank-sum test $p=0.44$). Time-phase slope and position-phase slope were strongly correlated ($r=0.65$, $p<10^{-10}$, Fig. 4D). Indeed, much of the variability between the phase-time and phase-position slope could be explained by variations in speed. Within the scatter graph of time-phase slope (in deg/s) plotted against position-phase slope (in deg/cm, see Fig. 4D), any straight line through the origin corresponds to a constant speed, with units of (deg/s)/(deg/cm) = cm/s. The 5-percentile lines bound a cone in which 90% of the rat's speeds fell, covering 6.5 cm/s to 44.1 cm/s; 82.0% of the scatter plot's points were found within this region. At the 1-percentile level, for speeds ranging from 2.7 cm/s and 59.9 cm/s, 90.1% of the points fell within the corresponding cone. We also tested the path-dependence of phase precession with respect to the phase-time slope and confirmed the effects of path length, tortuosity and eccentricity (Fig. S9 in File S1). The speed of the animal was negatively correlated with the phase-time slope. This result is consistent with the lack of a speed-effect on the phase-position slope for straight runs.

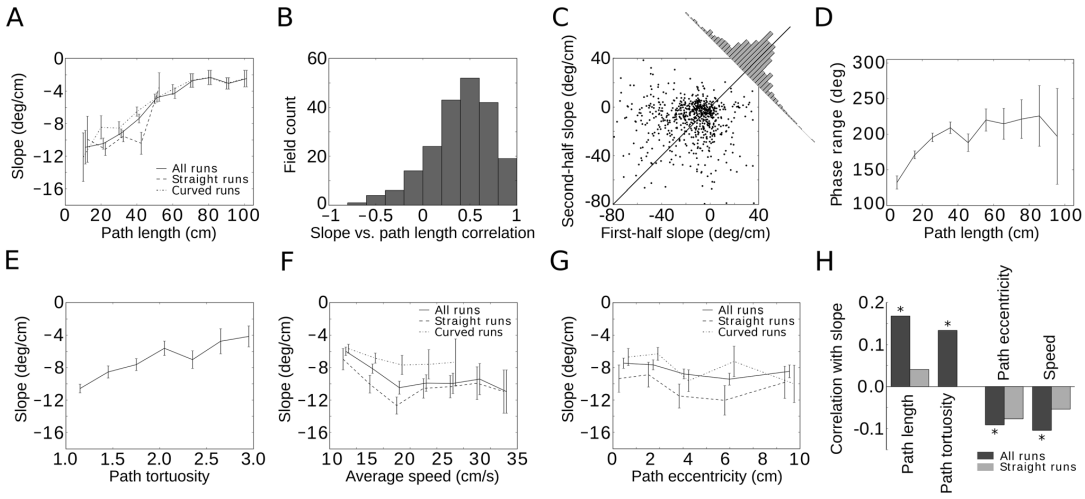

Figure 3. Salient features of the animal's path through a grid field affect phase precession. (A) The shorter the path is, the steeper the phase precession becomes. (B) The path length and phase precession correlate on a grid field by grid field basis, not just on average across grid fields. (C) First-half slopes are steeper than second-half slopes. The histogram in the inset shows the distance of data points from the diagonal, which is skewed towards smaller slopes in the second half of runs. (D) The phase range increases with path length and saturates at about 210°. (E) More meandering runs (increasing tortuosity) exhibit a less pronounced phase precession. As tortuosity correlates with the path length in a firing field, this finding is consistent with (A). (F) The animal's speed affects the phase-precession slope only weakly, and this effect primarily reflects a correlation between speed and tortuosity. For straight runs through the field, a statistically significant effect of speed on phase precession was not found. (G) Tangential paths lead to steeper phase precession than paths through the center of the field. The eccentricity measures the shortest distance between the path and the center of the firing field. For straight runs, the effect is not statistically significant. (H) Summary of the observed phenomena, with asterisks indicating statistical significance ($p<0.05$). For all investigated measures, restricting the analysis to straight runs weakens the effects. Error bars indicate one s.e.m. and are slightly offset for clarity in (A), (F), and (G).
doi:10.1371/journal.pone.0100638.g003

Layer specificity of EC phase precession

Earlier studies [11,17] suggested that phase precession is prominent in cortical layer II but weak in layer III. We reanalyzed this question by pooling across fields and runs. Although slopes of phase precession did not show significant differences across cortical layers (Fig. 5A, note the one exception), we confirmed that phase-precession correlations depend on the cell's layer in mEC (Fig. 5B). Spikes from layer II cells clearly precessed, while deep layers displayed a slightly weaker correlation between phase and the animal's position, and layer III showed hardly any correlation (Fig. 5B).

We then turned to the analysis of single runs and found that, on a run-by-run basis, phase-precession slopes did not show a statistical difference across different cortical layers (Fig. 5C, one-way ANOVA, $p = 0.35$). On the other hand, the correlation of phase precession was clearly smaller in layer III (t-test layer II versus layer III: $p<10^{-5}$, Fig. 5D, but note the differential effects for conjunctive cells and pure grid cells, Fig. S14 in File S1) – the phases were much more variable. Single-run phase precession in the deep layers of mEC was comparable to phase precession in layer II (t-test correlation in layer II versus layer V: $p = 0.12$, correlation II versus VI: $p = 0.006$ slope II versus V: $p = 0.92$, slope II versus VI: $p = 0.59$); no difference could be discerned between layers V and VI (t-test correlation in layer V versus VI: $p = 0.76$, slope V versus VI: $p = 0.65$). When we restricted the single-run analysis to traversals with a significant correlation between position and phase ($p<0.05$), we could confirm the findings described above: phase-precession slopes did not depend on cortical layer (one-way ANOVA, $p = 0.78$), whereas layer III showed a lower phase-precession correlation than layers II and VI (t-test of correlations in layer II versus layer III: $p = 0.003$, II vs. V: $p = 0.14$, II vs. VI: $p = 0.33$, III vs. V: $p = 0.35$, III vs. VI: $p = 0.02$, V vs. VI: $p = 0.40$).

Independently of the strength of phase precession, spikes may preferentially occur at a particular phase of the theta rhythm. The theta phase preference was not pronounced, though, and differed mildly from layer to layer, being strongest in layer V and weakest in layer II (Fig. 5E, vector strengths: layer II: 0.02, layer III: 0.02, layer V: 0.11, layer VI: 0.03; Rayleigh-test for circular uniformity: layer II: $p = 0.63$, layer III: $p = 4*10–6$, layer V: $p<10–10$; layer VI: $p<2*10–7$). Furthermore, phase precession implies that the first spike in a firing field should occur at a different phase than the "average" spike. Cells in layer II displayed a shift of about 220° between the first spike and the median spike (Fig. 5F), with the first spike occurring late in the theta cycle.

Comparison with oscillatory interference models

The observed properties of phase precession in 2D environments can serve to constrain computational models of phase precession in grid cells. As a last step of our analysis, we therefore asked whether the interference of oscillations at different frequencies [19,20,32] can explain the experimental data in two-dimensional arenas. We investigated different versions of oscillatory interference models for grid-cell formation (see Material and Methods) and compared the models to the in-vivo data (Fig. 6A). The original oscillatory interference model uses three speed- and head-direction-dependent oscillators and one reference oscillator that represents the theta rhythm. When the animal moves, the frequency of the oscillator aligned to the running direction increases relative to the reference frequency, which causes an

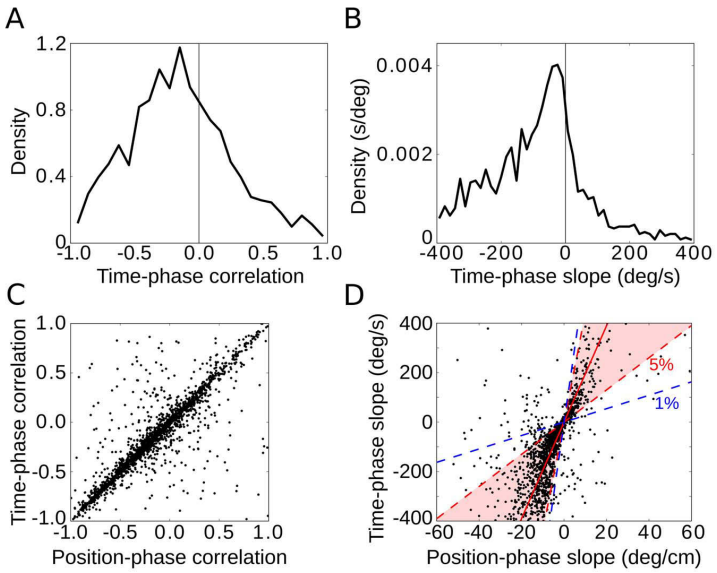

Figure 4. Phase precession in time. Negative values of time-phase correlation (A) and time-phase slope (B) of single runs indicate phase precession. (C) Time-phase correlation and position-phase correlation are statistically indistinguishable in single runs. (D) Time-phase slope and position-phase slope are highly correlated. The slope of the solid red line indicates the median of average speeds (19.5 cm/s) in single runs. Red and blue dashed lines mark 5-percentiles (6.5 cm/s and 44.1 cm/s, region shown in magenta) and 1-percentiles (2.7 cm/s and 59.9 cm/s) of the speed distribution, respectively. These data show that the variability between the phase-time and phase-position slope is mainly due to variations of the animals' running speed.
doi:10.1371/journal.pone.0100638.g004

interference pattern that oscillates at half of the frequency difference. A grid pattern can be formed by three speed-controlled oscillators with different preferred running directions. In a simple version of the model, the input oscillators have preferred directions that are 60° apart. This model leads to direction-dependent phase coding (also see [14]); Fig. 6B depicts an extreme case in which phase-recession (and not phase-precession) results along a particular direction. Such behavior was not observed in the in-vivo data. In fact, our data showed that phase precession occurs independently of heading direction of the rat in two dimensions.

A second version of the model uses three input oscillators whose preferred directions are separated by 120°. This model leads to phase coding that is independent of running direction. For this angular separation of oscillators, the sinusoidal modulation of frequency with heading direction implies that at least one oscillator's frequency falls below the reference frequency – for any direction of motion. The input oscillators' frequencies, therefore, fall both below and above the reference frequency, the phase changes non-monotonically with position (Fig. 6C). For this specific model, the phase first precesses and later recesses.

An extended version of the original model is based on six "dendritic" oscillators and a threshold nonlinearity so that the frequencies never fall below the overall theta frequency (Fig. 6D, [19]). This model leads to phase precession for runs in any direction. We simulated this model on the entire data set of measured runs in the 2D arena and analyzed how phase-precession slopes depend on properties of the run – just as we did for the in-vivo data. The model, by construction, makes the phase-precession slope independent of the animal's speed (Fig. 6E), which is in agreement with the experimental data for straight runs (Fig. 3F). However, the model also predicts that phase precession should be independent of path length, tortuosity, and eccentricity (Fig. 6F-H). In contrast, the in-vivo data revealed a significant dependence of phase precession on these variables (Fig. 3A, E, G). Furthermore, the model does not show a preferred phase at field entry ($p = 0.17$, Rayleigh test for circular uniformity), which implies that the phase offset is not constant from run to run. Although some grid fields clearly showed preferred entry phases in the in-vivo data (e.g. Fig. 2B), the overall preference was weak (Fig. 5F, Fig. S17 in File S1), such that this model prediction could not be tested with our data.

Discussion

Data from rats running on linear tracks provide evidence that the spike phases of mEC grid cells encode spatial distance [11,18]. This finding extends directly to two-dimensional environments, as was also recently shown by Climer et al. [14] and Jeewajee et al. [13] based on data pooled across multiple runs and firing fields. In addition, our run-by-run analysis revealed a number of unexpected results: spikes precessed at about twice the slope that one estimates from trial-averaged data; the slope of phase precession was the same across all layers of mEC, even for spikes of layer III cells, which were thought not to participate in phase precession [11]; and the sequence of spike phases depended on the properties of the rat's path through a firing field. Long or winding runs through a firing field led to weakest phase precession whereas runs that skirt the edge show steeper rates of phase precession. For this analysis, we measured phase against the total distance traveled within the field, as this distance is easily defined. Based on a more complex measure of the spatial variable and using pooled data, Climer et al. [14] and Jeewajee et al. [13] found that both the

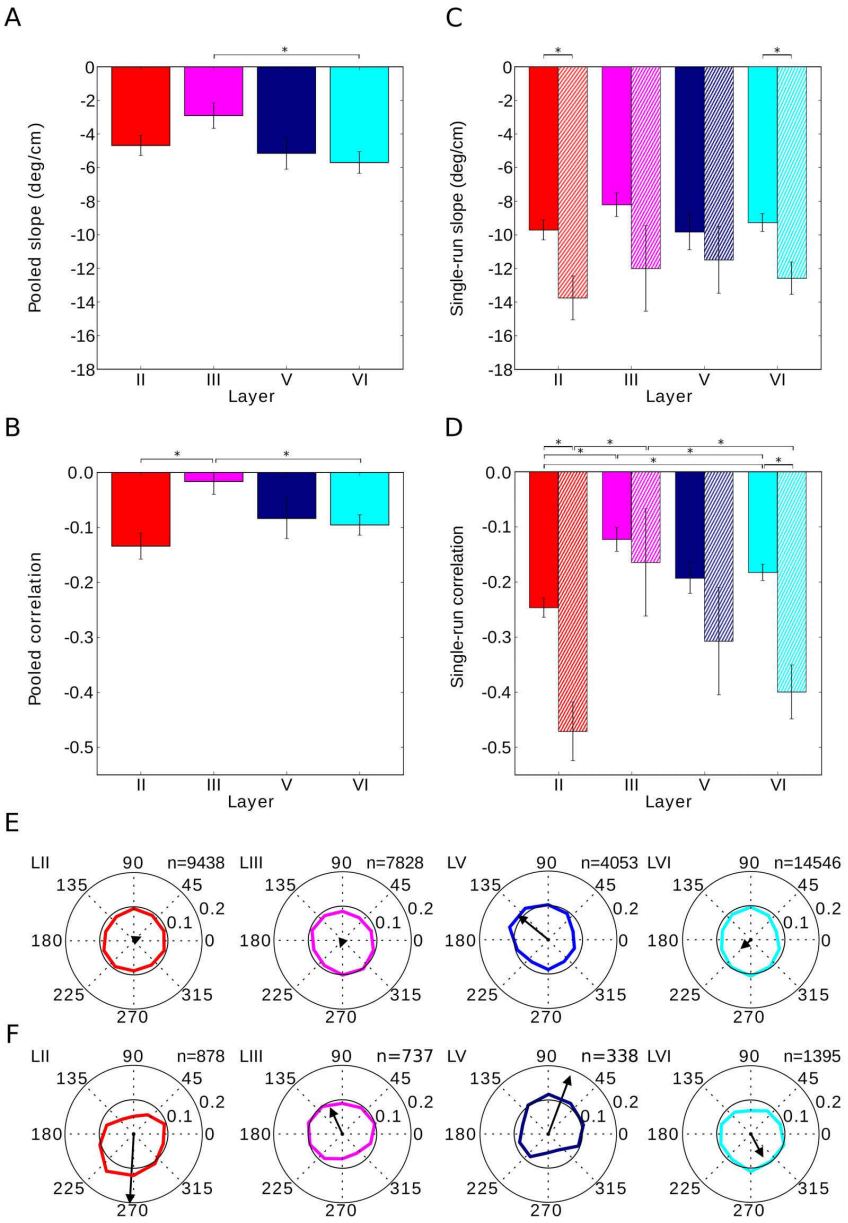

Figure 5. Phase precession in different cortical layers. Phase-precession slope generally does not depend on the cell's cortical layer (A and C). However, phase precession is decreased in layer III, as measured by the correlation (B and D). The single-run correlation of phase precession is lowest in layer III, and in layers II, V and VI the place-phase correlation is similar. Single-run effects are reproduced when the analysis is restricted to significantly correlated runs (cross-hatched bars). All bars show mean values, error bars depict one s.e.m. and asterisks indicate statistical significance ($p<0.05$). (E) Spikes show a preferred theta phase. The theta-phase preference is mild, and the weakest phase locking is encountered in layer III. (F) The first spike in a grid-field traversal generally occurs late in the theta cycle for layer II and VI, while it occurs rather early in layers III and V. In (E) and (F), the spike count histogram is normalized so that the sum of all ten bins equals 1. Colors label the cortical layer. Black arrows indicate the vector strength of the spike-phase theta modulation. All spikes were included in the analysis; no prior selection was made. The analysis is based on a total of 95 cells: 20 cells for layer II, 36 from layer III, 10 from layer V and 29 from layer VI.
doi:10.1371/journal.pone.0100638.g005

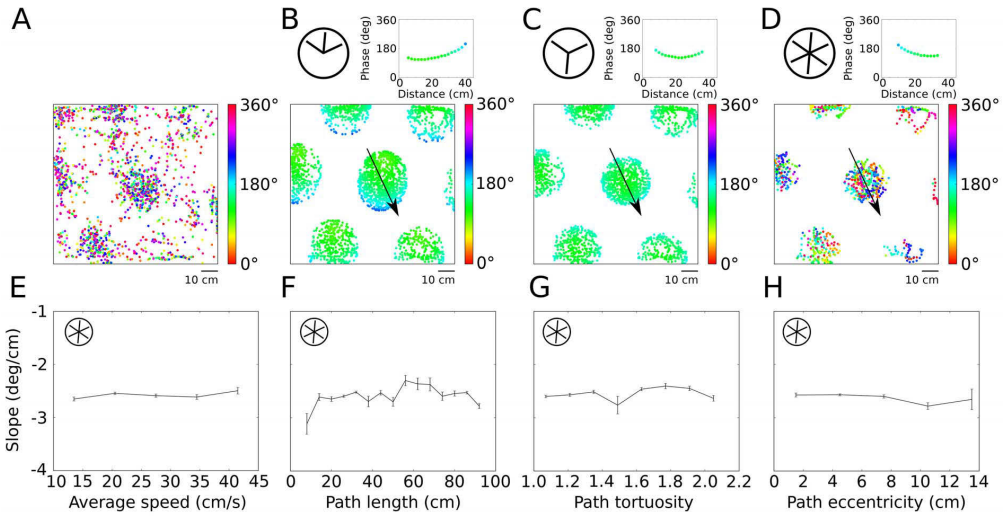

Figure 6. Testing predictions of oscillatory interference models. (A) Spikes (dots) of an example grid cell in a two-dimensional environment. Colors indicate the theta phase of spiking. (B) Oscillatory interference model with three "dendritic" oscillations; preferred directions are separated by 60°, as indicated in the inset at the top left, yields direction-dependent phase coding. The top right inset shows spike phases along a linear run through the central firing field as indicated by the arrow in the main panel. (C) Preferred directions separated by 120° lead to nonmonotonic phase coding so that spike phases first precess, then recess. Insets show phases for linear runs through the center, as in (B). (D) Model with six "dendritic" oscillators whose frequency modulation with speed is half-wave rectified such that the frequency never falls below theta frequency. This model leads to saturating phase precession for any run through a grid field, but the phase-precession slope is independent of path length (E), tortuosity (F), and eccentricity (G), which is in contrast to the data analysis in Figure 3. (H) The rate of phase precession does not depend on speed, which is consistent with the experimental data for straight runs.
doi:10.1371/journal.pone.0100638.g006

(normalized) slope and the correlation of phase precession were the same for runs closer to the edge versus those that passed through the center. These observations are in line with our results because a constant normalized slope implies steeper absolute slopes for the shorter tangential runs. Our run-by-run analysis revealed that the slopes are steeper at a field's periphery (Fig. 3G), despite the fact that both phase range and average path length for these runs were lower. Similar results were found by Huxter et al. [34] (cf. their Fig. S2); in their study on phase precession in CA1 place cells, they introduce a discontinuous measure of space to define phase precession in two-dimensional environments. These authors also noted that phase precession in CA1 depends on the path: for increasingly complicated trajectories, phase precession ceased.

Whereas the phase of hippocampal CA1 neurons for rats running on a linear track correlates more strongly with the distance traveled than with the time elapsed in pooled data [33], at the single-run level in two-dimensional environments, position and time correlated equally well with the phase variable in mEC (Fig. 4). The spike phases exhibit similar single-run position and time-correlations as reported for place cells in the hippocampus [15].

Mizuseki et al. [17] reported that only a minority of cells in mEC display pooled phase precession and that pooled phase precession is layer specific. However, on single runs, the phase *does* precess in many cells across all layers; in fact, the slopes of phase precession are statistically indistinguishable across layers (Fig. 5C). The correlation between phase and position in layer III, however, is weaker, but still more than five times larger than the pooled data suggest (Fig. 5B, 5D). As the phase of the theta rhythm at the time-point of field entry is generally random, one possible explanation is that superimposing data from different runs masked the weakly correlated phase precession in layer III. However, the data set's statistics are too limited to test this hypothesis.

Previous studies also report low rates of spike-phase precession in entorhinal cortex, with a slope of around -3 deg/cm in both Hafting et al. [11] and Mizuseki et al. [17]. This rate stands in stark contrast to the -10 deg/cm slope based on single runs drawn from the same data as in Hafting et al. [11] that we describe here (Fig. 2F). Part of the discrepancy can be explained by the difference between single runs and pooled data (Fig. 2E); while another part can be explained by the quantification of phase precession: Kempter et al. [28] showed that linear-linear regression tends to underestimate the slope and range of phase precession compared to circular-linear regression, as we have used. The slope of phase precession in mEC is in line with the phase-precession slope observed in hippocampus (−7.6 deg/cm on average) and medial prefrontal cortex (−9.4 deg/cm on average, both numbers from [35]). Jeewajee et al. [13] demonstrated pooled phase-precession in open environments in both hippocampal place cells and entorhinal grid cells, although the proportion of significantly phase-precessing cells was higher in hippocampus than in entorhinal cortex. In this study, the authors mapped individual runs to the unit circle, normalized running direction and pooled these normalized runs, which allows for a clear visualization of phase precession in open environments. However, using this procedure, it is rather complicated to investigate the impact of the animal's trajectory on phase precession as the properties of individual runs are lost by normalization and pooling.

Hafting et al. [11] found the average phase range – in pooled data – to be about 165°, which is in broad agreement with the

single-run phase ranges in our analysis (171° for runs <30 cm) and in hippocampus (180°) [15]. Phase precession, therefore, exhibits consistent characteristics throughout the entorhinal-hippocampal loop [12,34].

Which cells, therefore, drive phase precession? Even within the same layer of mEC, cellular biophysics and morphology vary [36–38]. Stellate cells in mEC are thought to support phase precession, as they display subthreshold resonance and membrane potential oscillations in the theta frequency range [39,40], which can also affect spike patterns [41–43]. On the other hand, pyramidal cells in layer III act as low-pass filters (at least at the soma). Interlaminar connections [44] could allow one layer to impose its phase precession onto another layer, or at least influence that layer. Likewise, the strong phase precession of principal cells in the hippocampal CA1 subregion may – at least in part – stem from single-run phase precession in mEC [45,46].

We found that the observed phenomena in mEC were not in agreement with oscillatory interference models [19,20,32], which explain both grid-cell formation and phase precession as the result of a common mechanism, namely the interference of oscillations at different frequencies. In such models, grid spacing and rate of phase precession are linked. Pure phase precession, as opposed to a mixture of phase precession and recession, required nonlinear rectification and the involvement of six oscillators, instead of three. While this oscillatory interference model is still consistent with omnidirectional and speed-independent phase precession, it did not reproduce the features of biological phase precession derived from the single-run analysis: the model displayed a constant rate of phase precession, regardless of the path taken. However, it seems that including a "somatic" baseline oscillation in the model would lead to steeper phase-precession slopes at the edges of a firing field [14]. Extensions of continuous-attractor networks that include mechanisms for spiking and oscillation [22,24] inherit phase precession from the oscillatory interference model and generate realistic grid spacings and rates of phase precession. However, the phase precession remains independent of the properties of the path, which is inconsistent with the experimental observations. Navratilova et al. [24] suggest that a conjunction of intrinsic and extrinsic mechanisms could generate different slopes of phase precession on field entry and field exit; but such a model cannot generate different rates of phase precession for tangential and central paths through a grid field. Therefore, it remains an open challenge to find a minimal model that accurately describes entorhinal phase precession in two-dimensional environments.

Supporting Information

File S1 Contains 18 additional figures.
(PDF)

Acknowledgments

We thank E. I. Moser and coworkers for their hospitality to E.T.R, and for making data recorded by T. Hafting, F. Sargolini and their coworkers publicly available.

Author Contributions

Conceived and designed the experiments: ER MS AH RK SS. Performed the experiments: ER. Analyzed the data: ER. Contributed reagents/materials/analysis tools: ER MS AH RK SS. Wrote the paper: ER MS AH RK SS.

References

1. Buzsáki G, Draguhn A (2004) Neuronal Oscillations in Cortical Networks. Science 304: 1926–1929.
2. Jensen O, Lisman JE (2000) Position Reconstruction From an Ensemble of Hippocampal Place Cells: Contribution of Theta Phase Coding. Journal of Neurophysiology 83: 2602–2609.
3. Kayser C, Montemurro MA, Logothetis NK, Panzeri S (2009) Spike-Phase Coding Boosts and Stabilizes Information Carried by Spatial and Temporal Spike Patterns. Neuron 61: 597–608.
4. Siegel M, Warden MR, Miller EK (2009) Phase-dependent neuronal coding of objects in short-term memory. Proceedings of the National Academy of Sciences 106: 21341–21346.
5. O'Keefe J, Recce ML (1993) Phase relationship between hippocampal place units and the EEG theta rhythm. Hippocampus 3: 317–330.
6. Fyhn M, Molden S, Witter MP, Moser EI, Moser M-B (2004) Spatial Representation in the Entorhinal Cortex. Science 305: 1258–1264.
7. Derdikman D, Whitlock JR, Tsao A, Fyhn M, Hafting T, et al. (2009) Fragmentation of grid cell maps in a multicompartment environment. Nature Neuroscience 12: 1325–1332.
8. Nitz DA (2011) Path shape impacts the extent of CA1 pattern recurrence both within and across environments. Journal of Neurophysiology 105: 1815–1824.
9. Singer AC, Karlsson MP, Nathe AR, Carr MF, Frank LM (2010) Experience-dependent development of coordinated hippocampal spatial activity representing the similarity of related locations. The Journal of Neuroscience 30: 11586–11604.
10. Hayman R, Verriotis MA, Jovalekic A, Fenton AA, Jeffery KJ (2011) Anisotropic encoding of three-dimensional space by place cells and grid cells. Nature neuroscience 14: 1182–1188.
11. Hafting T, Fyhn M, Bonnevie T, Moser M-B, Moser EI (2008) Hippocampus-independent phase precession in entorhinal grid cells. Nature 453: 1248–1252.
12. Skaggs WE, McNaughton BL, Wilson MA, Barnes CA (1996) Theta phase precession in hippocampal neuronal populations and the compression of temporal sequences. Hippocampus 6: 149–172.
13. Jeewajee A, Barry C, Douchamps V, Manson D, Lever C, et al. (2014) Theta phase precession of grid and place cell firing in open environments. Philosophical Transactions of the Royal Society B: Biological Sciences 369.
14. Climer JR, Newman EL, Hasselmo ME (2013) Phase coding by grid cells in unconstrained environments: two-dimensional phase precession. European Journal of Neuroscience 38: 2526–2541.
15. Schmidt R, Diba K, Leibold C, Schmitz D, Buzsáki G, et al. (2009) Single-Trial Phase Precession in the Hippocampus. Journal of Neuroscience 29: 13232–13241.
16. Hafting T, Fyhn M, Molden S, Moser M-B, Moser EI (2005) Microstructure of a spatial map in the entorhinal cortex. Nature 436: 801–806.
17. Mizuseki K, Sirota A, Pastalkova E, Buzsáki G (2009) Theta Oscillations Provide Temporal Windows for Local Circuit Computation in the Entorhinal-Hippocampal Loop. Neuron 67: 267–280.
18. Reifenstein ET, Kempter R, Schreiber S, Stemmler MB, Herz AVM (2012) Grid cells in rat entorhinal cortex encode physical space with independent firing fields and phase precession at the single-trial level. Proceedings of the National Academy of Sciences 109: 6301–6306.
19. Burgess N, Berry C, OKeefe J (2007) An Oscillatory Interference Model of Grid Cell Firing. Hippocampus 17: 801–812.
20. Zilli EA, Yoshida M, Tahvildari B, Giocomo LM, Hasselmo ME (2009) Evaluation of the Oscillatory Interference Model of Grid Cell Firing through Analysis and Measured Period Variance of Some Biological Oscillators. PLoS Computational Biology 5: e1000573.
21. Fuhs MC, Touretzky DS (2006) A Spin Glass Model of Path Integration in Rat Medial Entorhinal Cortex. The Journal of Neuroscience 26: 4266–4276.
22. Schmidt-Hieber C, Hausser M (2013) Cellular mechanisms of spatial navigation in the medial entorhinal cortex. Nature Neuroscience 16: 325–331.
23. Couey JJ, Witoelar A, Zhang S-J, Zheng K, Ye J, et al. (2013) Recurrent inhibitory circuitry as a mechanism for grid formation. Nature Neuroscience 16: 318–324.
24. Navratilova Z, Giocomo LM, Fellous J-M, Hasselmo ME, McNaughton BL (2012) Phase precession and variable spatial scaling in a periodic attractor map model of medial entorhinal grid cells with realistic after-spike dynamics. Hippocampus 22: 722–789.
25. Mehta M, Lee A, Wilson M (2002) Role of experience and oscillations in transforming a rate code into a temporal code. Nature 417: 741–746.
26. Sargolini F, Fyhn M, Hafting T, McNaughton BL, Witter MP, et al. (2006) Conjunctive Representation of Position, Direction, and Velocity in Entorhinal Cortex. Science 312: 758–762.
27. Langston RF, Ainge JA, Couey JJ, Canto CB, Bjerknes TL, et al. (2010) Development of the spatial representation system in the rat. Science 328: 1576–1580.
28. Kempter R, Leibold C, Buzsáki G, Diba K, Schmidt R (2012) Quantifying circular-linear associations: Hippocampal phase precession. Journal of Neuroscience Methods 207: 113–124.

29. Jammalamadaka SR, SenGupta A (2001) Topics in Circular Statistics. Singapore: World Scientific Publishing Co.
30. Zar JH (1999) Biostatiscal analysis. Biostatiscal analysis.
31. Berens P (2009) CircStat: a MATLAB toolbox for circular statistics. Journal of Statistical Software 31: 1–21.
32. Burgess N (2008) Grid cells and theta as oscillatory interference: Theory and predictions. Hippocampus 18: 1157–1174.
33. Huxter J, Burgess N, O'Keefe J (2003) Independent rate and temporal coding in hippocampal pyramidal cells. Nature 425: 828–832.
34. Huxter JR, Senior TJ, Allen K, Csicsvari J (2008) Theta phase-specific codes for two-dimensional position, trajectory and heading in the hippocampus. Nature Neuroscience 11: 587–594.
35. Jones MW, Wilson MA (2005) Theta rhythms coordinate hippocampal-prefrontal interactions in a spatial memory task. PLoS biology 3: e402.
36. Klink R, Alonso A (1997) Morphological characteristics of layer II projection neurons in the rat medial entorhinal cortex. Hippocampus 7: 571–583.
37. Varga C, Lee SY, Soltesz I (2010) Target-selective GABAergic control of entorhinal cortex output. Nature Neuroscience 13: 822–824.
38. Canto CB, Witter MP (2012) Cellular properties of principal neurons in the rat entorhinal cortex. II. The medial entorhinal cortex. Hippocampus 22: 1277–1299.
39. Erchova I, Kreck G, Heinemann U, Herz AVM (2004) Dynamics of rat entorhinal cortex layer II and III cells: characteristics of membrane potential resonance at rest predict oscillation properties near threshold. The Journal of Physiology 560: 89–110.
40. Alonso A, Llinás RR (1989) Subthreshold Na^+-dependent theta-like rhythmicity in stellate cells of entorhinal cortex layer II. Nature 342: 175–177.
41. Engel TA, Schimansky-Geier L, Herz AVM, Schreiber S, Erchova I (2008) Subthreshold Membrane-Potential Resonances Shape Spike-Train Patterns in the Entorhinal Cortex. J Neurophysiol 100: 1576–1589.
42. Schreiber S, Erchova I, Heinemann U, Herz AVM (2004) Subthreshold Resonance Explains the Frequency-Dependent Integration of Periodic as Well as Random Stimuli in the Entorhinal Cortex. Journal of Neurophysiology 92: 408–415.
43. Fernandez FR, Malerba P, Bressloff PC, White JA (2013) Entorhinal Stellate Cells Show Preferred Spike Phase-Locking to Theta Inputs That Is Enhanced by Correlations in Synaptic Activity. The Journal of Neuroscience 33: 6027–6040.
44. Beed P, Bendels MHK, Wiegand HF, Leibold C, Johenning FW, et al. (2010) Analysis of Excitatory Microcircuitry in the Medial Entorhinal Cortex Reveals Cell-Type-Specific Differences. Neuron 68: 1059–1066.
45. Chance FS (2012) Hippocampal Phase Precession from Dual Input Components. The Journal of Neuroscience 32: 16693–16703.
46. Jaramillo J SR, Kempter R (2014) J Neurosci: in press.

Supporting information
"Movement dependence and layer specificity of entorhinal phase precession in two-dimensional environments"
Eric Reifenstein, Martin Stemmler, Andreas Herz, Richard Kempter, Susanne Schreiber

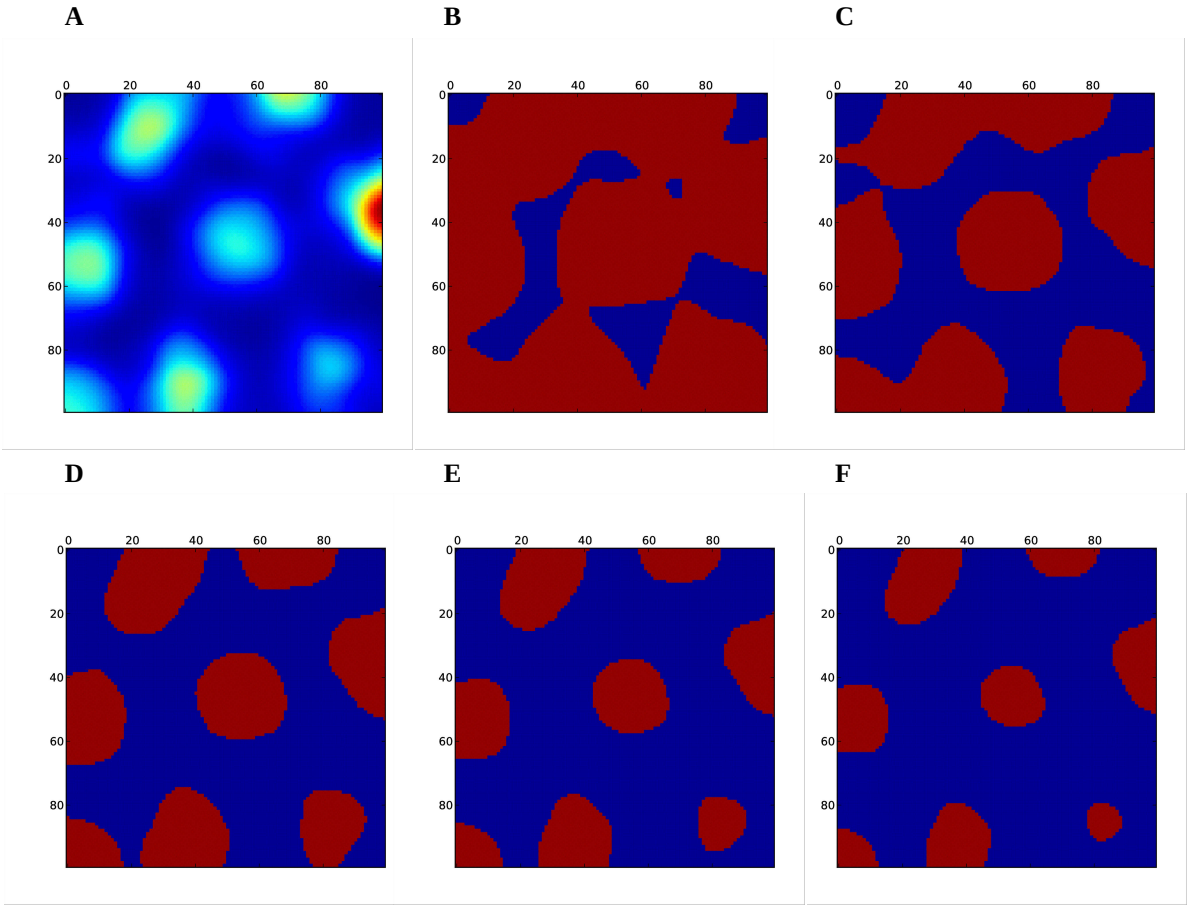

Figure S1: (A) Firing-rate map of a grid cell. (B)-(F) Different thresholds for the selection of firing fields (B: 5%, C: 10%, D: 15%, E: 20%, F: 25% of the peak firing rate). Too low thresholds led to merged fields, whereas too high values excluded weak fields from the analysis. We hence chose a threshold of 20% for all the analysis in the manuscript. The preliminary fields that were found by this criterion were then extended to 20% of the individual field's peak firing rate. For comparison we note that in hippocampal data, where firing rates are generally higher than in our data and often only a single firing field is present, frequent choices for threshold values are 5% or 10%.

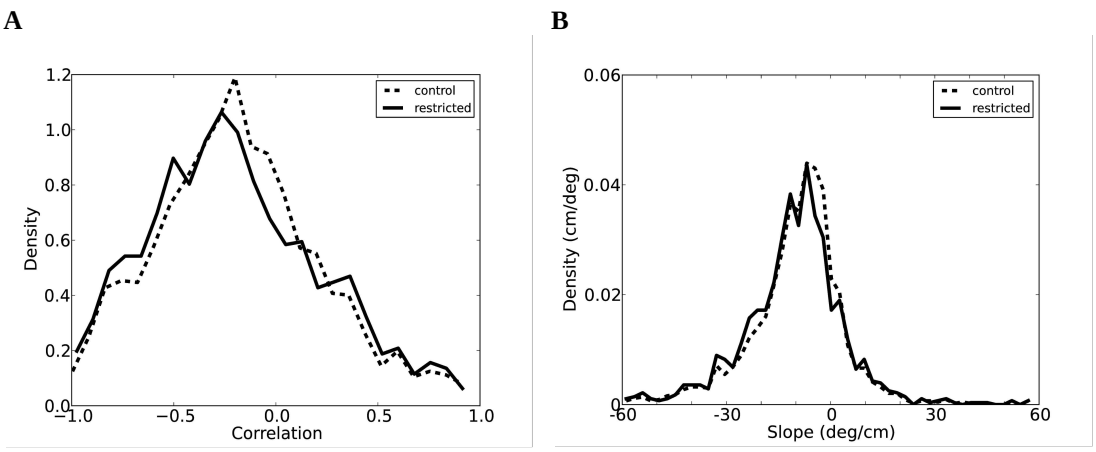

Figure S2: We tested two additional criteria for the selection of runs: a single run must not be shorter in duration than three theta cycles and the rat must not move slower than 1 cm/s during any time of the field traversal. The distribution of phase precession correlation (A) and slope (B) were affected only marginally; changes were not statistically significant (correlation: Wilcoxon test p=0.10, slope: t-test p=0.07).

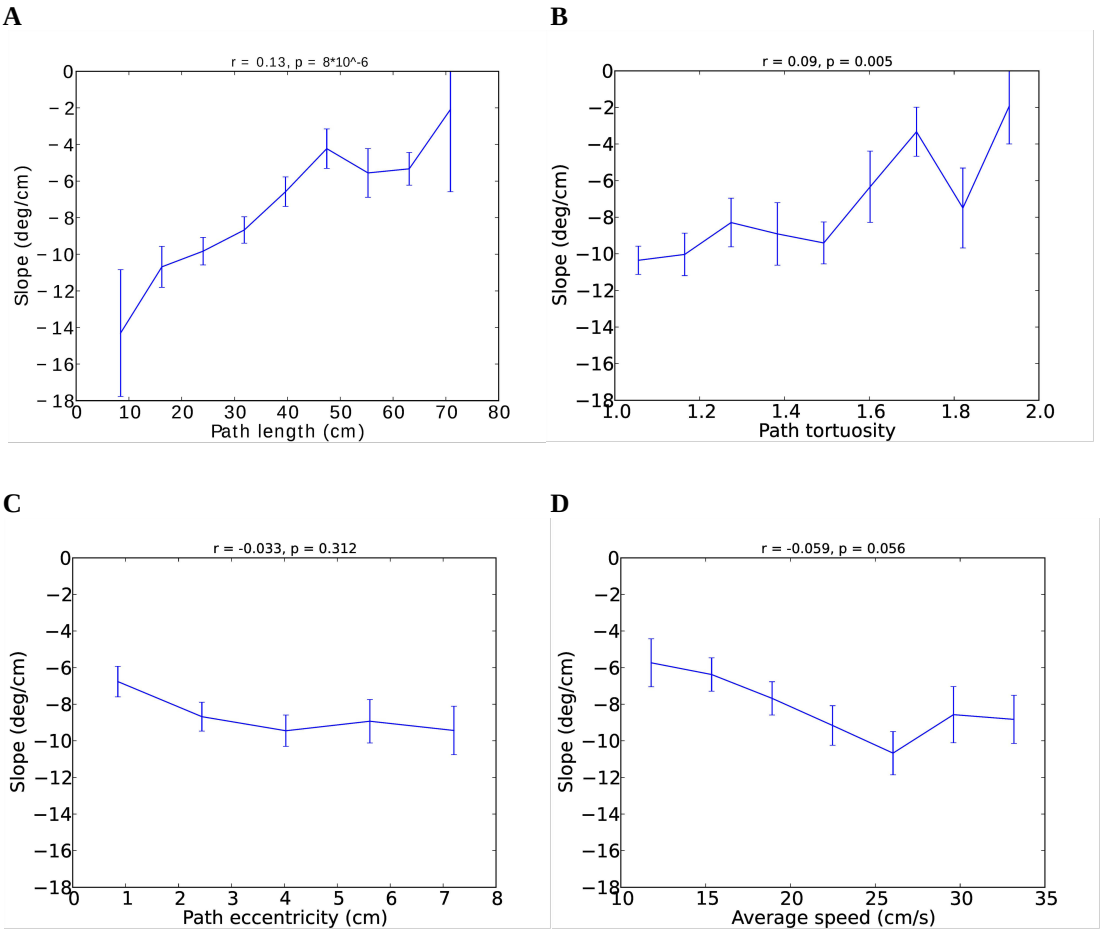

Figure S3: Using the same additional restrictions for selecting runs as in Fig. S2, i.e. runs must not be shorter than three theta cycles and speed is always larger than 1 cm/s, we could reproduce the effects of path length (A) and tortuosity (B). The restrictions reduced the number of runs included in the analysis (in particular those with lower speed), so that the dependence of phase precession slope on eccentricity (C) and running speed (D) did not meet the criterion for statistical significance anymore.

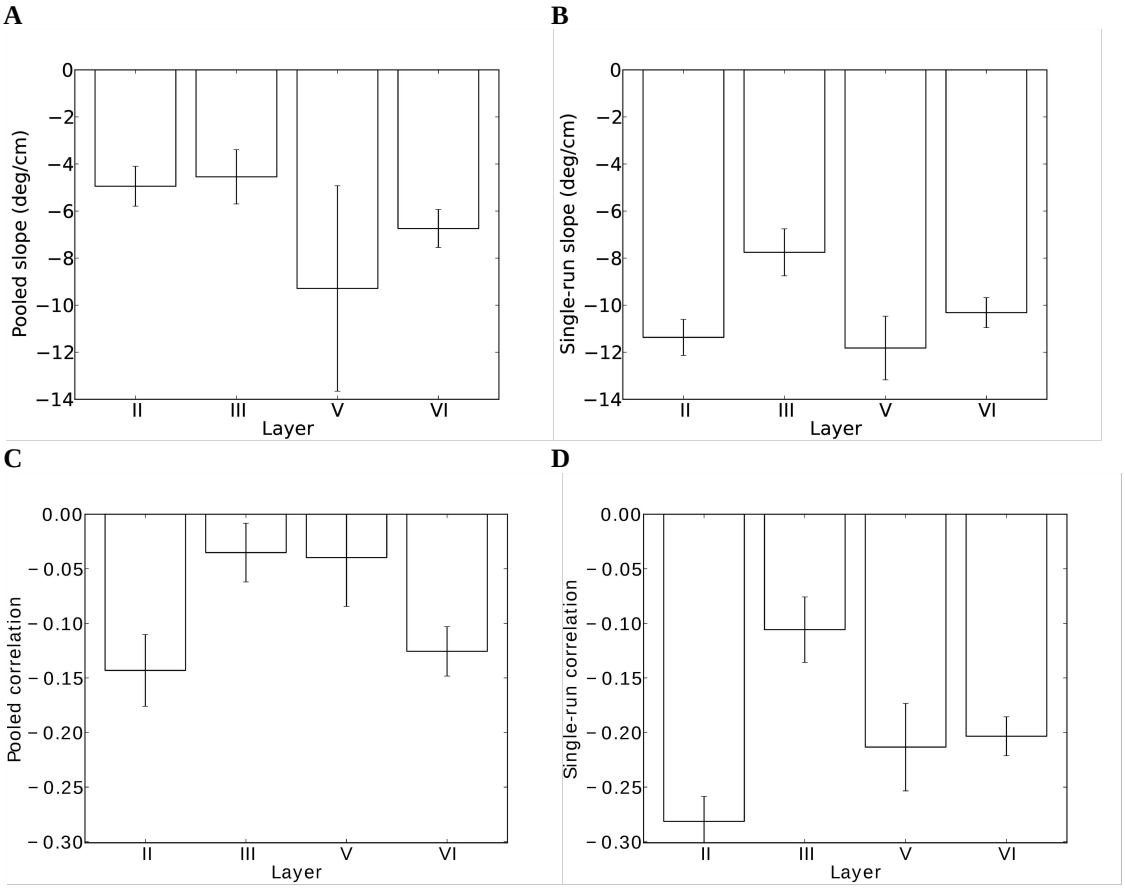

Figure S4: Layer specificity of phase precession for a stricter selection of runs. When the analysis is restricted to runs where the animal did not move slower than 1 cm/s, the results for pooled correlation (C) and single-run correlation (D) are well preserved. Interestingly, the difference in pooled slopes between layers II and III is reduced for the stricter selection of runs (A), whereas the difference in single-run slopes between layers II and III is increased (B).

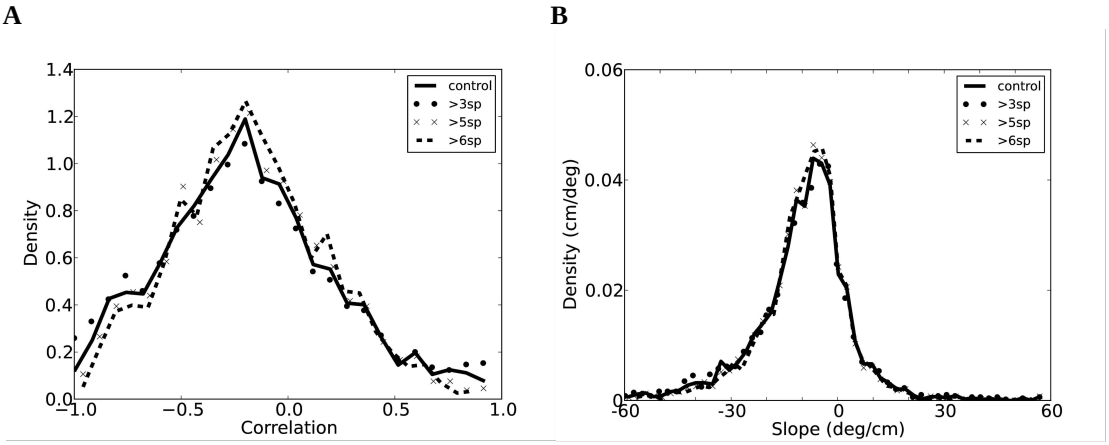

Figure S5: Throughout the manuscript, only runs with more than four spikes were included in the analysis (here termed control condition). To exclude a strong dependence of the results on this selection criterion, we also estimated phase precession correlation (A) and slope (B) for runs with more than 3, 5, or 6 spikes, respectively. Phase-precession estimates were only mildly affected by these different criteria.

Slopes restricted to [-80,80] deg/cm

Slopes restricted to [-50,50] deg/cm

A

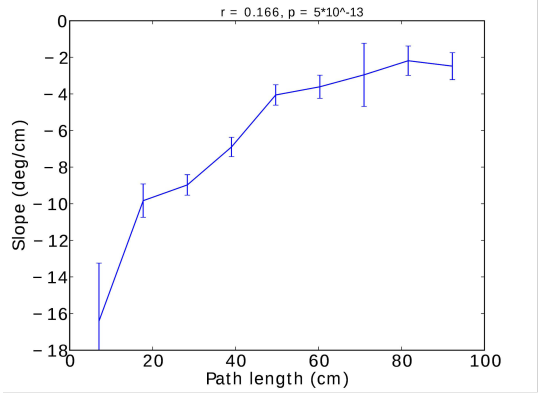

B

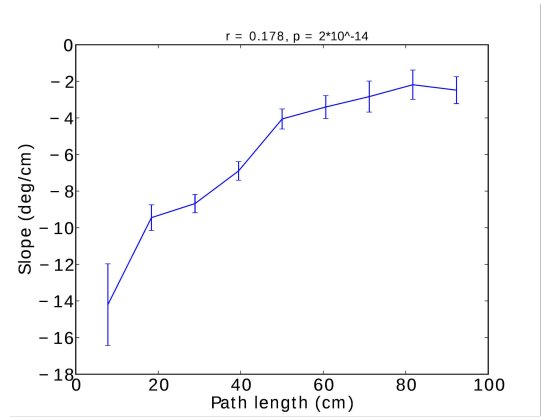

C

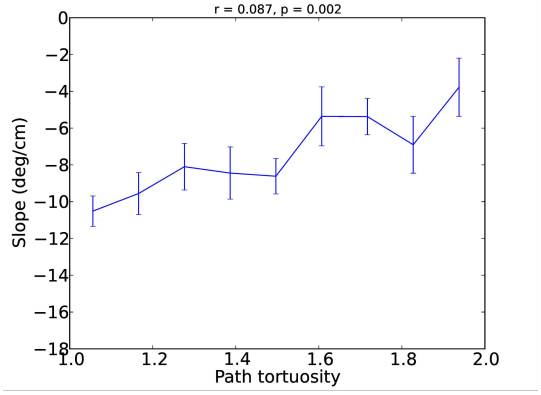

D

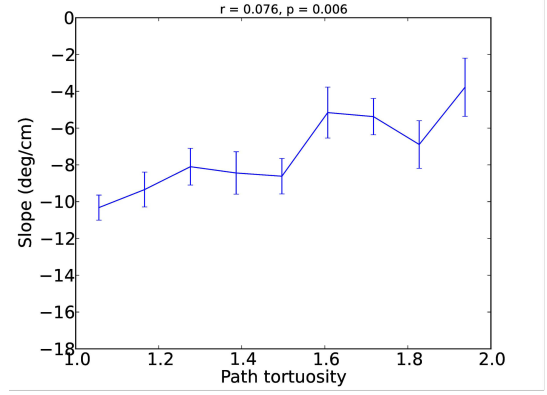

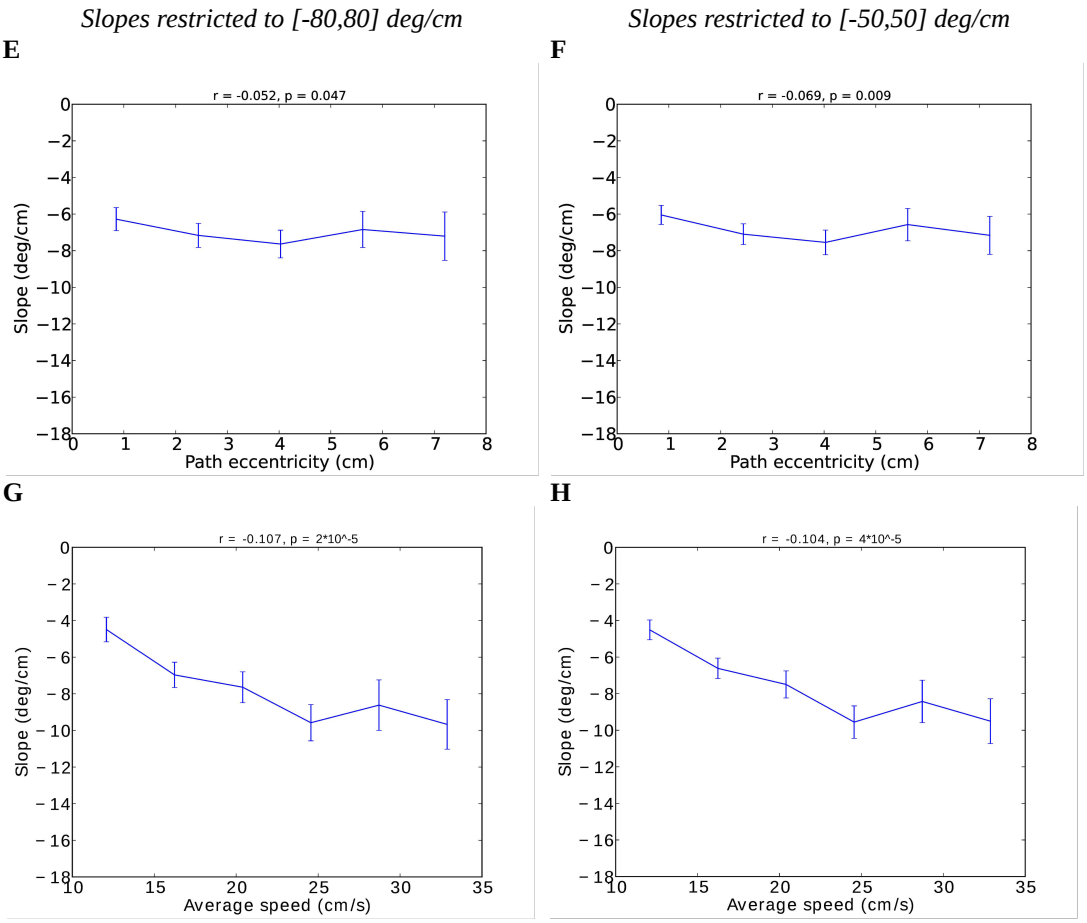

Figure S6: Single-run slopes were restricted to the range [-60,60] deg/cm throughout the manuscript. The dependence of phase precession on the properties of the path through a firing field can be reproduced when this restriction is relaxed, so that the slope is required to lie within the broader range of [-80,80] deg/cm (A, C, E,G), or tightened, so that the slope lies within [-50,50] deg/cm (B, D, F, H); compare to Fig. 3 in the manuscript.

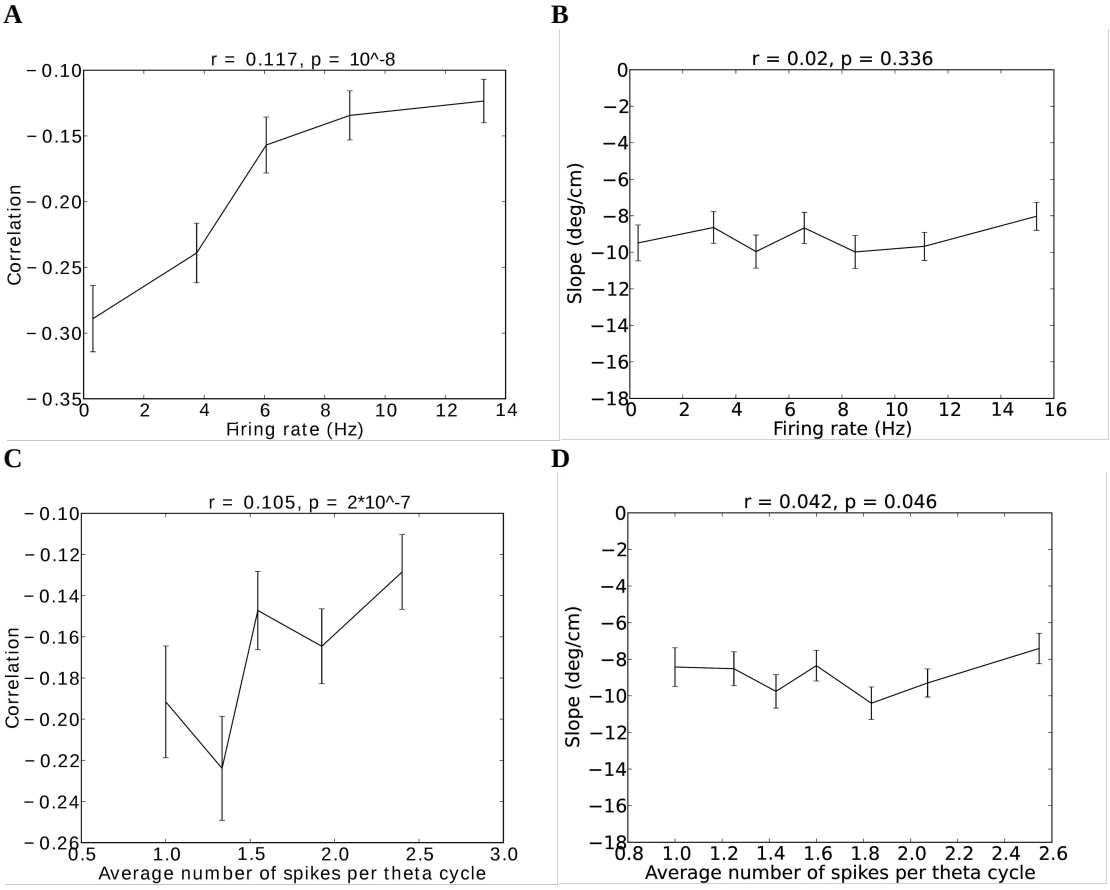

Figure S7: How does firing rate influence phase precession? Here we show the dependence of phase precession correlation (left column) and slope (right column) on firing rate using two estimates: the number of spikes divided by run duration (i.e. average firing rate; top row) and the average number of spikes per theta cycle in a run (bottom row). Firing activity and phase-precession correlation were weakly correlated (A and C), whereas slope was not affected by firing rate (B) or average number of spikes per theta cycle (D).

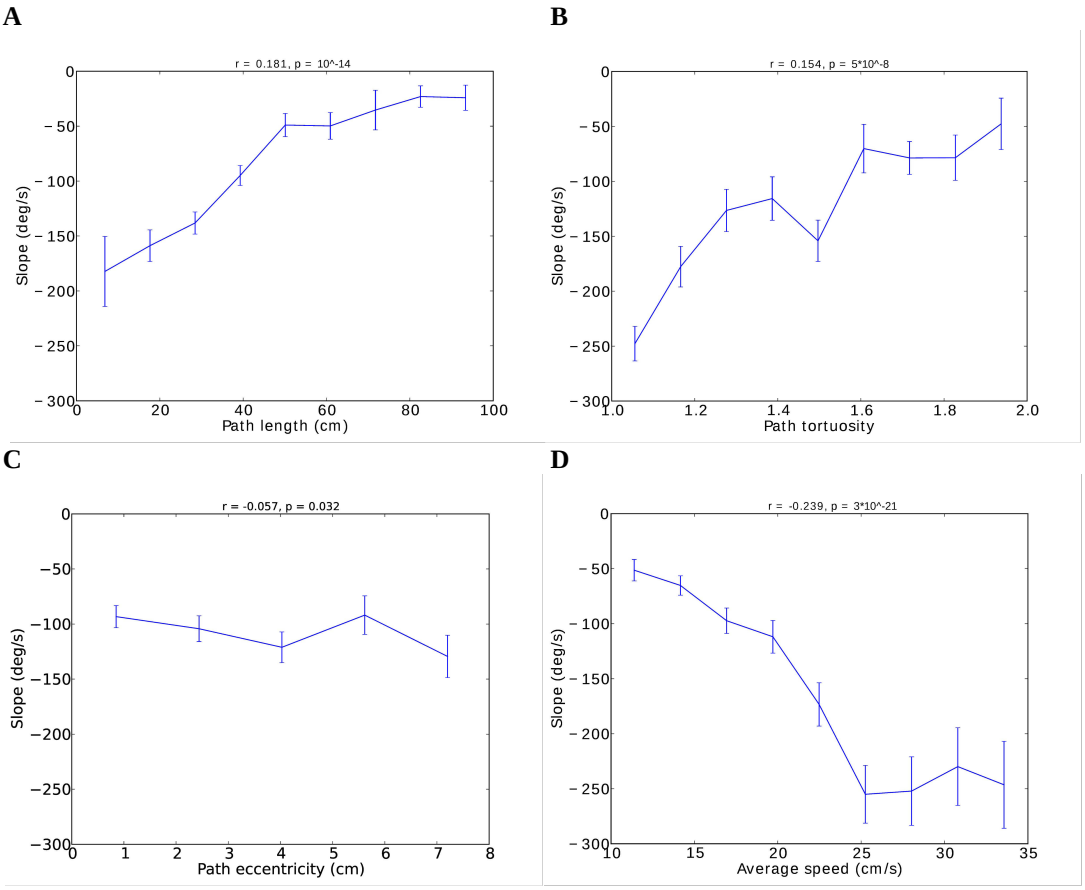

Figure S8: Salient features of the animal's path through a grid field affect the phase-time slope. For the phase-time slope, the path-length effect (A), the tortuosity effect (B) and the eccentricity effect (C) could be reproduced (see Fig. 3). (D) The phase-time slope correlated negatively with the speed of the animal – this is expected as there was no or only weak correlation of the phase-position slope with speed (Fig. 3F).

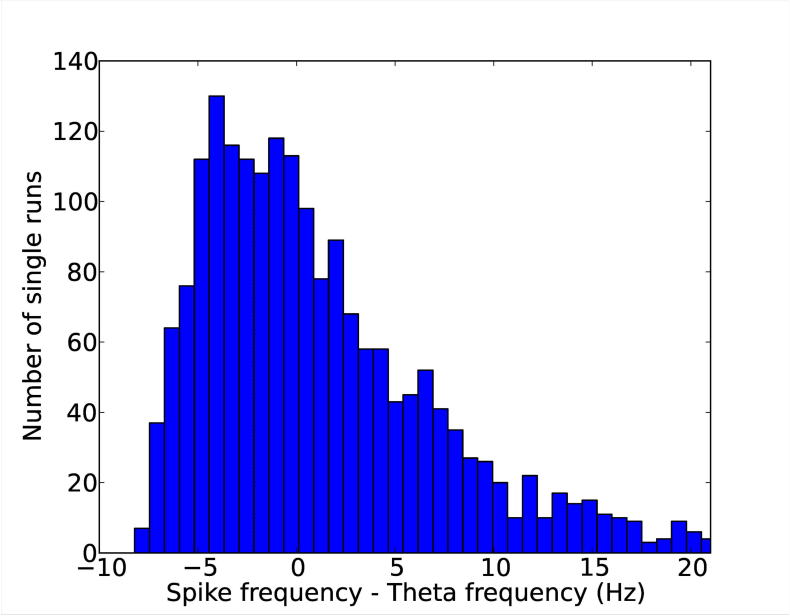

Figure S9: To investigate phase precession, previous studies measured the difference of the oscillation frequency of neuronal firing and the LFP's theta rhythm (Mizuseki et al., 2009). There, phase precession manifests itself as a positive frequency difference. In our single-run analysis, however, the difference was negative in many single runs (median difference -0.15 Hz) because cells often skipped theta cycles without spiking. Therefore, the frequency difference is not a suitable measure for assessing phase precession in entorhinal grid cells.

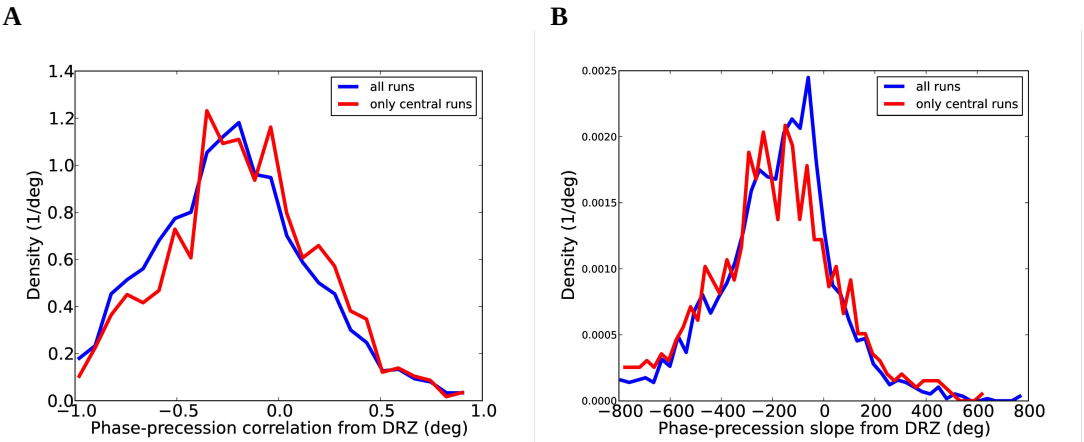

Figure S10: The so-called Directional Rate Zone measure (DRZ) was introduced by Huxter et al. (2008). Here, we show that phase precession was also evident with respect to the DRZ measure in our data for both correlation (A, -0.19 [-0.22, -0.18] for all runs, -0.15 [-0.17, -0.11] for central runs, median correlation ± 95% confidence interval) and slope (B; -164° ± 5° for all runs; -180° ± 9° for central runs, mean slope ± s.e.m.). Runs with an eccentricity of smaller than 3 cm were defined as central.

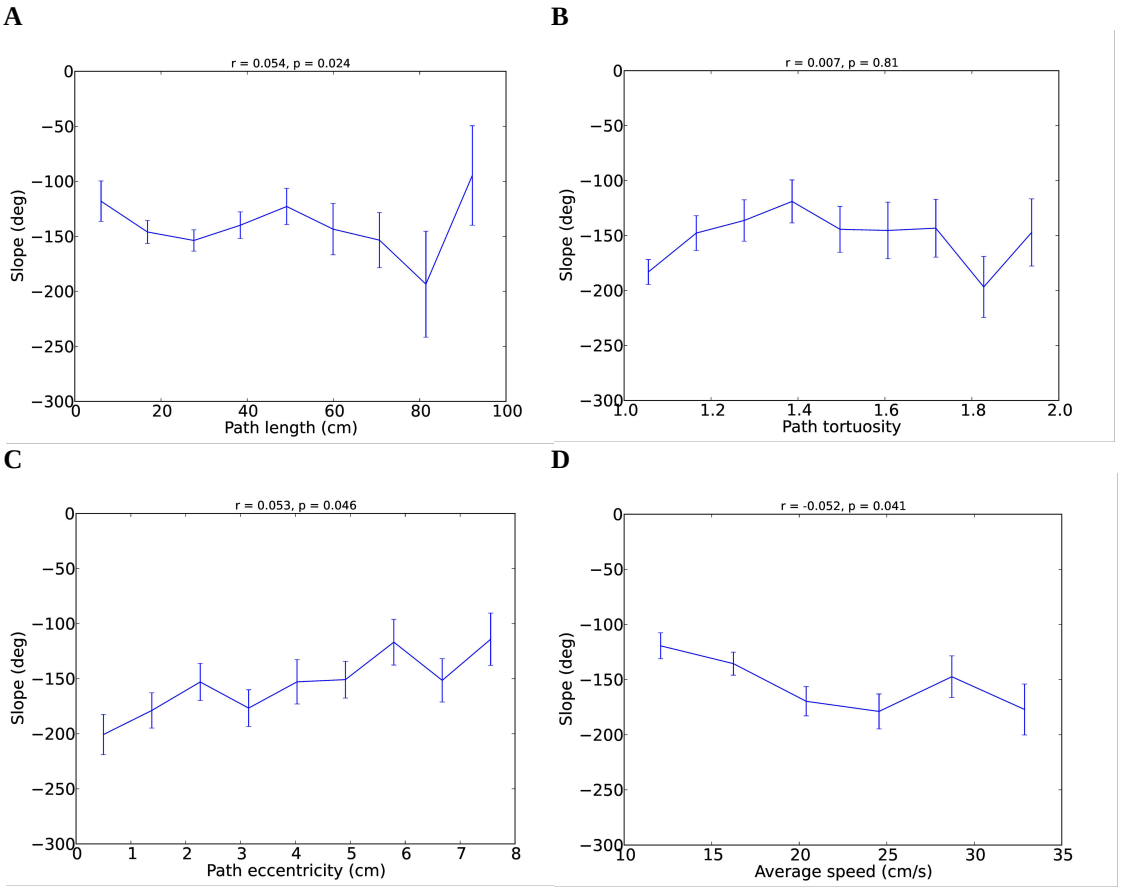

Figure S11: Although the DRZ measure can be used to show phase precession in our data, it does not capture the dependence of phase precession on the movement statistics during field traversals. The reason lies in the discontinuity of the measure along peripheral trajectories (i.e. trajectories that do not pass a field's center). For these runs, the absolute values of the measure are always non-zero and the sign inverts instantly when the animal changes from running 'towards' the center to running 'away' from it. This discontinuity distorted the estimate of phase-precession slope and weakened the effects of path length (A), tortuosity (B), or speed (D) on the phase-precession slope (from DRZ). The effect of eccentricity (C) was even inverted. The farther the path lies from the center of the firing field, the shallower the regression line between phase and DRZ became.

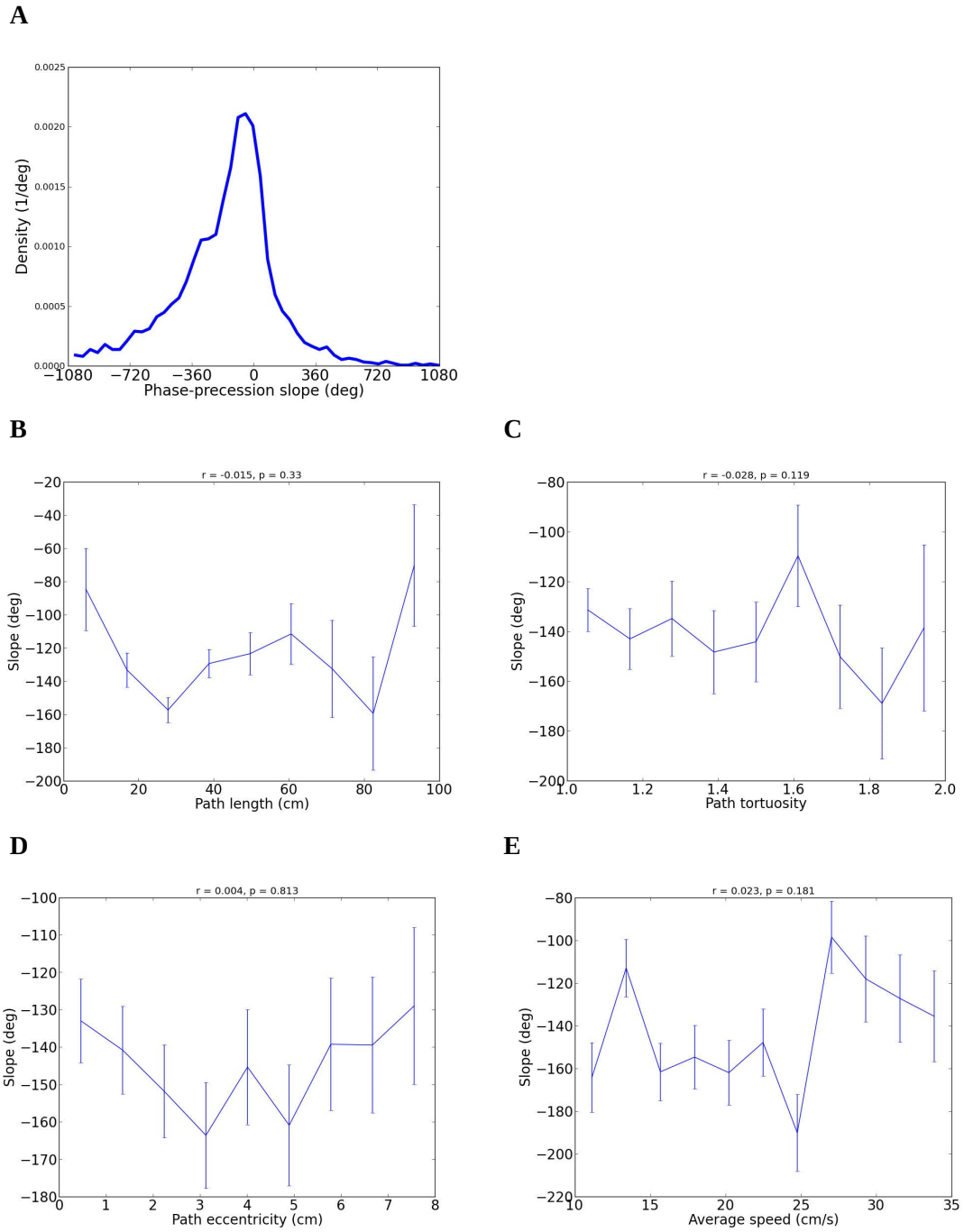

Figure S12: Single-run slopes calculated from normalized running distance do not depend linearly on the properties of the rat's trajectory. (A) Distribution of phase-precession slopes. Distance is normalized within each run, ranging from 0 (at field entry) to 1 (at field exit). (B) to (E) Properties of the rat's path are not significantly correlated with the slope of theta phase vs. normalized distance.

A **B**

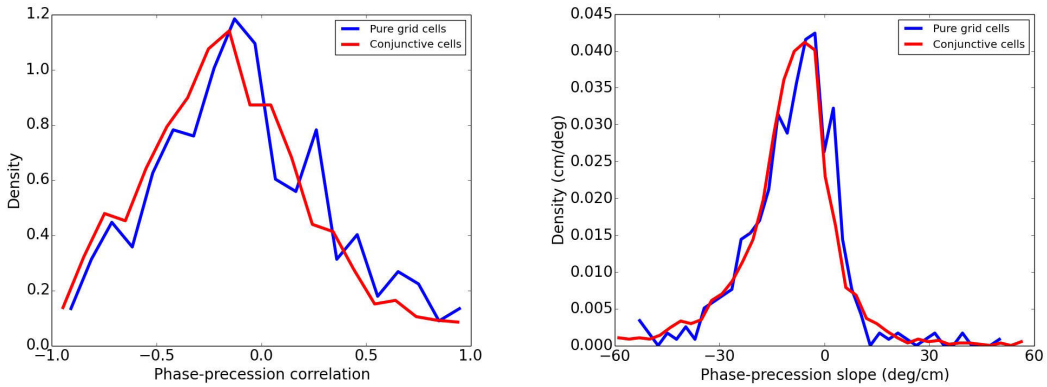

Figure S13: Conjunctive cells exhibit phase precession. (A) Phase-precession correlation in conjunctive cells appears to be slightly more negative compared to pure grid cells ($p<0.001$, Mann-Whitney rank test). (B) The slopes of pure grid cells and conjunctive cells are not significantly different. If at all, conjunctive cells exhibit slightly more negative slopes.

A **B**

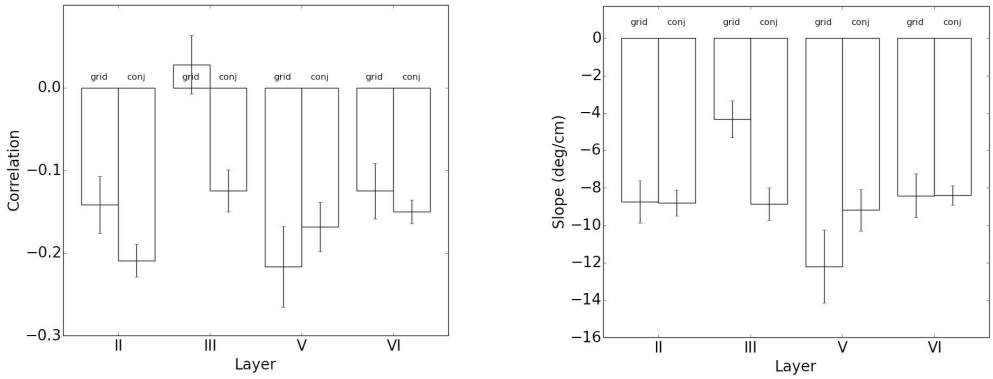

Figure S14: (A) Conjunctive cells in layer III exhibit clear phase precession whereas pure grid cells do not. Also in layer II, phase-precession correlation is tighter in conjunctive cells than in pure grid cells (layer II: $p=0.048$, layer III: $p<0.001$). (B) Phase-precession slopes in layer III are significantly steeper in conjunctive cells as compared to pure grid cells ($p=0.002$, t-test). For the slopes in layers II, V and VI no statistical differences could be found.

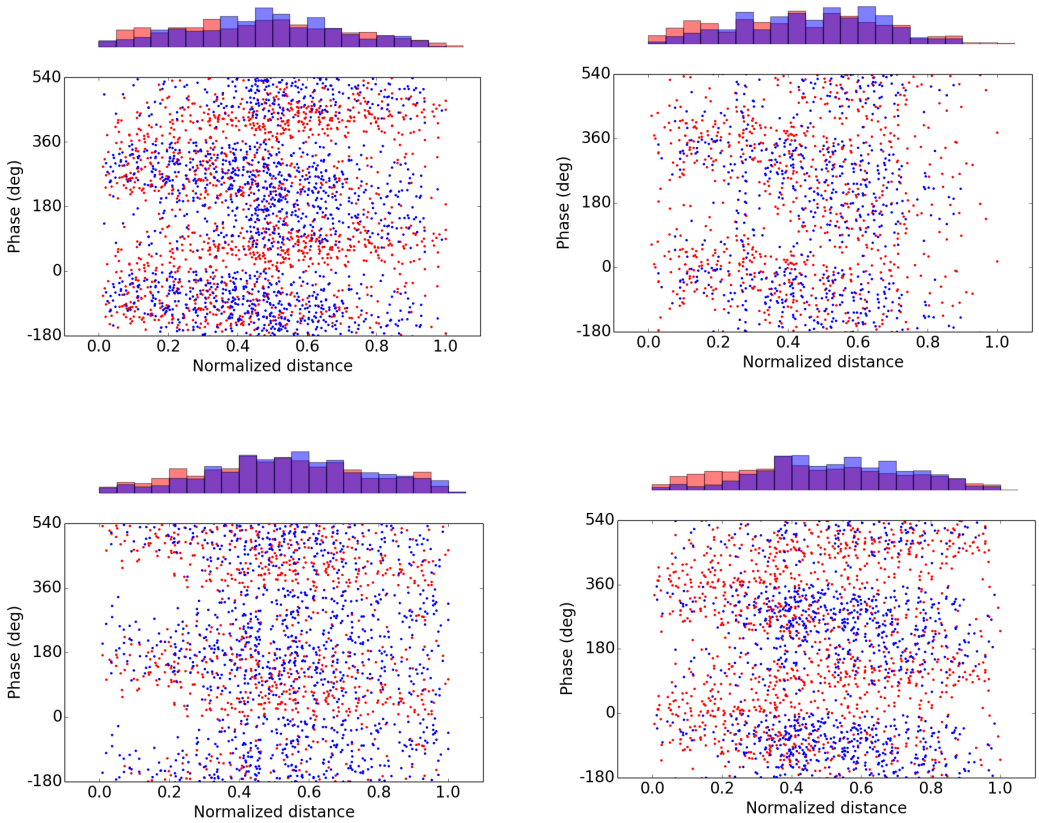

Figure S15: Burst firing is commonly observed in grid cells. Examples of pooled-data phase precession for four grid fields of different grid cells (the first three fields are the same as in Fig. 2B). Spikes within a theta cycle were separated in leading spike (the first spike in the cycle) and follower spikes (all spikes later in the cycle). Leading spikes are shown in red, follower spikes in blue. Histograms show the corresponding distributions of normalized distances (averaged across phases). Climer et al. (2013) found an increased portion of follower spikes towards the end of the run for linear-track data. In open environments, we find examples of grid fields that also show this behavior. For pooling, the distance is normalized by the total path length in each individual run.

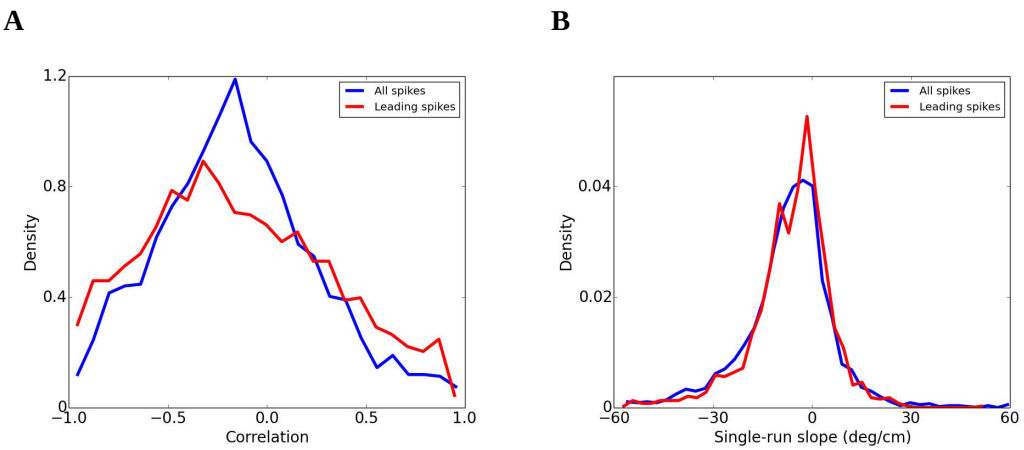

Figure S16: In open environments phase precession remains when the analysis is restricted to the leading spikes only. (A) Distribution of single-run correlation for all spikes and leading spikes. Leading spikes tend to result in a slightly tighter correlation of phase and distance, but this effect is statistically not significant. (B) Distribution of single-run slopes for all spikes and leading spikes. No statistical difference could be found.

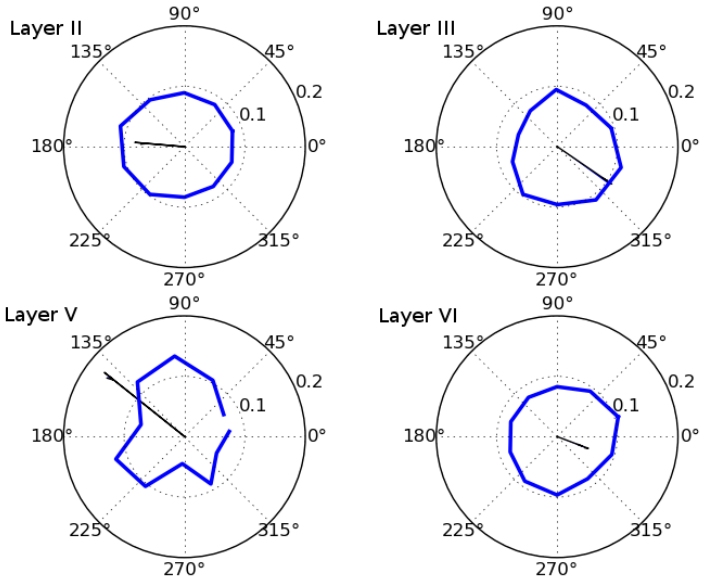

Figure S17: Single-run offsets from the circular-linear regression between travelled distance and theta phase. Layers II, III and VI show a non-uniform angular distribution of offsets (Rayleigh-test: p = 0.015, p = 0.0005, p = 0.035, respectively). For layer V (p = 0.2) only a limited amount of data was available. Although the distributions are mostly non-uniform, the vector strength is generally low (black lines), indicating large phase jitter. This might explain why the preferred offsets differ from the preferred phase of the first spike (Fig. 5F).

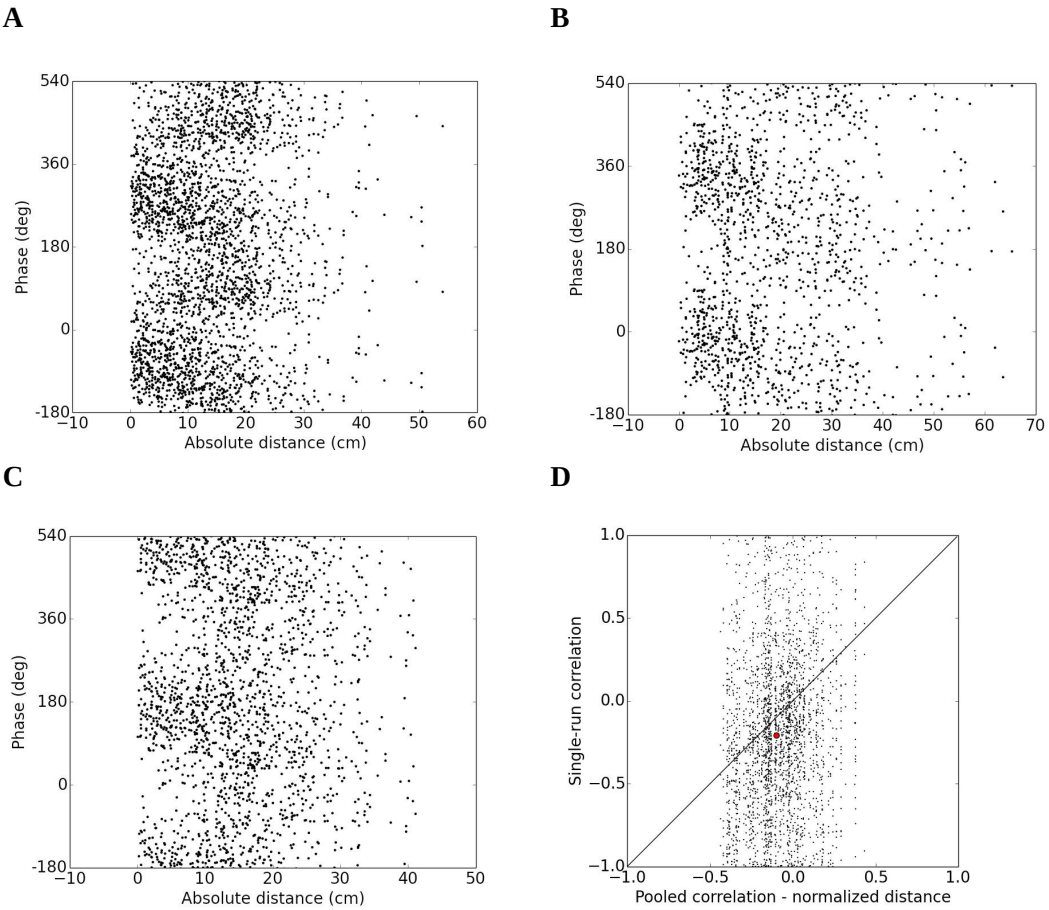

Figure S18: (A) – (C) Examples of pooled phase precession with respect to absolute distance along the path. Data represent the same three grid fields as in Figure 2B. Phase precession is also evident with respect to the absolute distance, though normalized distance seems to be the better regressor for theta phase. In the main text, we compared single-run correlation and pooled correlation, both calculated using the absolute distance. (D) reproduces this finding (Figure 2E) for pooled correlation that is calculated from the normalized distance. Phase-precession correlation is significantly stronger in single runs than in pooled data from normalized runs ($p<10^{-10}$, Mann-Whitney rank test). The red dot indicates medians of pooled correlation and single-run correlation.

4 Cell-Type Specific Phase Precession in Layer II of the Medial Entorhinal Cortex

Published in the *Journal of Neuroscience* on February, 17 2016.

Brief Communications

Cell-Type Specific Phase Precession in Layer II of the Medial Entorhinal Cortex

Eric T. Reifenstein,[1,2] Christian L. Ebbesen,[2,3] Qiusong Tang,[2] Michael Brecht,[2] Susanne Schreiber,[1,2] and Richard Kempter[1,2]

[1]Institute for Theoretical Biology, Department of Biology, Humboldt-Universität zu Berlin, 10115 Berlin, Germany, [2]Bernstein Center for Computational Neuroscience Berlin, 10115 Berlin, Germany, and [3]Berlin School of Mind and Brain, Humboldt-Universität zu Berlin, 10099 Berlin, Germany

The identity of phase-precessing cells in the entorhinal cortex is unknown. Here, we used a classifier derived from cell-attached recordings to separate putative pyramidal cells and putative stellate cells recorded extracellularly in layer II of the medial entorhinal cortex in rats. Using a novel method to identify single runs as temporal periods of elevated spiking activity, we find that both cell types show phase precession but putative stellate cells show steeper slopes of phase precession and larger phase ranges. As the two classes of cells have different projection patterns, phase precession is differentially passed on to different subregions of the hippocampal formation.

Key words: **entorhinal cortex; hippocampus; phase precession; pyramidal cell; stellate cell; temporal code**

Significance Statement

It is a great challenge for neuroscience to reveal the cellular basis of cognitive functions. One such function is the ability to learn and recollect temporal sequences of events. The representation of sequences in the brain is thought to require temporally structured activity of nerve cells. How different types of neurons generate temporally structured activity is currently unknown. In the present study, we use a computational classification procedure to separate different cell types and find that a subpopulation of cells, so-called stellate neurons, exhibits clear temporal coding. Contrary to the stellate cells, pyramidal cells show weaker temporal coding. This discovery sheds light on the cellular basis of temporal coding in the brain.

Introduction

Large-scale oscillations play an important role in many parts of the brain. They may functionally couple different brain regions and provide the basis for temporal coding (Buzsáki and Draguhn, 2004; O'Keefe and Burgess, 2005). Throughout the entorhinal–hippocampal network, large-amplitude theta oscillations (6–11 Hz) can be observed in the local field potential. Different cell types show different degrees of locking to the local theta oscillations (Klausberger and Somogyi, 2008; Mizuseki et al., 2009), and principal cells shift their firing phases consistently from late to early phases of the theta oscillations, a phenomenon termed phase precession (O'Keefe and Recce, 1993).

Phase precession can be observed in the hippocampus (O'Keefe and Recce, 1993; Skaggs et al., 1996), as well as the medial entorhinal cortex (Hafting et al., 2008; Reifenstein et al., 2012, 2014) and is one of the most extensively studied examples of temporal coding in the brain (Buzsáki and Draguhn, 2004; O'Keefe and Burgess, 2005). A subpopulation of cells in layer II of the medial entorhinal cortex (mECII) shows phase precession (Hafting et al., 2008; Mizuseki et al., 2009), but it is unclear if and how phase precession is passed from the mECII to the hippocampus.

mECII contains two morphologically and electrophysiologically (Alonso and Klink, 1993; Tang et al., 2014) different types of principal cells: stellate cells, which project to the dentate gyrus, and pyramidal cells, which send output to CA1 (Varga et al., 2010; Kitamura et al., 2014; Ray et al., 2014). Differences in phase coding between the two populations would suggest that mECII passes phase precession differentially to downstream areas. Furthermore, because pyramidal and stellate cells have distinct electrophysiological properties, such as subthreshold resonance (Alonso and Klink, 1993; Engel et al., 2008), differences in temporal coding between the two populations might give insights into mechanisms underlying the generation of phase precession.

Received Aug. 6, 2015; revised Jan. 5, 2016; accepted Jan. 9, 2016.

Author contributions: E.T.R., C.L.E., Q.T., M.B., S.S., and R.K. designed research; E.T.R., C.L.E., Q.T., M.B., S.S., and R.K. performed research; C.L.E., Q.T., and M.B. contributed unpublished reagents/analytic tools; E.T.R. analyzed data; E.T.R., C.L.E., Q.T., M.B., S.S., and R.K. wrote the paper.

This work was supported by the German Federal Ministry of Education and Research (BMBF; 01GQ0901, 01GQ0972, 01GQ1001A, 01GQ1403), the DFG (NeuroCure, Gottfried Wilhelm Leibniz Prize), and the ERC (NeuroBehavior grant).

The authors declare no competing financial interests.

Correspondence should be addressed to Eric T. Reifenstein, Institute for Theoretical Biology, Department of Biology, Humboldt-Universität zu Berlin, Philippstr. 13, Haus 4, 10115 Berlin, Germany. E-mail: eric.reifenstein@bccn-berlin.de.

DOI:10.1523/JNEUROSCI.2986-15.2016

 0270-6474/16/362283-06$15.00/0

Pyramidal and stellate cells can be reliably identified by immunohistochemistry: pyramidal cells are calbindin-positive and stellate cells are calbindin-negative (Varga et al., 2010; Tang et al., 2014). One way to directly investigate phase coding in pyramidal and stellate cells would be to perform juxtacellular recordings and labeling in freely-moving animals to directly assess the identity of the recorded cell (Tang et al., 2014). Although this approach provides unequivocal information about the cellular identity, the technique is exceedingly difficult and cannot yield sufficiently long recording durations to reliably assess phase precession. Alternatively, imaging cellular activity using fluorescent calcium indicators similarly allows for unequivocal information of cell type but does not provide the temporal resolution to measure the timing of individual spikes (Sun et al., 2015). Therefore, Tang et al. (2014) recently exploited the fact that pyramidal and stellate cells show differential locking to the local theta oscillations (Ray et al., 2014) and they developed a classifier that reliably predicts a cell's identity solely based on its spiking pattern. In the present study, we use this classifier to separate extracellularly recorded cells into putative pyramidal and putative stellate cells. This procedure allows us to perform a phase-precession analysis for sufficiently long recording durations from extracellular recordings while at the same time providing information about the identity of the cells. We are therefore able to tackle the question of whether there is a difference in phase precession between putative pyramidal and putative stellate cells in the mECII.

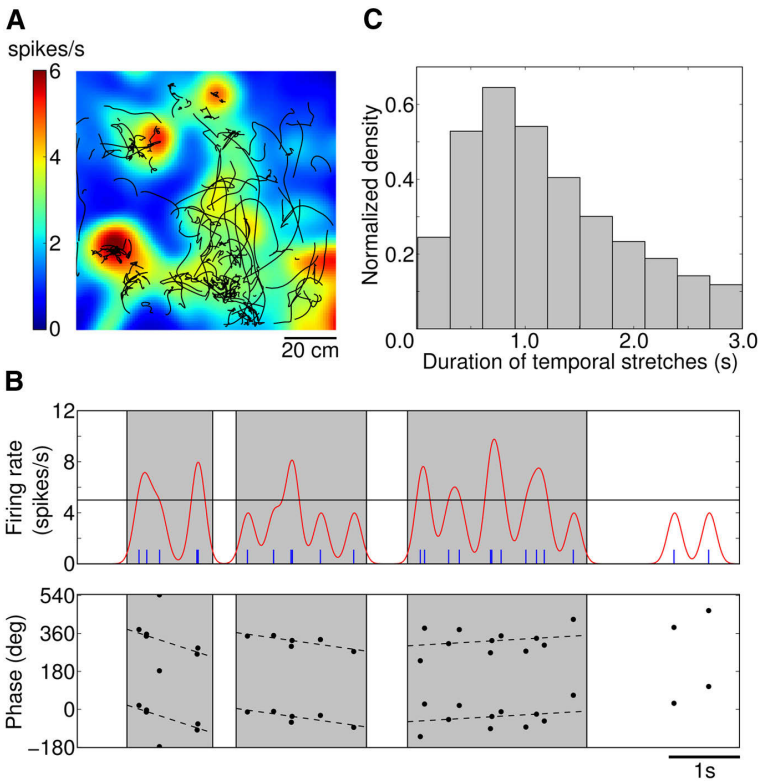

Figure 1. Detection of phase-precession patterns in temporally defined single runs of elevated firing. ***A***, Spatial tuning of a putative stellate cell from mEC layer II. The rat moves in a 1 m^2 box. Colors represent firing rates. Black lines depict temporally defined single runs. The cell has high spatial information (1.96 bits/s) and sparseness (0.49), yet this cell is not considered to be spatially modulated; see Materials and Methods for details. ***B***, Top, Illustration of the single-run selection. Blue ticks represent spike times. The red curve is an estimate of the firing rate. The horizontal black line at 5 spikes/s marks the firing-rate threshold for the temporal selection of single runs (see Results for details). Bottom, For all spikes (black dots) in each of the single runs (gray areas) circular–linear regression was performed. Dashed lines indicate the circular–linear fits. In contrast to the temporal selection procedure, firing fields have to be defined first when a spatial selection procedure is applied. For the cell in ***A***, the standard field definition yields field borders that encircle the light blue area (~1.5 spikes/s). As spatially defined single runs can only lie within this area, the temporal procedure can pick up additional runs (it is not limited to the spatial extent of the pooled firing fields). ***C***, Duration of temporal stretches (temporally defined single runs). The median duration is 1.39 s [1.36, 1.40].

Materials and Methods

We analyzed extracellularly recorded data obtained from layer II of the medial entorhinal cortex in male rats. During the experiment, the animal was moving freely in a 1 m^2 box. The data were previously published; see Tang et al. (2014) for details on the experimental procedures.

Isolated single units were divided into putative interneurons and putative principal cells according to spike-rate and spike-shape criteria. All recorded principal cells were assigned a label, either "putative stellate cell" (pSte) or "putative pyramidal cell" (pPyr), based on a classification procedure that was deduced from Calbindin-labeling experiments (Tang et al., 2014). The classifier was a support vector machine with a radial basis-function kernel. Two properties were used to train the classifier: the strength $S = \left|\frac{1}{N}\sum_{k=1}^{N}\exp(i\theta_k)\right|$ of theta phase locking of a cell's spike train (N spikes) with respect to the local theta rhythm, and the cell's preferred theta phase $\varphi = \arg\left(\frac{1}{N}\sum_{k=1}^{N}\exp(i\theta_k)\right)$ where θ_k depicts the theta phase of the kth spike (Tang et al., 2014). The Hilbert transform was used to calculate the instantaneous phase of the theta oscillation. Spikes were excluded from the analysis if the speed of the animal was <2 cm/s.

Only a minority of principal cells from the extracellular recordings showed clear spatial modulation (27 of 114; 21 pPyr and 6 pSte; Tang et al. (2014) shows the applied shuffling procedure). Moreover, the median spatial information was low (0.58 bits/s [0.49, 0.72]), and the median spatial sparseness had small values (0.30 [0.26, 0.34]; Aghajan et al., 2015). Therefore, we were not able to separate individual field traversals ("single runs") from the spatial firing fields. Instead we followed a different strategy based on the temporal structure of the recorded spike trains to identify coherent periods of elevated firing (Fig. 1; see Results for details).

For each of the single runs, the times and theta phases of all spikes were used to assess phase precession. We quantified phase precession by calculating the circular–linear correlation coefficient (Kempter et al., 2012; Reifenstein et al., 2012) and the slope of the circular-linear regression line.

To minimize errors in the classification of cells, we repeated the analysis with a "guard zone." The guard zone required cells to have a minimal distance to the decision boundary during the classification procedure. In three independent repetitions of the analysis, the width of the guard zone was chosen 0.1, 0.3, or 0.5 (Fig. 2*B*).

Unless stated otherwise, we used the median and a large-sample approximation for its 95% confidence interval to summarize the data as most of the data stem from skewed distributions. Accordingly, the Mann–Whitney U test was used to test for statistical significance (exceptions as noted in the Results). Effects were considered statistically significant if $p < 0.05$.

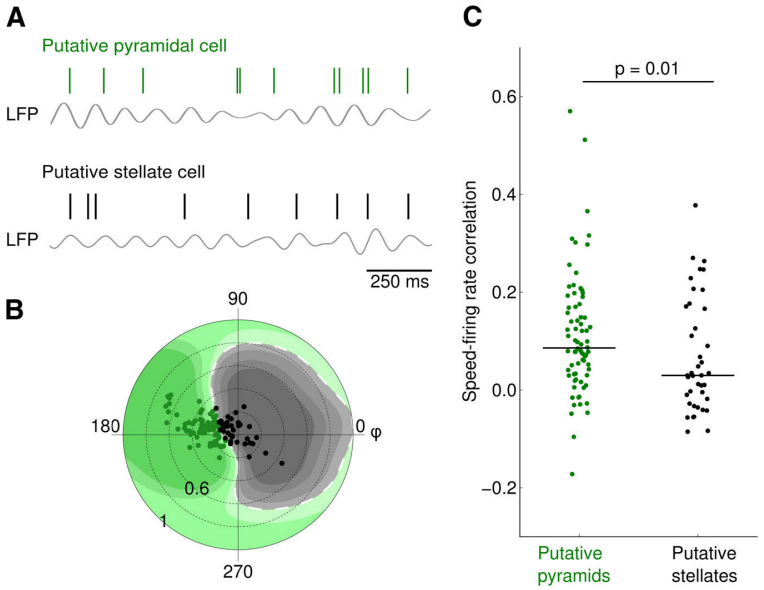

Figure 2. Classification of cells in layer II of the medial entorhinal cortex. ***A***, Example spike trains of cells classified as pyramidal cell (top) and stellate cell (bottom). Pyramidal cells locked to the theta rhythm more strongly and preferred phases around the trough of theta (180°). Stellate cells showed weaker locking and rather spiked around the peak of theta (0°). ***B***, The classifier by Tang et al. (2014) uses the strength of theta locking and the preferred theta phase to separate cells into putative stellate cells and putative pyramidal cells. The polar plot of the classified cells shows the average theta phase $\varphi \in [0, 360°]$ in the angular component, whereas the radial component is used for the phase-locking strength $S \in [0, 1]$. Black dots represent the putative stellate cells; green dots represent putative pyramidal cells. The white dashed line depicts the decision boundary. Differently shaded green and gray regions correspond to different values for the guard zone (0.1, 0.3, and 0.5). ***C***, The correlation between the animal's speed and the firing rate is stronger for putative pyramidal cells than for putative stellate cells. Each dot represents a cell. Horizontal black lines depict the median values.

Results

To quantify phase precession in mECII, we reanalyzed previously published data of extracellularly recorded principal cells while rats explored a 1 m^2 square arena (Tang et al., 2014). The activity of the recorded cells showed a wide spectrum of weak spatial modulations (Fig. 1*A*). Therefore, we focused on the temporal properties of the recorded cells and did not elaborate on the spatial properties.

For irregular spatial tuning of cells as in Figure 1*A*, it was difficult to define firing fields that could be used to select individual field traversals (single runs). Instead, following Aghajan et al. (2015), we obtained candidate single runs by temporal convolution of the spike train with a Gaussian kernel of width 100 ms, and identification of episodes above a firing-rate threshold of 5 spikes/s (Fig. 1*B*). As the firing rates of the cells did not vary much (2.0 spikes/s [1.7, 2.6], $n =$ 114), we chose the same threshold for all cells. The candidate single runs were extended in time until the firing rate dropped <10% of the single run's peak firing rate and remained <10% for >250 ms (~2 theta cycles) before and after the run. The latter criterion takes into account that the firing activity might skip theta cycles. Finally, the individual runs were required to have a minimal duration of 300 ms and to include at least four spikes (Fig. 1*B*).

To justify the choice of parameters to select single runs based on their temporal structure, we applied this method also to data from previous studies (Sargolini et al., 2006; Reifenstein et al., 2014) in which clear firing fields could be identified. Thus, we were able to apply both the "classical" spatial selection and the proposed temporal selection of single runs. The distributions of single-run phase precession correlations and slopes from the two procedures matched well (correlations: 0.01 bits Kullback–Leibler divergence; 94% overlap between the two distributions; slopes: 0.015 bits, 93% overlap), although the median values of the two distributions differed slightly (spatial: −0.17 [−0.18, −0.15], temporal: −0.14 [−0.15, −0.13], $p = 0.004$ for the correlations; spatial: −76 deg/s [−81, −72], temporal: −71 deg/s [−74, −69]; $p = 0.01$ for the slopes). To further quantify the similarity of the temporal and spatial selection procedures, we compared for each cell the number of spikes that were assigned to single runs by either method. We found that, on average, 97% of in-field spikes (according to the spatial criterion) were also picked up by the temporal criterion. Additionally, the temporal criterion included 13% more spikes, which occurred at the edges of firing fields or in isolated stretches of elevated firing or in fields with low maximum rate that did not pass the detection threshold in the spatial criterion. Hence, the temporal selection of single runs generalizes the classical spatial method. In summary, we identified 15,182 single runs in a total of 114 recorded cells.

The obtained spatial distribution of the temporally defined single runs generally matched the spatial tuning of a cell (Fig. 1*A*), although no spatial information was used to define the single runs. The temporal stretches of spiking activity had a median duration of 1.39 s ([1.36, 1.40] s; Fig. 1*C*).

For each single run, phase precession was quantified by circular–linear regression (Kempter et al., 2012). Negative slopes indicated phase precession, but also single runs with positive slopes were observed (Fig. 1*B*). The obtained slopes (−54 deg/s [−57, −51]) and correlations (−0.104 [−0.112, −0.095]) were slightly smaller than for the dataset used by Reifenstein et al. (2014) in which cells from all cortical layers were analyzed (data from Sargolini et al., 2006; slopes: −71 deg/s [−74, −69]; correlation: −0.14 [−0.15, −0.13], reanalysis using the temporal selection of single runs). Yet, the distributions of correlations overlapped strongly for the two datasets (94%), indicating that they match the ranges of values in Reifenstein et al. (2014). The difference in median values of slopes might be explained by the shorter single runs in the Sargolini dataset (0.97 s [0.96, 0.98] vs 1.39 s [1.36, 1.40] in our data, $p < 10^{-50}$). Shorter runs suggest that the average field sizes were smaller in the Sargolini data than in our data. As a consequence, the slopes in the Sargolini dataset would be steeper because smaller fields have steeper slopes (Reifenstein et al., 2014).

To quantify phase precession for pyramidal and stellate cells in layer II separately, we distinguished two classes of principal cells in our analysis. Tang et al. (2014) and Ray et al. (2014) showed that putative pyramidal cells tended to fire spikes around the trough of the local theta oscillation; on the other hand, the spiking activity of putative stellate cells showed a weak preference for the peak of theta (Fig. 2*A*). Based on this finding, we

were able to separate extracellularly recorded units into pPyr and pSte (Fig. 2*B*). In a total of 74 putative pyramidal cells and 40 putative stellate cells (an example of the activity a putative stellate cell was shown in Fig. 1*A*), we identified 11,684 and 3,498 single runs, respectively. Although the two populations strongly differed in phase-locking strength (pPyr: 0.33 ± 0.02, pSte: 0.15 ± 0.01; $p = 8 \times 10^{-12}$, *t* test), they showed similar overall firing rates (pPyr: 2.0 spikes/s [1.5, 2.9]; pSte: 2.1 spikes/s [1.4, 2.7]; $p = 0.19$) and similar bursting indexes (proportion of interspike intervals smaller than 0.15 s, pPyr: 0.50 [0.44, 0.58]; pSte: 0.47 [0.39, 0.55]; $p = 0.18$).

To gain more confidence in the classification procedure, we investigated the relationship between movement speed and firing rate for putative pyramidal cells and putative stellate cells. Sun et al. (2015) showed that pyramids have a stronger speed modulation of the firing rate. We tested this feature by calculating the correlation between the speed of the animal and the temporal fluctuations of the firing rate for each cell (Fig. 1*B*, see red curve for an example of firing-rate fluctuations). The firing rate and the speed were significantly correlated for both classes of cells, but the average correlation was significantly stronger for putative pyramidal cells (pPyr: $r = 0.09$ [0.07, 0.12]; pSte: $r = 0.03$ [−0.002, 0.09]; $p = 0.01$; Fig. 2*C*), confirming the classification proposed by Tang et al. (2014).

Interestingly, putative stellate cells displayed steeper phase precession than putative pyramidal cells (pPyr: −47 deg/s [−50, −44]; pSte: −81 deg/s [−87, −74]; $p = 10^{-13}$; Fig. 3*A*,*B*). To assess the size of the effect (difference of the median phase-precession slopes), we randomly assigned cell identities ("pPyr" or "pSte") to the single runs and calculated the effect size for each realization. We found that the measured effect size is larger than expected by chance in >99.8% of all cases (corresponds to $p = 0.013$).

To exclude sample size effects, we randomly downsampled the large number of single runs from the putative pyramidal cells ($n = 11,684$) to match the smaller number of runs from putative stellate cells ($n = 3,498$). In all 1000 repetitions of the downsampling, we found significantly shallower phase precession in the putative pyramidal cells as compared with the putative stellate cells ($p = 10^{-6}$ for all 1000 repetitions).

The correlation between time and theta phase was similar in putative pyramidal cells and putative stellate cells (pPyr: −0.10 [−0.11, −0.09]; pSte: −0.11 [−0.13, −0.09], $p = 0.1$). The steeper phase precession in putative stellate cells was accompanied by a larger phase range (pPyr: 110 deg [106, 113]; pSte: 169° [156, 178]; $p = 2 \times 10^{-6}$; Fig. 3*C*), because the duration of spike sequences did not differ for the two populations (pPyr: 1.40 s [1.37, 1.42]; pSte: 1.31 s [1.29, 1.37]; $p = 0.12$; Fig. 3*D*).

To minimize an erroneous classification of cells that were close to the decision boundary, we also implemented a guard zone: cells were required to have a minimal distance to the decision boundary during the classification procedure (Fig. 2*B*). For all tested minimal distances (0.1, 0.3, and 0.5), putative stellate cells exhibited significantly steeper phase precession than putative pyramidal cells ($p = 3 \times 10^{-14}$, minimal distance = 0.1; $p = 6 \times 10^{-12}$, minimal distance = 0.3; $p = 4 \times 10^{-5}$, minimal distance = 0.5).

The classification procedure of cells depended on the theta locking of spikes. Could this procedure bias the phase precession of the two populations? For example, perfect phase locking (phase-locking strength = 1) would impede phase precession. We measured the average phase-precession slope and the phase-locking strength for each cell. We found no correlation ($r = 0.14$, $p = 0.15$; Fig. 3*E*) between the two measures. Also for the two

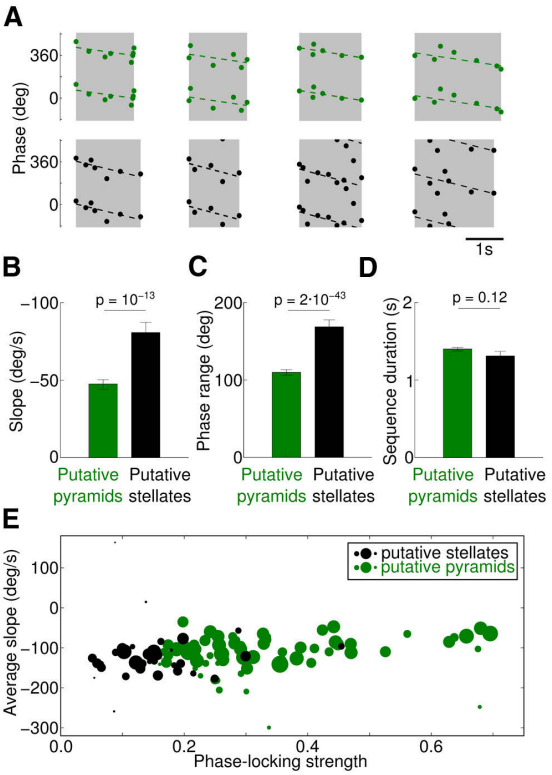

Figure 3. Phase precession was steeper in putative stellate cells. ***A***, Examples of single-run phase precession for a putative pyramidal cell (top) and a putative stellate cell (bottom). Green and black dots represent the spikes of the putative pyramidal and stellate cells, respectively. Dashed lines depict circular-linear fits. ***B***, Phase-precession slopes were significantly steeper in putative stellate cells. ***C***, Single-run phase ranges were significantly larger in putative stellate cells, consistent with the larger slope of phase precession. ***D***, The duration of single runs is statistically the same for the two populations. In ***B***–***D***, error bars depict the 95% confidence interval of the median. ***E***, Phase-locking strength and phase-precession slopes were not correlated in a cell-by-cell analysis. Green and black dots represent putative pyramidal cells and putative stellate cells, respectively. The area of each dot is proportional to the number of runs that the corresponding cell contributed to the analysis.

populations separately, phase-precession slope and phase-locking strength did not correlate (pPyr: $r = 0.19$, $p = 0.11$; pSte: $r = 0.05$, $p = 0.77$). Together, these results indicate that—within the physiological range of phase-locking strength <0.7 (Fig. 3*E*)—phase precession and phase locking can coexist.

Discussion

We found that putative stellate cells display steeper phase precession than putative pyramidal cells, which was accompanied by larger phase ranges. This is the first account of phase precession in different cell types within mECII. Hafting et al. (2008) and Mizuseki et al. (2009) showed entorhinal phase precession in extracellular recordings of unidentified cells in layer II, but did not relate the phase precession to pyramidal or stellate cells. Newman and Hasselmo (2014) investigated phase-precession of grid cells recorded in the superficial layers of mEC (both layers II and III) based on pooled-run data and found larger phase-precession correlations in trough-locking grid cells as compared with peak-locking grid cells. In contrast to this, we quantified phase precession in single runs of principal cells from only mECII and could

not find differences in the distributions of phase-precession correlations. Furthermore, Newman and Hasselmo (2014) suggested that trough-locking cells might be stellate cells, based on the stellate cells' tendency to fire in bursts during recordings in slices. We did not find differences in the bursting behavior of the putative pyramidal and putative stellate cells.

Newman and Hasselmo (2014) reported pooled-data phase-precession correlations in the range of −0.05. Because of the broader scatter of data points, pooled-data correlations are generally expected to be lower than single-run correlations (Schmidt et al., 2009). Therefore it is not surprising that we found twofold stronger correlations in our single-run analysis (in the range of −0.1). We argue that the animal needs to process information online and does not have the opportunity to pool over trials. Apart from that, functional hypotheses about temporal coding (Mehta et al., 2002) or sequence learning (Hasselmo and Eichenbaum, 2005) are usually discussed for phase precession in individual runs. Hence, it is appropriate to also analyze phase precession in single runs.

Aghajan et al. (2015) measured phase-precession correlations in temporally defined single runs and found correlations of around 0.2. The difference to our result might be explained by three facts: Aghajan et al. (2015) (1) recorded in CA1; (2) used a linear–circular correlation which is based on a sinusoidal model, in contrast to the circular-linear correlation we used (Kempter et al., 2012); and (3) restricted their analysis to significantly phase-precessing cells, whereas we included all cells in the analysis. The slopes of phase precession in our dataset were shallower than in the single-run analysis by Reifenstein et al. (2014) of mECII grid cells recorded by Sargolini et al. (2006). In the latter dataset, temporally defined single runs are shorter than in our data, suggesting that field sizes are smaller. Smaller field sizes were shown to correspond to steeper phase-precession slopes (Reifenstein et al., 2014). Therefore, it is likely that differences between our results and the findings by Reifenstein et al. (2014) are because of different field sizes in the two datasets.

It is presently unclear whether grid cells in mECII are predominantly pyramidal cells (Tang et al., 2014), stellate cells (Domnisoru et al., 2013), or if they show no preference for either cell type (Sun et al., 2015). Tang et al. (2014) found that in mECII calbindin-positive putative pyramidal cells on average showed higher grid scores than calbindin-negative putative stellate cells. Conversely, putative stellate cells generally showed higher border scores. We add to the picture that putative stellate cells exhibit steeper phase precession than putative pyramidal cells. It should be noted, however, that all conclusions rest on the assumption that the classifier of Tang et al. (2014) works correctly. To control for problems arising from our classification procedure, we performed three checks: first, we repeated the analysis using a variable guard zone, and found that our results did not depend on the guard zone width. Second, we replicated the recent finding from Sun et al. (2015) and found that the activity of putative pyramidal cells is more modulated by the animal's running speed than the activity of putative stellate cells. Third, we found no correlation between phase-precession slope and the phase-locking strength. This suggests that our results are not just an artifact of the known difference in phase-locking strength between pyramidal and stellate cells (Ray et al., 2014; Tang et al., 2014), but a real difference in the phase coding of the two cell populations.

Phase precession might be used to compress behavioral sequences to the time scale of synaptic plasticity (Skaggs et al., 1996). In this framework, a steeper phase-precession slope implies that the spikes of different cells in the compressed sequence are temporally more separated, which might be beneficial to retain the order of the sequence under the influence of temporal noise. On the other hand, a clearer temporal separation of the spikes from different cells poses a limit on the number of cells participating in the sequence.

Our results suggest that stellate cells send steeply phase-precessing output to the dentate gyrus, whereas the shallower precessing mECII pyramidal cells project to CA1 (Varga et al., 2010; Kitamura et al., 2014). Phase precession might thus be differentially inherited by different subregions of the hippocampal–entorhinal loop (Jaramillo et al., 2014; Schlesiger et al., 2015).

To conclude, our data indicate that even within the same layer of mEC principal cells can show different phase-precession patterns. This result compares with other observations which indicate that different groups of CA1 pyramidal cells can exhibit distinct temporal discharge patterns (Mizuseki et al., 2011). Also spiking activity of hippocampal interneurons is highly cell-type-specific (Klausberger and Somogyi, 2008). Hence, we argue that cell-type-specific temporal coding is a widespread phenomenon throughout the hippocampal formation. Future studies might aim to further investigate where phase precession originates and whether or how this temporal code is passed on between different subregions.

References

Aghajan ZM, Acharya L, Moore JJ, Cushman JD, Vuong C, Mehta MR (2015) Impaired spatial selectivity and intact phase precession in two-dimensional virtual reality. Nat Neurosci 18:121–128. CrossRef Medline

Alonso A, Klink R (1993) Differential electroresponsiveness of stellate and pyramidal-like cells of medial entorhinal cortex layer II. J Neurophysiol 70:128–143. Medline

Buzsáki G, Draguhn A (2004) Neuronal oscillations in cortical networks. Science 304:1926–1929. CrossRef Medline

Domnisoru C, Kinkhabwala AA, Tank DW (2013) Membrane potential dynamics of grid cells. Nature 495:199–204. CrossRef Medline

Engel TA, Schimansky-Geier L, Herz AV, Schreiber S, Erchova I (2008) Subthreshold membrane-potential resonances shape spike-train patterns in the entorhinal cortex. J Neurophysiol 100:1576–1589. CrossRef Medline

Hafting T, Fyhn M, Bonnevie T, Moser MB, Moser EI (2008) Hippocampus-independent phase precession in entorhinal grid cells. Nature 453:1248–1252. CrossRef Medline

Hasselmo ME, Eichenbaum H (2005) Hippocampal mechanisms for the context-dependent retrieval of episodes. Neural Netw 18:1172–1190. CrossRef Medline

Jaramillo J, Schmidt R, Kempter R (2014) Modeling inheritance of phase precession in the hippocampal formation. J Neurosci 34:7715–7731. CrossRef Medline

Kempter R, Leibold C, Buzsáki G, Diba K, Schmidt R (2012) Quantifying circular-linear associations: hippocampal phase precession. J Neurosci Methods 207:113–124. CrossRef Medline

Kitamura T, Pignatelli M, Suh J, Kohara K, Yoshiki A, Abe K, Tonegawa S (2014) Island cells control temporal association memory. Science 343:896–901. CrossRef Medline

Klausberger T, Somogyi P (2008) Neuronal diversity and temporal dynamics: the unity of hippocampal circuit operations. Science 321:53–57. CrossRef Medline

Mehta MR, Lee AK, Wilson MA (2002) Role of experience and oscillations in transforming a rate code into a temporal code. Nature 417:741–746. CrossRef Medline

Mizuseki K, Sirota A, Pastalkova E, Buzsáki G (2009) Theta oscillations provide temporal windows for local circuit computation in the entorhinal-hippocampal loop. Neuron 64:267–280. CrossRef Medline

Mizuseki K, Diba K, Pastalkova E, Buzsáki G (2011) Hippocampal CA1 pyramidal cells form functionally distinct sublayers. Nat Neurosci 14:1174–1181. CrossRef Medline

Newman EL, Hasselmo ME (2014) Grid cell firing properties vary as a function of theta phase locking preferences in the rat medial entorhinal cortex. Front Syst Neurosci 8:193. Medline

O'Keefe J, Burgess N (2005) Dual phase and rate coding in hippocampal place cells: theoretical significance and relationship to entorhinal grid cells. Hippocampus 15:853–866. CrossRef Medline

O'Keefe J, Recce ML (1993) Phase relationship between hippocampal place units and the EEG theta rhythm. Hippocampus 3:317–330. CrossRef Medline

Ray S, Naumann R, Burgalossi A, Tang Q, Schmidt H, Brecht M (2014) Grid-layout and theta-modulation of layer 2 pyramidal neurons in medial entorhinal cortex. Science 343:891–896. CrossRef Medline

Reifenstein ET, Kempter R, Schreiber S, Stemmler MB, Herz AV (2012) Grid cells in rat entorhinal cortex encode physical space with independent firing fields and phase precession at the single-trial level. Proc Natl Acad Sci U S A 109:6301–6306. CrossRef Medline

Reifenstein E, Stemmler M, Herz AV, Kempter R, Schreiber S (2014) Movement dependence and layer specificity of entorhinal phase precession in two-dimensional environments. PLoS One 9:e100638. CrossRef Medline

Sargolini F, Fyhn M, Hafting T, McNaughton BL, Witter MP, Moser MB, Moser EI (2006) Conjunctive representation of position, direction, and velocity in entorhinal cortex. Science 312:758–762. CrossRef Medline

Schlesiger MI, Cannova CC, Boublil BL, Hales JB, Mankin EA, Brandon MP, Leutgeb JK, Leibold C, Leutgeb S (2015) The medial entorhinal cortex is necessary for temporal organization of hippocampal neuronal activity. Nat Neurosci 18:1123–1132. CrossRef Medline

Schmidt R, Diba K, Leibold C, Schmitz D, Buzsáki G, Kempter R (2009) Single-trial phase precession in the hippocampus. J Neurosci 29:13232–13241. CrossRef Medline

Skaggs WE, McNaughton BL, Wilson MA, Barnes CA (1996) Theta phase precession in hippocampal neuronal populations and the compression of temporal sequences. Hippocampus 6:149–172. CrossRef Medline

Sun C, Kitamura T, Yamamoto J, Martin J, Pignatelli M, Kitch L, Schnitzer MJ, Tonegawa S (2015) Distinct speed dependence of entorhinal island and ocean cells, including respective grid cells. Proc Natl Acad Sci U S A 112:9466–9471. CrossRef Medline

Tang Q, Burgalossi A, Ebbesen CL, Ray S, Naumann R, Schmidt H, Spicher D, Brecht M (2014) Pyramidal and stellate cell specificity of grid and border representations in layer 2 of medial entorhinal cortex. Neuron 84:1191–1197. CrossRef Medline

Varga C, Lee SY, Soltesz I (2010) Target-selective GABAergic control of entorhinal cortex output. Nat Neurosci 13:822–824. CrossRef Medline

5 General Discussion

In Reifenstein et al. (2012), I argued that the theta phase of spikes from entorhinal grid cells can be used to estimate the position of the animal within a firing field. This is true for rats moving on a linear track, as phase changes monotonically with one-dimensional position. However, as shown in Reifenstein et al. (2014), this idea cannot be easily transferred to two-dimensional environments. The sequence of spike phases depends on the properties of the rat's path through a firing field. Long or winding runs through a firing field led to weakest phase precession whereas runs that skirt the edge show steeper rates of phase precession. The phase variable still changes monotonically along the animal's path, but variations in speed, direction, and path eccentricity disrupt the clear relationship between phase and space (also see Climer et al., 2013 and Jeewajee et al., 2014). Thus, it seems unlikely that the theta phase can be directly used by the nervous system to estimate the animal's position in two-dimensional space.

5.1 Phase-precession parameters influence the compression of sequences

As an alternative hypothesis, phase precession could be used to compress sequences of behavioral events to the time scale of synaptic plasticity (Skaggs et al., 1996). But how do the parameters of phase precession (slope, correlation, phase range, entry phase) influence the compression of sequences? In this framework, a steeper phase-precession slope implies that the spikes of different cells in the compressed sequence are further apart in time, which might be beneficial to retain the order of the events under the influence of temporal noise. On the other hand, a larger temporal separation of the spikes from different cells poses a limit to the number of cells participating in the sequence. Furthermore, phase-precession slopes of cells participating in the sequence should match. Too large a variability could disrupt the order

of events within individual theta cycles. Also the entry phase of the different cells plays an important role. If, for instance, the entry phase of cell 2 was too early compared to cell 1, the order of the two cells within a theta cycle would be constantly wrong. On the other hand, phase range does not seem to have such a drastic influence. If the entry phases and slopes of the two cells matched, changes in phase range would alter the number of theta cycles with overlapping activity. Hence, the order of the two cells would be conserved, but the phase range would dictate how many repetitions of spike pairs the synapse could experience. This could alter the speed of learning. Theta cycle skipping (i.e. the spiking activity skips one or more theta cycles) could have the same effect. If the spiking activity of a cell in the sequence skips theta cycles, the number of paired spikes and hence learning opportunities would be decreased. Theta cycle skipping has been observed in entorhinal recordings by many groups (Deshmukh et al., 2010, Quilichini et al., 2010, Newman and Hasselmo, 2014). As a last parameter discussed here, the phase-precession correlation also influences the speed of learning. The broader the scatter of spikes in phase and time, the more temporally jittered individual spikes are expected to be. This increases the likelihood of disrupting the right order in the sequence and would thus decrease the learning rate. These considerations will be extended in future work to provide a deeper understanding of the sequence-learning hypothesis as a potential function of phase precession.

5.2 Towards the origin of phase precession

As mentioned before, the events that are potentially linked by phase-precessing cells do not need to be spatial in nature. In Reifenstein et al. (2016), I applied a novel method to analyze phase precession independent from the spatial tuning of cells. In the analyzed data set, many spatially irregular cells showed phase precession. I believe that this approach – when applied to data from regions upstream of the hippocampus, where cells are generally not clearly tuned to space – will provide valuable insights about phase-precession generating mechanisms.

One such region of interest is the parasubiculum. It is a thin layer of tissue surrounding the medial entorhinal cortex, providing input to entorhinal layer II. Boccara et al. (2010) found grid cells in the parasubiculum. Tang et al. (2016) additionally reported significant fractions of border cells and strong head-direction tuning of many cells. With respect to

temporal properties, Tang et al. (2016) showed strong theta modulation for parasubicular neurons. We recently added to the picture that phase precession is only very weak in parasubiculum (Ebbesen et al., 2016).

From anatomical tracing experiments and an average spike-phase difference of approximately 19 degrees (corresponding to 7 ms), it seems very likely that parasubicular neurons project to the patches of pyramidal cells in layer II of the medial entorhinal cortex. Also these pyramidal cells express only a low degree of phase precession. Conversely, stellate cells in layer II and pyramidal cells in layer III phase precess with steep slopes. The latter finding is somewhat surprising as it challenges the long-held belief that cells in layer III do not phase precess (Hafting et al., 2008, Mizuseki et al., 2009).

Layer II stellate cells project to the dentate gyrus, whereas layer II pyramidal cells send output to CA1 (Varga et al., 2010, Kitamura et al., 2014, Ray et al., 2014). As layer II pyramidal cells show only weak phase precession, it seems unlikely that they substantially contribute to CA1 phase precession. Therefore, CA1 either generates phase precession de novo or receives phase-precessing inputs via the hippocampal loop, which originates from the strongly precessing stellate cells in layer II.

Phase precession in medial entorhinal cortex depends on the characteristics of the animal's trajectory. The longer and more curved the path, the shallower the phase-precession slope. Similar results were found by Huxter et al. (2008), who studied phase precession in CA1 place cells and noted that phase precession depends on the path: for increasingly complicated trajectories, phase precession ceased. In medial entorhinal cortex, position and time correlated equally well with the phase variable at the single-run level in two-dimensional environments (Reifenstein et al., 2014). The spike phases exhibit similar single-run position and time-correlations as reported for place cells in CA1 (Schmidt et al., 2009).

These observations indicate that the characteristics of single-run phase precession are similar in medial entorhinal cortex and CA1. Therefore, one might argue that phase precession in CA1 place cells could be inherited from the phase precession in the medial entorhinal cortex (Jaramillo et al., 2014, Schlesiger et al., 2015). Assuming that precisely timed activity of multiple grid cells is required to fire a single place cell, one might expect a reduction of the single-run phase range from entorhinal cortex to hippocampus – a prediction that is also made by Jaramillo et al. (2014) in their theoretical study on the inheritance of phase precession from one region to another. Indeed, the median single-run phase precession in

entorhinal grid cells on a linear track is 250 degrees, whereas Schmidt et al. (2009) observe that phase precession in CA1 during single runs on linear tracks typically extends over 180 degrees.

Recent studies provide evidence for direct connections from layer II pyramidal cells to layer II stellate cells (Fuchs et al., 2016). Keeping in mind that the stellates show clear phase precession whereas the pyramids do not, one could argue that layer II stellate cells are a plausible origin of phase precession. However, there is a possibility that layer II stellate cells could inherit phase precession from layer III.

Ongoing investigations by Winterer et al. suggest strong unidirectional feedforward projections from layer III to layer II. In recent work (Ebbesen et al., 2016), we demonstrate steep phase precession in layer III of the medial entorhinal cortex (slopes comparable to layer II stellate cells). Thus, layer III could pass on phase precession to layer II, but not the other way around, indicating that entorhinal phase precession could originate in layer III. In turn, layer III receives input from the lateral entorhinal cortex and the presubiculum. It is currently unclear whether cells in these regions show phase precession. These considerations and open questions will spark future work on identifying the origin of phase precession.

5.3 What are the underlying mechanisms of phase precession?

As discussed before, stellate cells in layer II of the medial entorhinal cortex could be one possible origin of phase precession. They display subthreshold resonance and membrane potential oscillations in the theta frequency range (Alonso and Llinás, 1989, Erchova et al., 2004) which can also affect spike patterns (Schreiber et al., 2004,Engel et al., 2008,Fernandez et al., 2013). A prominent class of phase-precession models – oscillatory interference models – makes use of membrane potential oscillations. These models explain phase precession as a result of the interference of oscillations at slightly different frequencies. I found that the observed phase precession in medial entorhinal cortex was not in agreement with oscillatory interference models (Burgess et al., 2007, Burgess, 2008, Zilli et al., 2009). In Reifenstein et al. (2014), I tested different versions of the model and found that it did not reproduce the features of phase precession derived from the single-run analysis of experimental data: in particular, the model predicted a constant slope of phase precession, regardless of the path

taken through two-dimensional firing fields.

An alternative mechanism relies on the idea of combining an oscillatory input in the theta range and a slowly increasing excitatory input. The subthreshold membrane potential would then reach the firing threshold earlier and earlier in successive theta cycles (Mehta et al., 2002). A variation of this idea uses the short-term facilitation of the Mossy fiber synapse to generate phase precession in CA3 (Thurley et al., 2008).

Similarly, pyramidal cells in layer III of the medial entorhinal cortex show short-term fascilitation of excitatory inputs (Heinemann et al., 2000). Although those inputs are not as strong as the ones by the Mossy fiber synapse, where individual inputs can generate a postsynaptic spike, the general idea might still work. It may require the coordinated activity of multiple excitatory, fascilitating synapses.

In a variation of that idea, one could imagine a scenario of inhibitory input undergoing short-term depression. Together with a strong and long excitatory drive, e.g. upon entering a firing field, depressing inhibition could lead to phase precession in stellate cells of medial entorhinal cortex layer II. However, this simple picture is complicated by the fact that it may require the coordinated activity of multiple inhibitory, depressing synapses in the medial entorhinal cortex to obtain phase precession, in contrast to the strong Mossy fiber synapse. I explore this possibility in ongoing work.

The depressing-inhibition mechanism makes two experimentally testable predictions. First, the overall firing rate must be low enough for the depressed synapse to return to its original state between two successive phase-precession sequences. Second, the spatial tuning of the postsynaptic (excitatory) cell should be matched by the spatial tuning of the presynaptic (inhibitory) cells.

To illustrate the first point, let us imagine a grid cell with multiple firing fields. When the animal traverses one firing field, the series of depressing inhibitory inputs results in phase precession. However, when the animal leaves the firing field, the synapse needs to relax to its original "undepressed" state to allow for phase precession in the next field traversal. For rats in open environments, it would take few seconds to get from one firing field to the next. This also sets a limit to the relaxation time constant of the synaptic depression.

In experimental data, many inhibitory cells show rather high firing rates (Buetfering et al., 2014), although there are a number of exceptions (Klausberger et al., 2003, Buetfering et al., 2014). In principal, it seems possible that inhibitory cells have low enough rates for the

depressed synapse to relax back to its original state. Particularly, if one keeps in mind that extracellular recordings are biased towards detecting highly active interneurons as compared to the low-activity ones.

The mechanism's second prediction is that the spatial tuning of the principal neuron should be matched by the presynaptic interneurons. For example, if the excitatory neuron is a grid cell, the series of depressing synaptic inputs should start when the animal enters the firing field. Consequently, the presynaptic (inhibitory) neurons would also be grid cells – at least in their collective tuning. Buetfering et al. (2014) found that parvalbumin-positive interneurons in the medial entorhinal cortex did not show clear spatial tuning. However, there remain many more classes of interneurons to be tested.

5.4 Phase precession in different classes of spatially modulated cells

The previous argument rests on the fact that grid cells show phase precession. But do different classes of spatially modulated neurons phase precess? In the data set by Tang et al. (2014), which I re-analyzed in Reifenstein et al. (2016), among a total of 114 cells there were 15 grid cells, 3 border cells, and 17 head-direction cells. I found that the single-run phase precession is shallower in grid cells than in border cells and head-direction cells. The phase-precession slopes in border cells and head-direction cells were statistically indistinguishable. [1] We did not include these results in the final publication because we felt that they should be taken with caution as the numbers of cells in each category were low. Particularly, when we separated those few cells into putative pyramids and putative stellates. Despite those statistical limitations, the main finding of the study could be reproduced for all groups: putative stellate cells showed significantly steeper phase precession than putative pyramidal cells. [2] Taken together, phase precession seems to occur in many different classes of cells, potentially allowing them to participate in sequences that are temporally compressed and stored in the synaptic weights.

In this thesis, I argued that phase precession might be the underlying neuronal mecha-

[1] grid: $-44\,[-51,-36]$ deg/s; border: $-68\,[-83,-51]$ deg/s; hd: $-71\,[-81,-59]$ deg/s; $p = 4\cdot10^{-5}$, Kruskal-Wallace H-test for the three groups; grid vs border: p=0.001, Mann-Whitney test; grid vs hd: $p = 3\cdot10^{-5}$, Mann-Whitney test; border vs hd: p=0.4, Mann-Whitney test

[2] grid: $p = 2\cdot10^{-7}$, border: $p = 0.009$, hd: $p = 0.001$

nism for remembering sequences of events, such as the one that happened to the hydraulic engineer Victor Hatherlay. For the other – arguably less pressing – open questions of Victor Hatherlay's story, I will not interfere with Sherlock Holmes and kindly direct the reader to the original story "The Adventure of the Engineer's Thumb" by Sir Arthur Conan Doyle.

Bibliography

Abbott L, Blum K (1996) Functional significance of long-term potentiation for sequence learning and prediction. *Cereb Cortex* 6:406–416.

Abeles M (1991) *Corticonics: Neural Circuits of the Cerebral Cortex* Cambridge University Press.

Allen T, Salz D, McKenzie S, Fortin N (2016) Nonspatial sequence coding in CA1 neurons. *J Neurosci* 36:1547–1563.

Alonso A, Klink R (1993) Differential electroresponsiveness of stellate and pyramidal-like cells of medial entorhinal cortex layer II. *J Neurophysiol* 70:128–143.

Alonso A, Llinás R (1989) Subthreshold Na+-dependent theta-like rhythmicity in stellate cells of entorhinal cortex layer II. *Nature* 342:175–177.

Amaral DG, Lavenex P (2007) *The Hippocampus Book* Oxford Univ. Press, New York.

Arnolds D, Lopes da Silva F, Aitink J, Kamp A, Boeijinga P (1980) The spectral properties of hippocampal eeg related to behaviour in man. *Electroencephalogr Clin Neurophysiol* 50:324–328.

Aviel Y, Pavlov E, Abeles M, Horn D (2002) Synfire chain in a balanced network. *Neurocomput* 44:285–292.

Bi G, Poo M (1998) Synaptic modifications in cultured hippocampal neurons: dependence on spike timing, synaptic strength, and postsynaptic cell type. *J Neurosci* 18:10464–10472.

Bland B (1986) Physiology and pharmacology of hippocampal formation theta rhythms. *Prog Neurobiol* 26:1–54.

Boccara C, Sargolini F, Thoresen V, Solstad T, Witter M, Moser E, Moser M (2010) Grid cells in pre- and parasubiculum. *J Neurosci* 13:987–994.

Broglio C, Gómez A, Durán E, Ocaña F, Jiménez-Moya F, Rodríguez F, Salas C (2005) Hallmarks of a common forebrain vertebrate plan: specialized pallial areas for spatial, temporal and emotional memory in actinopterygian fish. *Brain Research Bulletin* 66:397–399.

Buetfering C, Allen K, Monyer H (2014) Parvalbumin interneurons provide grid cell-driven recurrent inhibition in the medial entorhinal cortex. *Nat Neurosci* 17:710–718.

Burgess N (2008) Grid cells and theta as oscillatory interference: theory and predictions. *Hippocampus* 18:1157–1174.

Burgess N, Barry C, O'Keefe J (2007) An oscillatory interference model of grid cell firing. *Hippocampus* 17:801–812.

Burgess N, Recce M, O'Keefe J (1994) A model of hippocampal function. *Neural Netw* 7:1065–1081.

Buzsáki G (2002) Theta oscillations in the hippocampus. *Neuron* 33:325–340.

Cembrowski M, Wang L, Sugino K, Shields B, Spruston N (2016) Hipposeq: a comprehensive RNA-seq database of gene expression in hippocampal principal neurons. *eLife* 5:e14997.

Climer J, Newman E, Hasselmo M (2013) Phase coding by grid cells in unconstrained environments: two-dimensional phase precession. *Eur J Neurosci* 38:2526–2541.

Colombo M, Broadbent N (2000) Is the avian hippocampus a functional homologue of the mammalian hippocampus? *Neuroscience and Biobehavioral Reviews* 24:465–484.

Deshmukh S, Yoganarasimha D, Voicu H, Knierim J (2010) Theta modulation in the medial and the lateral entorhinal cortices. *J Neurophysiol* 104:994–1006.

Domnisoru C, Kinkhabwala A, Tank D (2013) Membrane potential dynamics of grid cells. *Nature* 495:199–204.

Ebbesen C, Reifenstein E, Tang Q, Burgalossi A, Ray S, Schreiber S, Kempter R, Brecht M (2016) Cell type-specific differences in spike timing and spike shape in rat parasubiculum and superficial medial entorhinal cortex. Manuscript in review.

Engel TA, Schimansky-Geier L, Herz AVM, Schreiber S, Erchova I (2008) Subthreshold membrane-potential resonances shape spike-train patterns in the entorhinal cortex. *J Neurophysiol* 100:1576–1589.

Erchova I, Kreck G, Heinemann U, Herz A (2004) Dynamics of rat entorhinal cortex layer II and III cells: characteristics of membrane potential resonance at rest predict oscillation properties near threshold. *J Neurosci* 560:89–110.

Fernandez F, Malerba P, Bressloff P, White J (2013) Entorhinal stellate cells show preferred spike phase-locking to theta inputs that is enhanced by correlations in synaptic activity. *J Neurosci* 33:6027–6040.

Fuchs E, Neitz A, Pinna R, Melzer S, Caputi A, Monyer H (2016) Local and distant input controlling excitation in layer II of the medial entorhinal cortex. *Neuron* 89:194–208.

Gerstner W, Kempter R, van Hemmen J, Wagner H (1996) A neuronal learning rule for sub-millisecond temporal coding. *Nature* 383:76–81.

Gerstner W, Ritz R, van Hemmen J (1993) Why spikes? hebbian learning and retrieval of time-resolved excitation patterns. *Biol Cybern* 69:503–515.

Giocomo L, Stensola T, Bonnevie T, Van Cauter T, Moser M, Moser E (2014) Topography of head direction cells in medial entorhinal cortex. *Nature* 24:252–262.

Goldman-Rakic P (1987) Circuitry of the prefrontal cortex and the regulation of behavior by representational memory In Plum F, editor, *Handbook of Physiology*, Vol. 5, pp. 373–417. Bethesda: American Physiological Society.

Gross C, Rocha-Miranda C, Bender D (1972) Visual properties of neurons in infero-temporal cortex of the macaque. *J Neurophysiol* 35:96–111.

Hafting T, Fyhn M, Bonnevie T, Moser MB, Moser EI (2008) Hippocampus-independent phase precession in entorhinal grid cells. *Nature* 453:1248–1252.

Hafting T, Fyhn M, Molden S, Moser M, Moser E (2005) Microstructure of a spatial map in the entorhinal cortex. *Nature* 436:801–806.

Harris K, Csicsvari J, Hirase H, Dragoi G, Buzsáki G (2002) Organization of cell assemblies in the hippocampus. *Nature* 424:552–556.

Hartley T, Lever C, Burgess N, O'Keefe J (2013) Space in the brain: how the hippocampal formation supports spatial cognition. *Phil Trans R Soc B* 369.

Hasselmo M, Eichenbaum H (2005) Hippocampal mechanisms for the context-dependent retrieval of episodes. *Neural Netw* 18:1172–1190.

Heinemann U, Schmitz D, Eder C, Gloveli T (2000) Properties of entorhinal cortex projection cells to the hippocampal formation. *Ann N Y Acad Sci* 911:112–126.

Huxter J, Burgess N, O'Keefe J (2003) Independent rate and temporal coding in hippocampal pyramidal cells. *Nature* 425:828–832.

Huxter J, Senior T, Allen K, Csicsvari J (2008) Theta phase-specific codes for two-dimensional position. *Nat Neurosci* 11:587–594.

Jaramillo J, Schmidt R, Kempter R (2014) Modeling inheritance of phase precession in the hippocampal formation. *J Neurosci* 34:7715–7731.

Jeewajee A, Barry C, Douchamps V, Manson D, Lever C, Burgess N (2014) Theta phase precession of grid and place cell firing in open environments. *Phil. Trans. R. Soc. B* 369:20120532.

Jung M, McNaughton B (1993) Spatial selectivity of unit activity in the hippocampal granular layer. *Hippocampus* 3:165–182.

Kamondi A, Acsády L, Wang XJ, Buzsáki G (1998) Theta oscillations in somata and dendrites of hippocampal pyramidal cells in vivo: activity dependent phase-precession of action potentials. *Hippocampus* 8:244–261.

Kempter R, Gerstner W, van Hemmen J (1997) Hebbian learning and spiking neurons. *Phys Rev E Stat Nonlin Soft Matter Phys* 59:4498–4514.

Kinkhabwala A, Aronov D, Tank D (2015) Visual cue-related activity of MEC cells during navigation in virtual reality In *2015 Neuroscience Meeting Planner, Washington, DC*, number 632.21/CC2. Society for Neuroscience.

Kistler W, van Hemmen J, De Zeeuw C (2000) Time window control: a model for cerebellar function based on synchronization, reverberation, and time slicing. *Prog Brain Res* 124:275–297.

Kitamura T, Pignatelli M, Suh J, Kohara K, Yoshiki A, Abe K, Tonegawa S (2014) Island cells control temporal association memory. *Science* 343:896–901.

Klausberger T, Magill P, Márton L, Roberts J, Cobden P, Buzsáki G, Somogyi P (2003) Brain-state- and cell-type-specific firing of hippocampal interneurons in vivo. *Nature* 421:844–848.

Koene R, Gorchetchnikov A, Cannon R, Hasselmo M (2003) Modeling goal-directed spatial navigation in the rat based on physiological data from the hippocampal formation. *Neural Netw* 16:577–584.

Kraus BJ, Robinson 2nd RJ, White JA, Eichenbaum H, Hasselmo M (2013) Hippocampal 'time cells': time versus path integration. *Neuron* 78:1090–1101.

Kreiman G, Koch C, Fried I (2000) Category-specific visual responses of single neurons in the human medial temporal lobe. *Nat Neurosci* 3:946–953.

Kropff E, Carmichael J, Moser M, Moser E (2015) Speed cells in the medial entorhinal cortex. *Nature* 523:419–424.

Lavenex P, Amaral D, Lavenex P (2006) Hippocampal lesion prevents spatial relational learning in adult macaque monkeys. *J Neurosci* 26:4546–4558.

Leibold C, Gundlfinger A, Schmidt R, Thurley K, Schmitz D, Kempter R (2008) Temporal compression mediated by short-term synaptic plasticity. *Proc Natl Acad Sci U S A* 105:4417–4422.

Lengyel M, Huhn Z, Erdi P (2005) Computational theories on the function of theta oscillations. *Biol Cybern* 92:393–408.

Leutgeb S, Leutgeb J (2007) Pattern separation, pattern completion, and new neuronal codes within a continuous CA3 map. *Learn. Memory* 14:745–757.

Levy W, Steward O (1983) Temporal contiguity requirements for long-term associative potentiation/depression in the hippocampus. *Neuroscience* 8:791–797.

Lisman J, Talamini LM, Raffone A (2005) Recall of memory sequences by interaction of the dentate and CA3: a revised model of the phase precession. *Neural Netw* 18:1191–1201.

Llorens-Martín M, Blazquez-Llorca L, Benavides-Piccione R, Rabano A, Hernandez F, Avila J, DeFelipe J (2014) Selective alterations of neurons and circuits related to early memory loss in alzheimer's disease. *Front Neuroanat* 8.

Logothetis N, Sheinberg D (1996) Visual object recognition. *Ann Rev of Neurosci* 19:577–621.

Lorente de Nó R (1934) Studies on the structure of the cerebral cortex II. continuation of the study of ammonic system. *J Psychol Neurol* 46:113–177.

Lynch J, Mountcastle V, Talbot W, Yin T (1977) Parietal lobe mechanisms for directed visual attention. *J Neurophysiol* 40:362–389.

MacDonald CJ, Lepage KQ, Eden UT, Eichenbaum H (2011) Hippocampal 'time cells' bridge the gap in memory for discontiguous events. *Neuron* 71:737–749.

Malhotra S, Cross R, van der Meer M (2012) Theta phase precession beyond the hippocampus. *Rev Neurosci* 23:39–65.

Mankin E, Diehl G, Sparks F, Leutgeb S, Leutgeb J (2015) Hippocampal ca2 activity patterns change over time to a larger extent than between spatial contexts. *Neuron* 85:190–201.

Markram H, Lübke J, Frotscher M, Sakmann B (1997) Regulation of synaptic efficacy by coincidence of postsynaptic aps and epsps. *Science* 275:213–215.

Markram H, Wang Y, Tsodyks M (1998) Differential signaling via the same axon of neocortical pyramidal neurons. *Proc Natl Acad Sci U S A* 95:5323–5328.

Mehta MR, Lee AK, Wilson MA (2002) Role of experience and oscillations in transforming a rate code into a temporal code. *Nature* 417:741–746.

Melamed O, Gerstner W, Maass W, Tsodyks M, Markram H (2004) Coding and learning of behavioral sequences. *Trends Neurosci* 27:11–14.

Mizuseki K, Sirota A, Pastalkova E, Buzsáki G (2009) Theta oscillations provide temporal windows for local circuit computation in the entorhinal-hippocampal loop. *Neuron* 64:267–280.

Moser E, Roudi Y, Witter M, Kentros C, Bonhoeffer T, Moser M (2014) Grid cells and cortical representation. *Nature Rev Neurosci* 15:466–481.

Newman EL, Hasselmo ME (2014) Grid cell firing properties vary as a function of theta phase locking preferences in the rat medial entorhinal cortex. *Front Syst Neurosci* 8:193.

O'Keefe J (1976) Place units in the hippocampus of the freely moving rat. *Experimental Neurology* 51:78–109.

O'Keefe J, Dostrovsky J (1971) The hippocampus as a spatial map: Preliminary evidence from unit activity in the freely-moving rat. *Brain Res* 34:171–175.

O'Keefe J, Recce ML (1993) Phase relationship between hippocampal place units and the EEG theta rhythm. *Hippocampus* 3:317–330.

Quilichini P, Sirota A, Buzsáki G (2010) Intrinsic circuit organization and theta-gamma oscillation dynamics in the entorhinal cortex of the rat. *J Neurosci* 30:11128–11142.

Ramón y Cajal S (1893) Estructura del asta de ammon y fascia dentata. *Anales de la Sociedad Española de Historia Natural* 22:53–126.

Ray S, Naumann R, Burgalossi A, Tang Q, Schmidt H, Brecht M (2014) Grid-layout and theta-modulation of layer 2 pyramidal neurons in medial entorhinal cortex. *Science* 343:891–896.

Reifenstein E, Ebbesen C, Tang Q, Brecht M, Schreiber S, Kempter R (2016) Cell-type specific phase precession in layer II of the medial entorhinal cortex. *J Neurosci* 17:2283–2288.

Reifenstein E, Kempter R, Schreiber S, Stemmler M, Herz A (2012) Grid cells in rat entorhinal cortex encode physical space with independent firing fields and phase precession at the single-trial level. *Proc Natl Acad Sci U S A* 109:6301–6306.

Reifenstein E, Stemmler M, Herz A, Kempter R, Schreiber S (2014) Movement dependence and layer specificity of entorhinal phase precession in two-dimensional environments. *PLoS ONE* 9:e100638.

Rodríguez F, López J, Vargas J, Broglio C, Gómez Y, Salas C (2002) Spatial memory and hippocampal pallium through vertebrate evolution: insights from reptiles and teleost fish. *Brain Research Bulletin* 57:499–503.

Rosenbaum R, McKinnon M, Levine B, Moscovitch M (2004) Visual imagery deficits, impaired strategic retrieval, or memory loss: disentangling the nature of an amnesic person's autobiographical memory deficit. *Neuropsychologia* 42:1619–1635.

Sargolini F, Fyhn M, Hafting T, McNaughton BL, Witter MP, Moser MB, Moser EI (2006) Conjunctive representation of position, direction, and velocity in entorhinal cortex. *Science* 312:758–762.

Savage L, Buzzetti R, Ramirez D (2004) The effects of hippocampal lesions on learning, memory, and reward expectancies. *Neurobiol Learn Mem* 82:109–119.

Schlesiger MI, Cannova CC, Boublil BL, Hales JB, Mankin EA, Brandon MP, Leutgeb JK, Leibold C, Leutgeb S (2015) The medial entorhinal cortex is necessary for temporal organization of hippocampal neuronal activity. *Nature Neurosci* 18:1123–1132.

Schmidt RC, Diba K, Leibold C, Schmitz D, Buzsáki G, Kempter R (2009) Single-trial phase precession in the hippocampus. *J Neuro* 29:13232–13241.

Schoenbaum G, Eichenbaum H (1995) Information coding in the rodent prefrontal cortex. i. single-neuron activity in orbitofrontal cortex compared with that in pyriform cortex. *J Neurophysiol* 74:733–750.

Schreiber S, Erchova I, Heinemann U, A.V.M. H (2004) Subthreshold resonance explains the frequency-dependent integration of periodic as well as random stimuli in the entorhinal cortex. *J Neurophysiol* 92:408–415.

Scoville WB, Milner B (1957) Loss of recent memory after bilateral hippocampal lesions. *J Neurol Neurosurg Psychiatry* 20:11–21.

Shettleworth S (2003) Memory and hippocampal specialization in food-storing birds: challenges for research on comparative cognition. *Brain, Behavior and Evolution* 62:108–116.

Skaggs WE, McNaughton BL, Wilson MA, Barnes C (1996) Theta phase precession in hippocampal neuronal populations and the compression of temporal sequences. *Hippocampus* 6:149–172.

Solstad T, Boccara C, Kropff E, Moser M, Moser E (2008) Representation of geometric borders in the entorhinal cortex. *Science* 322:1865–1868.

Tang Q, Burgalossi A, Ebbesen CL, Ray S, Naumann R, Schmidt H, Spicher D, Brecht M (2014) Pyramidal and stellate cell specificity of grid and border representations in layer 2 of medial entorhinal cortex. *Neuron* 84:1191–1197.

Tang Q, Burgalossi A, Ebbesen C, Sanguinetti-Scheck J, Schmidt H, Tukker J, Naumann R, Ray S, Preston-Ferrer P, Schmitz D, Brecht M (2016) Functional architecture of the rat parasubiculum. *J Neurosci* 36:2289–2301.

Thurley K, Leibold C, Gundlfinger A, Schmitz D, Kempter R (2008) Phase precession through synaptic facilitation. *Neural Comput* 20:1285–1324.

Tsodyks M, Skaggs W, Sejnowski T, McNaughton B (1996) Population dynamics and theta rhythm phase precession of hippocampal place cell firing: a spiking neuron model. *Hippocampus* 6:271–280.

van der Meer M, Redish A (2011) Theta phase precession in rat ventral striatum links place and reward information. *J Neurosci* 31:2843–2854.

van Strien N, Cappaert N, Witter M (2000) The anatomy of memory: an interactive overview of the parahippocampal-hippocampal network. *Nat Rev Neurosci* 10:272–282.

van Vreeswijk C, Hansel D (2001) Patterns of synchrony in neural networks with spike adaptation. *Neural Comput* 13:959–992.

Varga C, Lee S, Soltesz I (2010) Target-selective GABAergic control of entorhinal cortex output. *Nature Neurosci* 13:822–824.

Wilson M, McNaughton B (1993) Dynamics of the hippocampal ensemble code for space. *Science* 261:1055–1058.

Winterer J, Maier N, Wozny C, Beed P, Breustedt J, Evangelista R, Peng Y, D'Albis T, Kempter R, Schmitz D (2016) Excitatory wiring within a grid cell network. Manuscript in preparation.

Zilli E, Yoshida M, Tahvildari B, Giocomo L, Hasselmo M (2009) Evaluation of the oscillatory interference model of grid cell firing through analysis and measured period variance of some biological oscillators. *PLoS Comput Biol* 5:e1000573.

Danksagung

Ich bin einigen Menschen zu tiefstem Dank verpflichtet:

- Susanne Schreiber für ihre grenzenlose Geduld, großes Vertrauen und die damit verbundenen Freiheiten – nichts davon ist selbstverständlich, vielen Dank!
- Richard Kempter für seine Vorbildfunktion in unerschöpflicher Neugier und unaufgeregter Moderation sowie einer Vielzahl wertvoller fachlicher Beiträge
- Andreas Herz und Martin Stemmler dafür, dass sie mich mit unglaublichem Vertrauen und endloser Geduld an das Feld heran führten und durch ihren Scharfsinn stets begeistern
- Prateep Beed, Dietmar Schmitz, Qiusong Tang, Christian Ebbesen, Michael Brecht sowie May-Britt und Edvard Moser, die großzügig ihre Daten bereit stellten, geduldig alle noch so naiven Fragen über sich ergehen ließen und stets angenehme Gesprächspartner sind
- Willi Gottstein und José Donoso für Freundschaft, Humor und die Tatsache, dass sich der Weg nach Mitte allein schon für die Pausen gelohnt hätte
- allen in Haus 4, die die Arbeit am ITB mit Freude füllen – ich kann mir keine bessere Umgebung vorstellen
- meiner wundervollen Familie für Liebe, bedingungslose Unterstützung und mehr Verständnis als ich mir jemals hätte wünschen können
- dem einen Menschen, der mich besser kennt als sonst irgendjemand – du bist alles für mich

Selbständigkeitserklärung

Ich erkläre, dass ich die vorliegende Arbeit selbständig und nur unter Verwendung der angegebenen Literatur und Hilfsmittel angefertigt habe.

Berlin, den 02.05.2016 Eric Torsten Reifenstein